

Doctoral Dissertation

博士論文

**Development of Multichannel Cardiac Murmurs Analysis Method and
Monitoring System on Congenital Heart Disease**

先天性心疾患に対する多チャネル心雜音解析法と
モニタリングシステムの開発

March 2016

平成 28 年 3 月

Ting TAO

陶 婷

Graduate School of Science and Engineering

Yamaguchi University

山口大学大学院理工学研究科

Abstract

Congenital heart defect (CHD) is the most frequent form of major birth defects in newborns, common CHDs can not always be found and cured during pregnancy or at birth, and they must be monitored throughout life. Thus, if life-style related diseases could not be monitored continuously during a long period in the early stage, they might be difficult to be diagnosed appropriately in an early step. Furthermore, auscultating and analyzing heart murmurs from different positions during a physical examination are the vital diagnosis for CHDs. The needs for the primary health care physicians to improve the cardiac auscultation skill, and computer-aided analysis skill of heart murmurs, are still strong in the primary screening examination, and become stronger for the general users to perform the auscultation at home.

The aim of this study is to develop a multichannel cardiac murmurs analysis method and monitoring system on CHD. Firstly, the background of CHD, HS and common murmurs, reviews of cardiac murmurs analysis were introduced in Chapter one. Next, four electronic stethoscopes were fixed on the auscultation cloth, the HSs collection method which reflected the cardiac valvular opening and closure sounds at the same time was proposed, this measuring system helped to make the relation between four cardiac valvular opening and closure sounds and murmurs clear in Chapter 2. The acquired data were transformed to analysis server by network for data transmission, save and analysis.

Heart murmurs are pathological sounds produced by turbulent blood flow due to cardiac defects.

In order to make the murmurs features easy to use for general users, the murmur index extraction methods based on quantitatively analysis of cardiac murmurs was proposed in Chapter 3. Although, there are some evaluation studies about cardiac murmurs, the quantitative analysis of evaluation indexes has not been decided. In our study, the evaluation indexes of energy analysis under five frequency bands, and murmurs duration time parameters at systolic and diastolic periods were extracted. Firstly, the approach on analysis of the pathologic cardiac murmurs based on the wavelet packet decomposition technique was proposed. The HS signals were divided into five bands and the energy ratios at each frequency band were calculated and compared. Based on the analysis of clinic HSs data, three evaluation indexes of cardiac murmurs (ICM) were proposed for the analysis of the pathologic murmurs. Finally, the threshold values between the innocent and pathologic murmurs were determined based on the statistical results of the normal HSs. The statistic results showed that ICM of multichannel signals not only evaluated the murmur quantitatively, but also revealed the murmurs generating reason by analyzing signals from four positions simultaneously.

Furthermore, in order to further quantitatively analyze the cardiac murmurs at each cardiac cycle, the murmurs time duration indexes extraction based on cardiac vibration state by describing the shape of different-scale window moment waveform (MW) was proposed in Chapter 3. Firstly, homomorphic MW extraction was proposed and the HS cycle and S1S2 segmentation were implemented by locating the maximum and minimum of MW respectively. Secondly, considering the segmentation points of HS S1S2 and cycle as MW centers respectively, to extract the systolic MW (SMW) and diastolic MW (DMW), furthermore, extracting systolic murmur index (SMI) and diastolic murmurs index (DMI) which were proposed based on SMW and DMW. Finally, many experiments show that the murmurs indexes are efficient to judge the murmurs occurring periods and murmurs time duration. Importantly, DMF can be computed by moment analysis very fast and simple, and therefore it's very useful to auto-diagnosis or aided-diagnosis in an artificial intelligence cardiac murmur analysis system.

The noises coming from various sources contaminate HS signals and affect HS auscultation, in order to improve the auscultation, an unexpected noise reduction method based on frequency slice wavelet transform (FSWT) that can consummate the filtrating in time and frequency domain

simultaneously was proposed. This method was assessed by signal noise ratio (SNR), correlation coefficient (CC) and mean square error (MSE) evaluation indicators and comparing with the total variation de-noise (TVD) and discrete wavelet transform (DWT) methods, experimental results showed HCA method was much more effective for external (ambient noise, speech noise, stethoscope device power interference) and certain internal (respiratory or lung sounds, and skin movements) disturbances noise reduction.

Finally, the multichannel murmurs monitoring system which is composed of multichannel HSs measuring system, analysis server and analysis result display was designed. The measuring system which consists of multichannel cardiac signals recorders acquires the signals and sends them to analysis server through internet network by computer. And the data transmission (upload and download) and analysis were implemented by the analysis server. The analysis results which show the multichannel heart murmur analysis indexes are useful and efficient to diagnose the CHDs, meanwhile, further reveal the heart murmurs physiological and pathological information. And the results data were not only saved in the server, but also displayed in the website for murmurs auscultation and diagnosis. Therefore, monitoring on CHDs by clinical HSs auscultation and analysis remain important for general daily health care. The pre-monitoring for CHD sounds will greatly improve the prevention of clinical CHD in advance, and helpful to the primary screening examination, and becomes stronger for the general users to perform the auscultation at home.

要旨

近年、心疾患は死亡原因に2位となっている。また、新生児1000人中約8人が先天性心疾患を患っており、特に中国内陸山間部はより深刻である。先天性心疾患の発見と治療が遅れると、心不全さらに死亡をもたらすこともある。心疾患の検査方法として、超音波による心エコーヤ CT画像診断が最も有効されているが、病院や関連施設等を通う必要がある。在宅などで簡便な検査法として心雜音の聴診は昔からある。しかしながら、聴診による診断は熟練の医師でないと判断は困難である。「入院より在宅」医療費抑制を目指すためにも、一般使用者が自宅で容易に心疾患の早期発見とモニタリングができるシステムへの要望が高まっている。本研究ではこのような現状に基づいて、心音、心雜音を中心に一般家庭で心音の聴診を簡便に行える多チャンネル同期聴診方法の開発を行う。また、心房中隔欠損症(ASD)や心室中隔欠損症(VSD)、ファロー四徴症(TOF)などの心雜音を定量的に評価する解析方法について検討・提案し、一般家庭でも使いやすい心音聴診と解析システムを開発する。

本論文は緒論、結言を含め6章から構成されている。

1章では、本研究の技術的な背景と本論文の構成について述べている。

2章では、自宅での多チャンネル心音計測システム開発について述べている。医者は心音を聴診する場合、複数箇所の心音を聴診し、心雜音の様々な特性から心臓の病状を推定する。しかし、一般家庭使用者は心音の聴診部位に関する知識がなく正確に聴診することができない可能性がある。この点に対して、四つの聴診器を搭載したウェアラブル聴診システムを開発し、心臓の四つの弁が開閉時に発生する音を四箇所で同時に採集する方法を提案した。今まで聴診の結果から分かりにくかった四つの弁で発生する心雜音の関係がより分かるようになった。

3章では、心雜音の評価に対して多くの研究がなされているが、心雜音を定量的に評価するパラメータが定まっていない。本章では、心雜音の強さと周波数特性、心雜音の発生タイミングとその持続時間を、心雜音の評価指数として提案し、これらのパラメータの解析方法と抽出アルゴリズムを提案した。具体的には、五つの周波数領域における心雜音のパワー指數並びに心臓の収縮期と拡張期における心雜音の持続時間指數を提案した。心雜音のパワー指數として、ウェーブレット解析法を用いて心雜音を五つの周波数域(VLF, LF, SF, MF, HF)に分割し、心雜音エネルギー評価パラメーター(ICM)を提示した。また、心雜音の持続時間指數を求めるには、心音の1音と2音を高精度に分割するアルゴリズムを開発するとともに、心雜音の収縮期と拡張期における心雜音の持続時間を計算するガウス近似方法を開発した。さらに、臨床先天性心疾患データ(ASD: 心房中隔欠損症、VSD: 心室中隔欠損症、TOF: ファロー四徴症)ならび健康者心音データ(NHS)を用いて検証を行い、その有効性を検証した。

4章では、一般家庭で聴診する際に環境ノイズが聴診データに含まれることが多いため、遠隔聴診を行う際に医師の聞きやすい心音データの提供が必要である。本章では、聴診データに含まれる環境ノイズの軽減方法について検討している。本論文では、当研究グループが開発している周波数スライスウェーブレット変換(FSWT)方法を画像処理技術と組み合わせることにより効果的な環境ノイズの軽減方法を提案している。具体的には、FSWTによるスペクトログラムを求め、特定周波数領域における環境ノイズのエネルギーを軽減する重み関数を自動的に計算し、スペクトログラムにかけて調整する。調整後の FSWT スペクトログラムに対して逆 FSWT を施し、環境ノイズを軽減された心音信号に再構成する。本方法を適用することで、環境ノイズを軽減すると同時に心音の聴覚効果を保つことが特徴的である。

5章では、一般家庭在宅で利用できる心雜音のモニタリング用多チャンネル心音聴診解析システムの開発を行う。このシステムの主要部分は2章で開発した四チャンネル心音同時計測システム、3章で抽出した心雜音定量解析により評価指數の表示、4章で提案した環境ノイズ軽減法による心音再構築アルゴリズムで構成されている。これにより、一般家庭在宅でも心疾患に対する心雜音の計測、評価及び環境ノイズを軽減した心音が聴診可能な支援システムを構築している。このシステムにおいては心雜音レベルの定量評価を示す一方、その結果を遠隔で医者に診てもらうことで、より正確な心疾患の診断と予防が可能となる。

6章は、結言であり、本論文で得られた成果について要約している。

Contents

I. Introduction	1
1. Background.....	1
1.1 <i>Congenital heart disease</i>	2
1.2 <i>Heart sounds and common murmurs</i>	4
2. Review of cardiac murmurs analysis	6
3. Aim of this thesis	8
4. Outline	9
References	12
II. Clinical Heart Sound Acquisition	16
1. The existing heart sound acquisition system	16
2. Multichannel acquisition system	18
3. Clinical HS data statistics	26
4. Summary.....	26
References	27
III. Multichannel Cardiac Murmurs Analysis Method and Murmurs Indexes	29
1. Pre-processing.....	30
2. Murmurs indexes extraction based on energy analysis.....	31
2.1 <i>Frequency band definition</i>	32
2.2 <i>Murmurs index evaluation based on wavelet packet energy</i>	32
2.3 <i>Result and discussion for one channel signal</i>	36
2.4 <i>Result and discussion for four channel signals</i>	44
2.5 <i>Summary</i>	47
3. Murmurs indexes extraction based on heart vibration states	48
3.1 <i>The heart sound segmentation of multichannel signals</i>	49
3.1.1 <i>Envelop waveform extraction</i>	50
3.1.2 <i>Homomorphic envelop waveform extraction of multichannel signals</i>	51
3.1.3 <i>Moment waveform extraction based on homomorphic envelop waveform</i>	52
3.1.4 <i>Calculate heart rate with FFT analysis</i>	53
3.1.5 <i>Calculation of heart sound cycle and heart sound segmentation</i>	53
3.2 <i>Murmurs indexes extraction based on dual moment features</i>	55

3.2.1	<i>The introduction of moment method</i>	58
3.2.2	<i>Murmurs indexes extraction</i>	59
3.3	<i>Result and discussion</i>	61
3.3.1	<i>Heart rate of clinical four channel signals</i>	61
3.3.2	<i>Homomorphic segmentation of clinical four channels signals</i>	62
3.3.3	<i>Murmurs indexes of clinical four channels signals</i>	67
3.4	<i>Summary</i>	69
References		70
IV. Unexpected Noise Reduction for Improvement of Auscultation		71
1.	Unexpected noise problems of clinical heart sound.....	71
2.	Reviews of noise reduction methods	73
2.1	<i>Introduction of frequency slice wavelet transform method</i>	74
2.2	<i>A natural assumption</i>	75
3.	Noise reduction methods	76
3.1	<i>Noise reduction by discrete wavelet transform method</i>	76
3.2	<i>Noise reduction by total variance de-noise method</i>	77
3.3	<i>Noise reduction by histogram curve adjusting method</i>	78
4	Validation.....	79
5	Comparison of noise reduction methods.....	80
5.1	<i>Comparison of standard HS noise reduction</i>	80
5.2	<i>Comparison of clinical noise reduction</i>	84
5	Summary.....	87
References		88
V. Multichannel Heart Murmurs Monitoring System		90
1.	System design	91
2.	Analysis engine.....	92
3.	Murmurs analysis indexes display	93
3.1	<i>Discussion of normal heart sound (NHS) case</i>	93
3.2	<i>Discussion of atrioventricular septal defect (ASD) case</i>	98
3.3	<i>Discussion of ventricular septal defect (VSD) case</i>	101
3.4	<i>Discussion of Tetralogy of Fallot (TOF) case</i>	103
4.	Summary.....	106
References		107
VI. Conclusions		108
Acknowledgment		111

- Main Technical Term and Notations

Terminology Nouns	Notations	Pages
Congenital Heart Defects	CHD	p.1
Atrioventricular Septal Defects	ASD	p.1
Ventricular Septal Defects	VSD	p.1
Tetralogy of Fallot	TOF	p.2
Aortic Area	A	p.4
Pulmonic Area	P	p.4
Tricuspid Area	T	p.4
Mitral Area	M	p.4
Heart Sound	HS	p.5
First Heart Sound	S1	p.5
Second Heart Sound	S2	p.5
Normal Heart Sound	NHS	p.5
Wavelet Decomposition	WD	p.7
Frequency Slice Wavelet Transform	FSWT	p.9
Indexes of Cardiac Murmurs	ICM	p.10
Dual Moment Feature	DMF	p.10
Moment Waveform	MW	p.10
Homomorphic Envelops Waveform	HEW	p.11
Systolic Murmur Index	SMI	p.11
Diastolic Murmur Index	DMI	p.11
Time Frequency Representation	TFR	p.11
Signal Noise Ratio	SNR	p.11
Correlation Coefficient	CC	p.11
Mean Square Error	MSE	p.11
Total Variation De-noise	TVD	p.11

Discrete Wavelet Transform	DWT	p.11
Histogram Curve Adjustment	HCA	p.11
Abnormal Heart Sound	AHS	p.26
Wavelet Packet Decomposition	WPD	p.30
Very Low Frequency	VLF	p.31
Standard Frequency	SF	p.31
Low Frequency	LF	p.31
Middle Frequency	MF	p.31
High Frequency	HF	p.31
Threshold for Cardiac Murmurs	TCM	p.36
True Positives	TP	p.41
False Negatives	FN	p.41
True Negatives	TN	p.41
False Positives	FP	p.41
Accuracy	Acc	p.41
Sensitivity	Se	p.41
Specificity	Sp	p.41
Homomorphic MW	HMW	p.47
Systolic MW	SMW	p.47
Diastolic MW	DMW	p.47
Homomorphic Envelop Waveform	HEW	p.48
Envelop Waveform	EW	p.49
Heart Rate	HR	p.52
Murmur Index Level	MIL	p.66
Systolic MIL	SMIL	p.66
Diastolic MIL	DMIL	p.66
Majorization-Minimization	MM	p.76

- List of Figures

I. Introduction

Fig.1. Cross-section of a normal heart and a heart with an ASD.

Fig.2. Cross-section of a normal heart and a heart with a VSD.

Fig.3. Cross-section of a normal heart and a heart with TOF.

Fig.4. Auscultation sites.

Fig.5. The structure schematic drawing of normal heart sound (NHS).

Fig.6. The structure schematic drawing of abnormal HS.

Fig.7. Murmur patterns of NHS and common CHDs.

II. Clinical Heart Sound Acquisition

Fig.1. Block diagram of single channel HS measurement and analysis system.

Fig.2. Big and small chest pieces.

Fig.3. Male vest.

Fig.4. Female vest.

Fig.5. Simple graph of auscultation clothes.

Fig.6. Auscultation clothes sample.

Fig.7. Measuring system with BIOPAC.

Fig.8 (a) HS real-time display graph of BIOPAC acquisition system (NHS).

Fig.8 (b) HS real-time display graph of BIOPAC acquisition system (VSD).

Fig.9. Measuring system with BIOPAC for clinical HS recording.

Fig.10. Measuring system with IC recorders fixed by plastic case for clinical HS recording

(a) Measuring system with IC recorders (b)~(c) IC recorders fixed by plastic case(front~side).

Fig.11. Measuring system with IC recorders.

Fig.12. Multichannel signals measuring system.

Fig.13. Multichannel NHS.

Fig.14. Multichannel ASD signals.

Fig.15. Multichannel VSD signals.

Fig.16. Multichannel TOF signals.

III. Multichannel Cardiac Murmurs Analysis Method and Murmurs Indexes

Fig.1. A block diagram of the study on cardiac murmurs evaluation based on the (WP) technique.

Fig.2. HS signal examples of NHS, ASD, VSD, TOF and their reconstructed signals at different corresponding frequency band, Original, VLF, SF, LF, MF and HF.

Fig.3. Energy distribution at SF frequency.

Fig.4. Energy distribution at LF frequency.

Fig.5. Energy distribution at MF frequency.

Fig.6. Energy distribution at HF frequency.

Fig.7. Energy distribution at VLF.

Fig.8. Distributions of the indexes of cardiac murmurs at LF band (ICM_{LF}).

Fig.9. Example of pulmonary sound due to a normal breath, indicated by case Pa in Fig.8.

Fig.10. Example of pulmonary sound due to a normal breath, indicated by case Pb in Fig.8.

Fig.11. Example of pulmonary sound due to a normal breath, indicated by case Pc in Fig.8.

Fig.12. Distributions of the indexes of cardiac murmurs at MF band (ICM_{MF}).

Fig.13. Example of pulmonary sound due to a normal breath, indicated by Pd in Fig.12.

Fig.14. Distributions of the indexes of cardiac murmurs at HF band (ICM_{HF})

Fig.15. Example of pulmonary sound due to a normal breath, indicated by Pe in Fig.14.

Fig.16. Example of pulmonary sound due to a normal breath, indicated by Pf in Fig.14.

Fig.17. Mean values of the ICM_{LF} at four positions.

Fig.18. Mean values of the ICM_{MF} at four positions.

Fig.19. Mean values of the ICM_{HF} at four positions.

Fig.20. Original multichannel signals, each EW and HEW of NHS.

Fig.21. Original multichannel signals, each EW and HEW of abnormal HS (TOF).

Fig.22. HEW extraction and homomorphic segmentations based on HEW of NHS.

(a)HEW extraction (b) cycle, S1S2 segmentation based on MW ($l=T/2$).

Fig.23. HEW extraction and homomorphic segmentations based on HEW of abnormal HS (TOF).

(a)HEW extraction (b) cycle, S1S2 segmentation based on MW ($l=T/2$).

Fig.24. The HS segmentation flow chart.

Fig.25. Systolic and diastolic MW of NHS with different window lengths. (a)Original NHS, (b) HEW extraction, (c) MW($l=T/8$), (d) MW($l=3T/8$).

Fig.26. Systolic and diastolic MW of VSD with different window lengths (a)Original VSD signal, (b)

HEW extraction, (c) MW($l = T/8$), (d) MW($l = 3T/8$).

Fig.27. Systolic and diastolic MW of NHS with different window lengths (a) EW extraction, (b) MW($l = T/8$), dotted box shown the systolic MW shape, (c) MW($l = 3T/8$) , dotted box shown the systolic MW shape.

Fig.28. Systolic and diastolic MW of VSD with different window lengths (a)EW extraction, (b) MW($l = T/8$), dotted box shown the systolic MW shape, (c) MW($l = 3T/8$) , dotted box shown the systolic MW shape.

Fig.29. Schematic diagram of signal moment.

Fig.30. The four-channel VSD original sound signals and their MW.

Fig.31. S1S2 and cycle segmentation points as the time centers (t_i, t_j).

Fig.32. A block diagram of homomorphic segmentation of multichannel HS technique

Fig.33. RH of NHS and CHDs.

Fig.34. The original of the multichannel ASD signals (deleted sample).

Fig.35. The homomorphic cycle segmentation of multichannel VSD (case 1) signals, the part in the red dotted box is noise which influence the homomorphic cycle segmentation.

Fig.36. The homomorphic S1S2 segmentation of multichannel VSD (case 1) signals, the part in the black dotted box is error segmentation of S1S2.

Fig.37. The homomorphic cycle segmentation of multichannel VSD (case 2) signals, the part in the dotted box is noise which influence the homomorphic cycle segmentation.

Fig.38. The homomorphic S1S2 segmentation of multichannel VSD (case 2) signals, the part in the black dotted box is error segmentation of S1S2.

Fig.39. The histogram statistics of double moment feature values in systole.

Fig.40. The histogram statistics of double moment feature values in diastole.

IV. Unexpected Noise Reduction for Improvement of Auscultation

Fig.1. Original Normal HS and the signals at different frequency bands (SF, LF, MF, HF) The door slam noises shown in red box

Fig.2. Original CHD HS and the signals at different frequency bands (SF, LF, MF, HF), the electronic noise and car whistle noise shown in red box

Fig.3. Original Normal HS and the signals at different frequency bands (SF, LF, MF, HF), the strong breath sounds shown in red box

Fig.4. Original CHD HS and the signals at different frequency bands (SF, LF, MF, HF), the strong breath sounds shown in red box

Fig.5. The original clinical normal HS signal and its time-frequency representation (TFR) image with real-life noise.

Fig.6. The original clinical abnormal HS signal and its time-frequency representation (TFR) image of ventricular septal defect with real-life noise.

Fig.7. Histogram curves of FSWT from a standard NHS original signal s0, adding white noise from 10% to 50% respectively.

Fig.8. HCA method: SNRs and correlation coefficients tendency with different adjustment parameters α for different noise levels from 10% to 50% respectively, and the blue '*' is the optimal adjustment parameter at each noise level.

Fig.9. TVD method: SNRs and correlation coefficients tendency with different regularization parameters for different noise levels from 10% to 50% respectively, and the blue star mark '*' is the optimal regularization parameter at each noise level.

Fig.10. DWT method: SNRs and correlation coefficients tendency with different adjustment parameters for different noise levels from 10% to 50% respectively, and the blue star mark '*' is the optimal adjustment parameter at each noise level.

Fig.11. The SNR, CC and MSE curve at different noise levels with HCA, TVD and DWT methods.

Fig.12. Time domain noised signals (green) and de-noised signals (blue) by HCA, TVD and DWT methods. (a) Plus 10%noise (b) Plus 30%noise

Fig.13. Noise (in Fig.1) reduction by DWT.

Fig.14. Noise (in Fig.4) reduction by DWT.

Fig.15. Noise (in Fig.1) reduction by TVD.

Fig.16. Noise (in Fig.4) reduction by TVD

Fig.17. Noise (in Fig.1) reduction by HCA.

Fig.18. Noise (in Fig.4) reduction by HCA

Fig.19. Time diagrams. (a) The raw clinical HS signal. (b) De-noised signal with HCA method. (c) De-noised signal with TVD method. (D) De-noised signal with DWT method.

Fig.20. The phase space maps of HS signal. (a) The raw clinical HS signal. (b) De-noised signal with HCA method. (c) De-noised signal with TVD method. (D) De-noised signal with DWT method.

V. Multichannel Heart Murmurs Monitoring System

Fig.1. The multichannel heart murmur monitoring system.

Fig.2. Multichannel heart murmur monitoring system.

Fig.3. The GUI monitoring system.

Fig.4. The GUI monitoring system of four channels NHS case (WBD).

Fig.5. The multichannel cardiac murmur diagnosis parameters of NHS case (WBD).

Fig.6. The GUI monitoring system of NHS case (CSY).

Fig.7. The multichannel cardiac murmur diagnosis parameters of NHS case (CSY).

Fig.8. Waveforms of NHS case (CSY) at different frequencies in Mitral position (M), and the part in the red box showed the body organ sounds at LF and MF bands.

Fig.9. The GUI monitoring system of ASD case (MSJ).

Fig.10. The multichannel cardiac murmur diagnosis parameters of ASD case (MSJ).

Fig.11. The multichannel signals of ASD case (MSJ), the basic HS (S1 and S2), systolic murmur (SM) are marked, and the strong external noise at T and M positions are marked with red box.

Fig.12. Waveforms of ASD case (MSJ) at different frequencies in Tricuspid position (T), and the part in the red box showed the strong external sound at MF and HF bands.

Fig.13. The GUI monitoring system of VSD case (XY).

Fig.14. The multichannel cardiac murmur diagnosis parameters of VSD case (XY).

Fig.15. The multichannel signals of VSD case (XY), the basic HS (S1 and S2), systolic murmur (SM) are marked, and some systolic murmurs at T and M positions.

Fig.16. Waveforms of VSD case (XY) at different frequencies in Pulmonary (P) position, and the part in the red box showed the strongest at LF, MF and HF bands.

Fig.17. The GUI monitoring system of TOF case (ZZL).

Fig.18. The multichannel cardiac murmur diagnosis parameters of TOF case (ZZL).

Fig.19. The multichannel signals of TOF case (ZZL), the basic HS (S1 and S2), systolic murmur (SM) are marked, and some diastolic murmurs at P position.

- List of Tables

I. Introduction

II. Clinical Heart Sound Acquisition

Table1. Specification of the IC recorder.

Table2. Specification of the microphone (audio technical®, AT805F).

III. Multichannel Cardiac Murmurs Analysis Method and Murmurs Indexes

Table1. Murmurs frequency bands definition.

Table2. Means and variances of the energy ratios at four frequency bands.

Table3. TN, FN, TP, FP, sensitivity (Se), specificity (Sp) and accuracy (Acc) of evaluation indexes of cardiac murmurs ICM_L .

Table4. Energy ratios values at different frequency bands of CHD heart sound below the threshold TCM_{HF} .

Table5. Means and variances of the ICM_{LF} at four positions.

Table6. Means and variances of the ICM_{MF} at four positions.

Table7. Means and variances of the ICM_{HF} at four positions.

Table8. The threshold of TCM_{LF} , TCM_{MF} and TCM_{HF} at four positions.

Table9. Means and variances of the HR between NHS and CHD.

Table10. The statistic of cycle automatic segmentation accuracy.

Table11. The statistic of S1S2 automatic segmentation accuracy.

Table12. The murmurs indexes in systole ($SMI \pm \sigma_{SMI}$).

Table13. The murmurs indexes in diastole ($DMI \pm \sigma_{DMI}$).

Table14. The MIL of systole (SMI) and diastole (DMI).

Table15. The MIL definition of systole and diastole.

IV. Unexpected Noise Reduction for Improvement of Auscultation

Table1. Optimal parameters at five noise level with three de-noised methods.

Table2. The energy ratio at LF, MF and HF frequency bands of case 1 (door slam noise) in Fig 1.

Table3. The energy ratio at LF, MF and HF frequency bands of case 2 (strong breath sounds) in Fig2.

V. Multichannel Heart Murmurs Monitoring System

Chapter 1

Introduction

In this introduction chapter the background, review of cardiac murmur analysis and aim of this thesis which develop a multichannel heart murmur analysis method and monitoring system on congenital heart disease (CHD) are introduced.

1. Background

Heart disease is the leading or the second cause of death for people in the world, according to American Heart Association report, in the United States, killing nearly 787,000 people alone in 2011, and the total cost is estimated to be 298 billion dollar [1]. 80% of the total mortality occurs in low and middle-income countries. And a type of heart disease called CHD is the most frequent form of major birth defects in newborns affecting close to 1% of newborn babies (8 per 1,000) [2].

1.1 Congenital heart disease

CHDs are structural problems that arise from abnormal formation of the heart or major blood vessels, and defects range in severity from tiny pinholes between chambers that may resolve spontaneously to major malformations that can require multiple surgical procedures before school age and may result in death in utero, in infancy, or in childhood. CHDs are serious and common conditions that have significant impact on morbidity, mortality, and healthcare costs in children and adults. And continental variations in birth prevalence have been reported, from 6.9 per 1000 births in Europe to 9.3 per 1000 in Asia [3]. There are many types of CHDs. Some are simples, such as atrioventricular septal defects (ASD), ventricular septal defects (VSD). Other heart defects are more

complex, they include combinations of simple defects, and the most common complex heart defect is Tetralogy of Fallot (TOF). And, the most common types of defects in children are (at a minimum) VSD and the most common lesions seen in adults are ASD and TOF [4]. In the following, there are some pathology informations of ASD, VSD and TOF in detail [4].

An ASD is a hole in the part of the septum that separates the atria and the upper chambers of the heart. The hole allows oxygen-rich blood from the left atrium to flow into the right atrium, instead of flowing into the left ventricle as it should. Many children who have ASDs have few, if any, symptoms. In Fig. 1, ① shows the structure and blood flow inside a normal heart. ② shows a heart with an ASD. The hole allows oxygen-rich blood from the left atrium to mix with oxygen-poor blood from the right atrium.

A VSD is a hole in the part of the septum that separates the ventricles—the lower chambers of the heart. The hole allows oxygen-rich blood to flow from the left ventricle into the right ventricle, instead of flowing into the aorta and out to the body as it should. In Fig. 2, ① shows the structure and blood flow inside a normal heart. ② shows two common locations for a VSD. The defect allows oxygen-rich blood from the left ventricle to mix with oxygen-poor blood in the right ventricle. Large VSDs allow a lot of blood to flow from the left ventricle to the right ventricle. As a result, the left side of the heart must work harder than normal. Extra blood flow increases blood pressure in the right side of the heart and the lungs. The heart's extra workload can cause heart failure and poor growth. If the hole isn't closed, high blood pressure can scar the arteries in the lungs.

The most common complex heart defect is TOF, which is a combination of four defects: pulmonary valve stenosis, a large VSD, an overriding aorta, and right ventricular hypertrophy. In TOF, not enough blood is able to reach the lungs to get oxygen, and oxygen-poor blood flows to the body. In Fig. 3, ① shows the structure and blood flow inside a normal heart. ② shows a heart with the four defects of TOF. Babies and children who have TOF have episodes of cyanosis, which can be severe. In the past, when this condition wasn't treated in infancy, older children would get very tired during exercise and might faint. TOF must be repaired with open-heart surgery, either soon after birth or later in infancy. The timing of the surgery will depend on how narrow the pulmonary artery is.

Children who have had this heart defect repaired need lifelong medical care from a specialist to make sure they stay as healthy as possible.

CHDs are not always found during pregnancy or at birth, they also can not be cured, and they must be monitored throughout life [2]. Thus, if life-style related diseases could not be monitored continuously during a long period in the early stage, they might be difficult to be diagnosed appropriately.

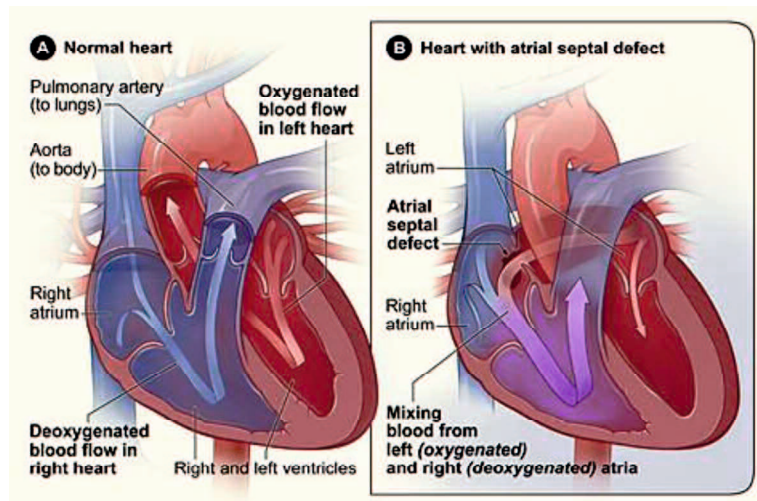


Fig. 1. Cross-section of a normal heart and a heart with an ASD.

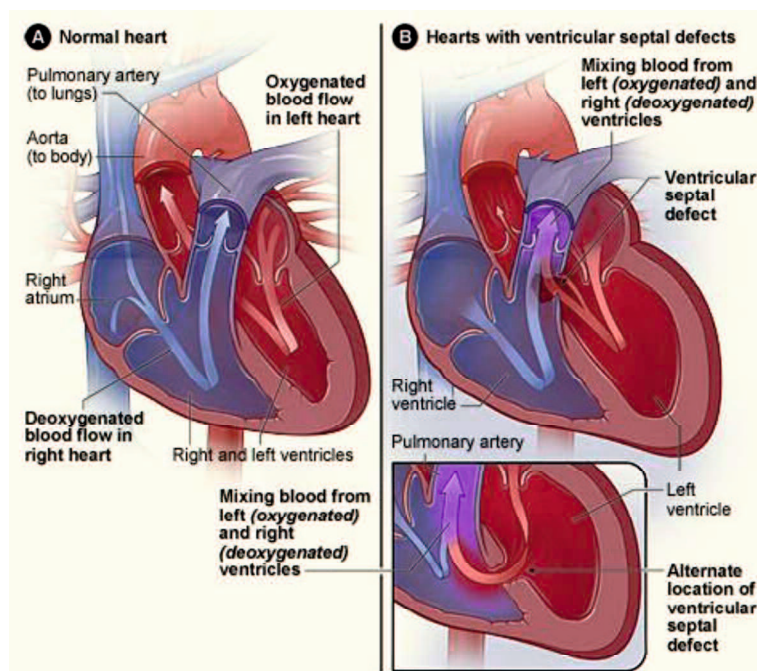


Fig. 2. Cross-section of a normal heart and a heart with a VSD.

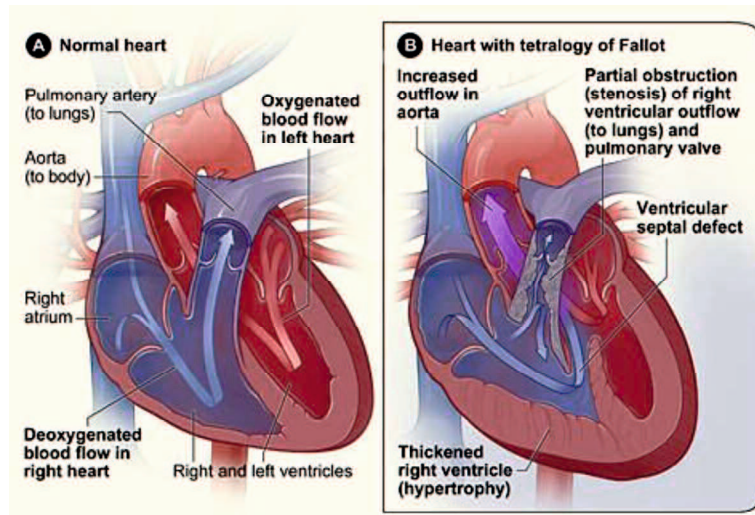


Fig. 3. Cross-section of a normal heart and a heart with TOF.

1.2 Heart sounds and common murmurs

HSs are produced by acoustic vibrations of the valvular, muscular, vascular and blood circulation. There are four important areas used for listening to heart sounds. Those are: aortic area (A), pulmonic area (P), tricuspid area (T), mitral area (M) (Apex), shown in Fig. 4. The four cardiac valves are classified into two types—the atrioventricular (mitral and tricuspid) and the semilunar (aortic and pulmonic) valves. This is an important distinction. During systole, atrioventricular (tricuspid and mitral) valves are closed and semilunar valves are open, while in diastole the opposite is true.

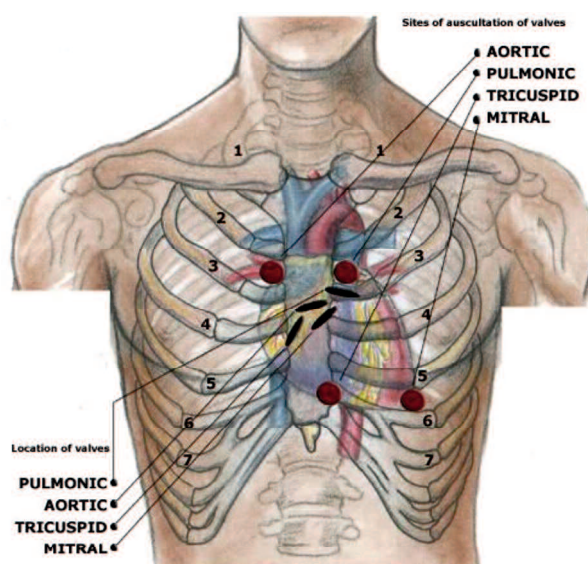


Fig. 4. Auscultation sites.

The heart sound (HS) signals provide vital clinical information, such as fundamental sounds, systolic murmurs, diastolic murmurs, and so on to physicians for analyzing and diagnosing different heart abnormalities. A common notation for a sound heard at an auscultatory site is to use the first initial of the site and the number 1 or 2 to describe the first heart sound (S1) and second heart sound (S2) respectively. In general both the S1 and S2 can be heard at all sites, but some pathologic and normal sounds are heard best at one site or another. The structure schematic drawings of normal heart sound (NHS) shown in Fig. 5 and abnormal HS shown in Fig.6.

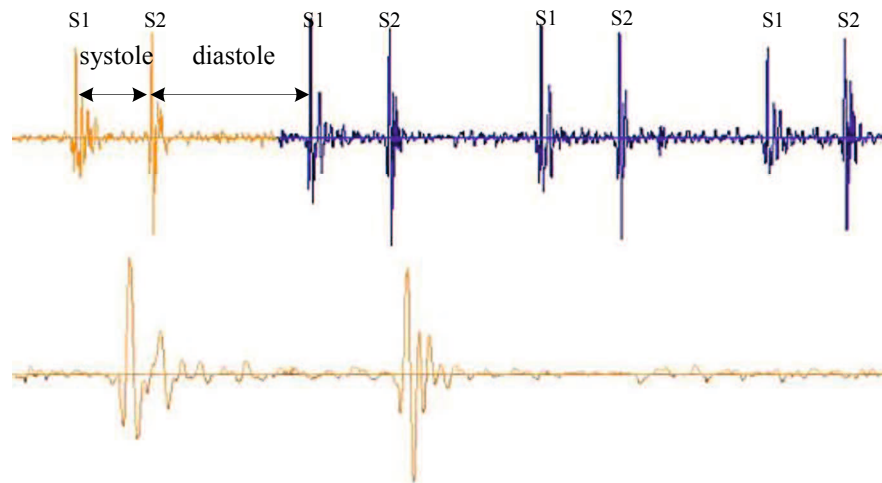


Fig. 5. The structure schematic drawing of normal heart sound (NHS).

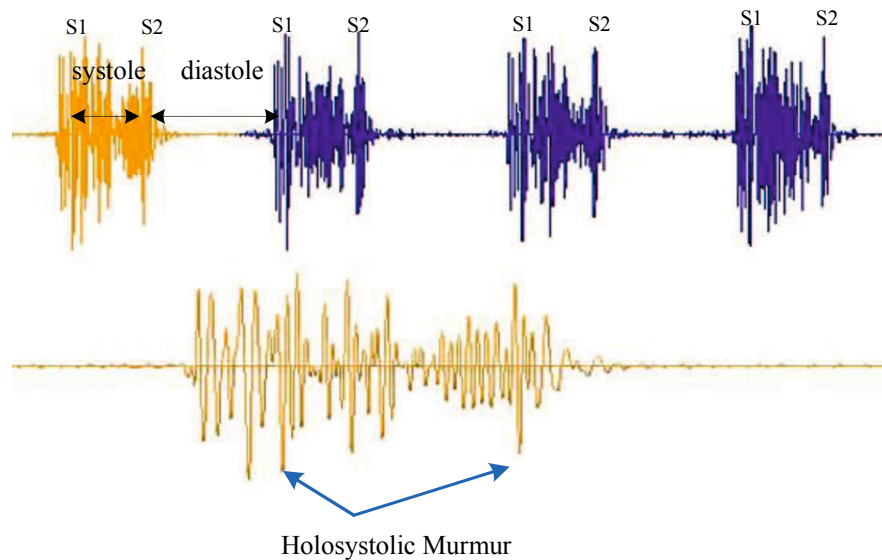


Fig. 6. The structure schematic drawing of abnormal HS.

A heart murmur is an extra or unusual sound hearing during a heartbeat. The doctor may hear

abnormal HSs when listening to the chest with a stethoscope. Hearing and detecting heart murmurs during a physical examination is the vital diagnosis for common clinical heart diseases, including the CHD, if the heart murmurs are detected, physicians will refer to go to a cardiologist for further diagnosis. The murmur patterns of NHS and common CHDs are showed in Fig. 8.

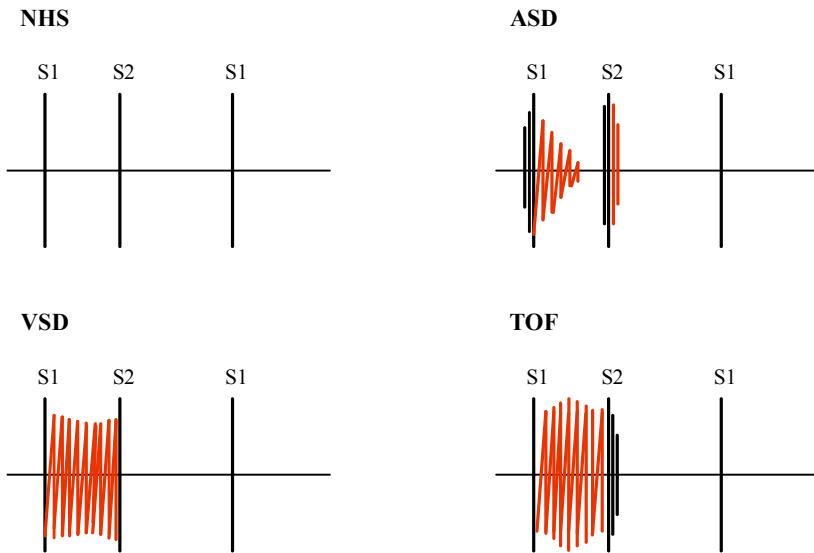


Fig. 7. Murmurs patterns of NHS and common CHDs.

In order to describe and compare the characters of the murmurs, the time occur of murmurs, murmur property, intensity, and position, also including the relation between murmur and breadth, body position when the objects are detected, are pay attention to.

2. Review of cardiac murmurs analysis

CHD sounds including abundant helpful physiological and pathological information, especially the murmurs of clinical CHD. In consequence, monitoring on heart diseases by clinical HS auscultation and cardiac murmur analysis remain important for general daily health care.

Heart murmurs are pathological sounds produced by turbulent blood flow due to certain cardiac defects, and they are the most common reasons for referral to the pediatric cardiologist. In children, about 50-70% of these murmurs are clinically insignificant [5], but if the child is crying, uncooperative to the examiner or breathing loudly, some other murmurs may occur. Because of the difficulty of mastering auscultation skills, innocent and organic heart murmurs cannot be readily distinguished. Therefore, heart murmur quantitative analysis is necessary. Recently, the demand for

evaluation of the murmurs from auscultation of cardiac sounds has been addressed by researchers and clinicians [6-9]. To detect and analyze the heart murmurs, many approaches have been carried out, including a multivariate matching pursuit method [8] used to model the murmurs by decomposing them into a series of parametric time-frequency atoms, and then the model parameters used to identify the cardiac sound signals. An adaptive singular spectrum analysis approach [9] was applied to the changes in the statistical properties of the sound data for detection of murmurs.

Since the heart murmurs show clearly different characteristics in the frequency domain compared with the time domain, many researchers have focused on the characteristic extraction by local frequency analysis method, such as the wavelet decomposition (WD) or wavelet packet decomposition [10-15, 24], the neural network [7, 16-19], support vector machine [20-22]. Sepehri, et al. [19], studied a method for automatic screening of congenital heart diseases in children with neural network classifier. The pathological murmurs of CHD were identified by examining the HS energy over special frequency bands called Arash-Bands. However, the Arash-Bands determined for each CHD in the study were overlapped with the frequencies 16-121 Hz. Based on our study, the main energy distributions either for normal or abnormal HSs are concentrated in the frequency range of 10-100Hz. We also found that frequency band is much influenced by measurement situations, ages, body types, mixed heart defects, etc. We have tried many methods but it seems difficult to identify some murmurs by the Arash-Bands. Furthermore, Samjin Choi, et al. [10, 24] proposed insufficiency murmur identification and valvular disorders detection using wavelet packet decomposition, and HS signals with frequency range 20-700Hz were preferred; furthermore, the features were extracted from WP coefficient calculated for each subdivision. However, the subjects in these two studies were from the medical text book [27] or internet web [28]. It is not clear whether WP coefficient calculated for each subdivision with the frequency range 20-700Hz can identify the CHD signals in general auscultation environment in hospital.

Furthermore, in time domain HS and murmurs feature analysis aspect, the features, such as, sound intensity, content, timing, duration, shape, systolic and diastolic intervals, amplitude ratio of S1 and S2, and the ratio of diastolic duration to systolic duration, which contain abundant physiological and pathological information are extracted in [29-30]. And then, in frequency domain

aspect, the frequency components and their width bands, maximum of amplitude of heart sound were proposed [31-36]. Many features presented in previous literatures can be also expressed by the time-frequency analysis and moment analysis of signals, such as, time center and duration, the frequency center and frequency bands etc. However, time-frequency analysis need a lot of computation, it is not easy adapt to the situations based on real-time processing systems, especially for those systems of mobile platform. The moment method [37-38] which can be used to realize the segmentation analysis of HS pattern and feature extraction is validated actually simper and faster than the wavelet method. However, firstly, the time window size of moment is an important parameter need to be determined, a fixed size in [37] is not easy to adapt to all situations. Further, the different time window moments of the HSs have different characteristics; these characteristics can be used to obtain the rhythm features of HSs more accurately. And then, the homomorphic segmentation by multichannel signals will improve the automatic segmentation accuracy much more than single channel signals.

3. Aim of this thesis

As we summarized from previous research, there are several problems of clinical cardiac murmurs analysis and monitoring. Aim at above problems, in this thesis we focused on the development of multichannel cardiac murmurs analysis method and monitoring system on CHD.

Firstly, due to the closure and opening of the human cardiac valves and blood flowing are occurring at the same time, especially, the cardiac murmurs from different body positions which are related with different disease, therefore, the one channel signal auscultation and analysis are not enough to diagnose the heart diseases accurately and comprehensively. So the multichannel clinical signals are even more valuable to obtain more abundant pathology information and corresponding positions information, which are great significance in clinical diagnosis and in-home heart healthcare. These part is introduced in Chapter one.

Meanwhile, the HS data which the previous research used usually obtained from the textbook and internet, which may not reflect the clinical HS auscultation problems, and the patients who suffered CHDs are always children and adolescents, and if the child is crying, uncooperative to the

examiner or breathing loudly, it is very difficult to collect high-quality clinical HSs. Therefore a portable multichannel acquisition system with auscultation clothes which can collect high-quality clinical HSs synchronously by a simple and effect way is introduced in Chapter 2.

And then, because of the difficulty of mastering auscultation skills, innocent and organic heart murmurs cannot be readily distinguished. Therefore, the study of computer-aided cardiac murmurs analysis is very important for CHD diagnosis. While, as we summarized from previous research, most of the research focus on HS or murmurs feature extraction and diseases classification by qualitative analysis, the quantitative analysis of clinical multichannel cardiac murmurs has not been pay attention to, therefore, in this thesis, in order to evaluate the clinical CHD murmurs quantitatively, the murmur index extraction methods based on murmur energy and heart vibration state are implemented in Chapter 3.

Furthermore, the unexpected noises from external and internal disturbances always affect the clinical auscultation and analysis seriously. Therefore, noise reduction method based on frequency slice wavelet transform (FSWT) that can consummate the filtrating in time and frequency domain simultaneously will be proposed in this study in Chapter 4.

At last, CHDs are not always found during pregnancy or at birth, they also can not be cured, and they must be monitored throughout life [2]. Thus, if life-style related diseases could not be monitored continuously during a long period in the early stage, they might be difficult to be diagnosed appropriately. Therefore, based on the murmurs index extraction analysis and unexpected noises reduction, a monitoring system on CHDs is developed to monitor continuously during a long period, further which will greatly improve the prevention of clinical CHD in advance, and helpful to the primary screening examination, and becomes stronger for the general users to perform the auscultation at home.

4. Outline

The contents of this study are to develop a multichannel cardiac murmurs analysis method and monitoring system on CHD. In the following, the contents in each chapter will be described in detail.

In chapter 1, the introduction of this study is introduced, they consist of background of CHD, HS and common murmurs, reviews of cardiac murmurs analysis and the aim of these thesis.

In chapter 2, the clinical HSs acquisition is introduced. At first, the existing single channel HS acquisition system which consists of an IC recorder, a microphone, a traditional chest piece, an earphone and a computer for analysis and display is introduced. However, this single channel system costs much more time to collect clinical HS from different positions at the same time, especially, if the child is crying, uncooperative to the examiner or breathing loudly, it is very difficult to collect high-quality clinical HSs. in order to solve the above problems, a multichannel signals acquisition system which is composed of computer, audio amplifier, and multichannel physiological signal recorders and auscultation cloth with four stethoscopes is developed. Moreover, the clinical HS data statistics is implemented.

In chapter 3, since the heart murmurs are pathological sounds produced by turbulent blood flow due to cardiac defects. In order to quantitatively analyze cardiac murmurs, a murmur index extraction method based on murmur energy analysis is proposed in this chapter. This approach which analyses both low and high frequency sub-bands of HS signals based on the wavelet packet decomposition technique is very simple. The HS signals are divided into five bands and the energy intensity at each frequency band is calculated and compared. Based on the analysis of clinic HS data, three evaluation indexes for cardiac murmurs are proposed for the analysis of the pathologic murmurs. Finally, the threshold values between the innocent and pathologic murmurs are determined based on the statistical results of the normal HSs. A pulmonary HS case study on the NHS and CHD signals is performed to validate the usefulness and performance of the proposed method. At last, the quantitative indexes of cardiac murmurs (ICM) parameters are calculated with the same method. The statistic results show that ICM parameters of multichannel signals can not also evaluate the murmur quantitatively, but also reveal the murmurs generating reason by analyzing signals from four positions simultaneously.

Furthermore, the dual moment feature (DMF) of systole and diastole HS signals as new indexes that can be used to evaluate heart vibration states by describing the shape of different-scale window moment waveform (MW). Firstly, the homomorphic segmentation of multichannel HS cycle (T) and

fundamental HS (S1S2) is proposed based on homomorphic envelops waveform (HEW) and homomorphic MW extraction with window length ($l=T/2$), the HS cycle segmentation is implemented by locating the maximum of MW and meanwhile the HR is also calculated, and the S1S2 segmentation is implemented by locating the minimum of MW. Secondly, considering the segmentation points of HS S1S2 and cycle as MW centers respectively, to extract the systolic MW with window length $T/8$, and diastolic MW with window length $3T/8$, furthermore, extracting DMF as systolic murmur index (SMI) which is proposed based on SMW with window length $T/4$ with one cycle time length, and also extracting diastolic murmur index (DMI) based on diastolic MW. Finally, many experiments show that the original clinical HS signal included more murmur components when the DMF is high and its value over 0.2. Importantly, DMF can be computed by moment analysis very fast and simple, and therefore it's very useful to auto-diagnosis or aided-diagnosis in an artificial intelligence cardiac murmur analysis system.

In chapter 4, the noises coming from various sources contaminate HS signals and affect heart disease detection. Therefore, in this chapter, a novel noise reduction method based on FSWT that can consummate the filtrating in time and frequency domain simultaneously will be proposed in this study. The image process idea of time frequency representation (TFR) is used instead of designing filter directly. This method is assessed using signal noise ratio (SNR), correlation coefficient (CC) and mean square error (MSE) evaluation indicators and comparing with the total variation de-noise (TVD) and discrete wavelet transform (DWT) methods, experimental results show that the proposed histogram curve adjustment (HCA) method was much more effective for external (ambient noise, speech noise, stethoscope device power interference) and internal (respiratory or lung sounds, and skin movements) disturbances noise reduction. Finally, a case of clinical HS is implemented to validate the proposed method which can cancel the HS noise and interference adaptive, simple and correctly.

In chapter 5, the multichannel murmurs monitoring system which is composed of multichannel HSs measuring system, analysis server and analysis result display was designed. The measuring system which consists of multichannel cardiac signals recorders acquires the signals and sends them to analysis server though internet network by computer. And the data transmission (upload and

download) and analysis were implemented by the analysis server. This monitoring on CHDs by clinical HSs auscultation and analysis remain important for general daily health care. The pre-monitoring for CHD sounds will greatly improve the prevention of clinical CHD in advance, and helpful to the primary screening examination, and becomes stronger for the general users to perform the auscultation at home.

In chapter 6, the conclusions of this study are presented.

References

- [1] The Heart Foundation, HEART DISEASE FACTS, ABOUT HEART DISEASE, 2015. Available at, <http://www.theheartfoundation.org/heart-disease-facts/heart-disease-statistics>. Accessed in 2015.02.03.
- [2] Congenital Heart Defects UK, 2007-2015. Available at, <http://www.chd-uk.co.uk/what-is-chd-abbreviation-for-congenital-heart-defects>. Accessed in 2015.02.03.
- [3] American Heart Association, Statistical Fact Sheet 2013 Update, 2013.
- [4] National Heart, Lung, and Blood Institute, Congenital Heart Defects, 2011. Available at, <http://www.nhlbi.nih.gov/health/health-topics/topics/chd/types>. Accessed in 2015.02.05.
- [5] Amer Abdullah Lardhi, Prevalence and clinical significance of heart murmurs detected in routine neonatal examination, *Journal of the Saudi Heart Association*, 2010, 22(1): 25-27.
- [6] Reichlin S., Dieterle T., Camli C., Leimenstoll B., Schoenenberger A. and Martina B., Initial clinical evaluation of cardiac systolic murmurs in the ED by noncardiologists, *American Journal of Emergency Medicine*, 2004, 71-75.
- [7] Higuchi k., Sato K., Makuuch H., Furuse A., Takamoto S. and Takeda H., Automated diagnosis of heart disease in patients with heart murmurs: application of a neural network technique, *International Journal of Medical Engineering and Technology*, 2006, 30: 61-68.
- [8] Sepideh Jabbari, Hassan Ghassemian, Modeling of heart systolic murmurs based on multivariate matching pursuit for diagnosis of valvular disorders, *Computers in Biology and Medicine*, 2011, 41(9): 802-811.
- [9] Saeid Sanei, Mansoureh Ghodsi, Hossein Hassani, An adaptive singular spectrum analysis

- approach to murmur detection from heart sounds, *Medical Engineering & Physics*, 2011, 33(3): 362-367.
- [10] Samjin Choi, Youngkyun Shin, Hun-Kuk Park, Selection of wavelet packet measures for insufficiency murmur identification, *Expert Systems with Applications*, 2011, 38(4): 4264-4271.
- [11] Yuerong Chen, Shengyong Wang, Chia-Hsuan Shen, Fred K. Choy, Matrix decomposition based feature extraction for murmur classification, *Medical Engineering & Physics*, 2012, 34(6): 756-761.
- [12] Zümrat Dokur, Tamer Ölmez, Heart sound classification using wavelet transform and incremental self-organizing map, *Digital Signal Processing*, 2008, 18(6): 951-959.
- [13] Fatemeh Safara, Shyamala Doraisamy, Azreen Azman, Azrul Jantan, Asri Ranga Abdullah Ramaiah, Multi-level basis selection of wavelet packet decomposition tree for heart sound classification, *Computers in Biology and Medicine* 2013, 43 (10): 1407-1414.
- [14] M. Hariharan ^{a,*}, C.Y. Fook ^a, R. Sindhu ^b, Abdul Hamid Adom^a, Sazali Yaacob^a, Objective evaluation of speech dysfluencies using wavelet packet transform with sample entropy, *Digital Signal Processing* 2013, 23 (3): 952-959.
- [15] Shivnarayan Patidar, Ram Bilas Pachori, Segmentation of cardiac sound signals by removing murmurs using constrained tunable-Q wavelet transform, *Biomedical Signal Processing and Control*, 2013, 41(4): 559-567.
- [16] Sanjay R. Bhatikar, Curt DeGroff, Roop L. Mahajan, A classifier based on the artificial neural network approach for cardiologic auscultation in pediatrics, *Artificial Intelligent in Medicine*, 2005, 33: 251-260.
- [17] Abdulkadir Sengur, An expert system based on principal component analysis: artificial immune system and fuzzy k-NN for diagnosis of valvular heart diseases, *Computers in Biology and Medicine*, 2008, 329-338.
- [18] Sepideh Babaei and Amir Geranmayeh, Heart sound reproduction based on neural network classification of cardiac valve disorders using wavelet transforms of PCG signals, *Computers in Biology and Medicine*, 2009, 8-15.
- [19] Amir A. Sepehri, Joel Hancq, Thierry Dutoit, Arash Gharehbaghi, Armen Kocharian, A. Kiani, Computerized screening of children congenital heart diseases, *Computer Methods and Programs in Biomedicine*, 2008, 92(2): 186-192.

- [20] Samit Ari, Koushik Hembram, Goutam Saha, Detection of cardiac abnormality from PCG signal using LMS based least square SVM classifier, *Expert Systems with Applications*, 2010, 37(12): 8019-8026.
- [21] Samjin Choi, Zhongwei Jiang, Cardiac sound murmurs classification with autoregressive spectral analysis and multi-support vector machine technique, *Computers in Biology and Medicine*, 2010, 40 (1): 8-20.
- [22] Shuping Sun, Haibin Wang, Zhongwei Jiang, Yu Fang, Ting Tao, Segmentation-based heart sound feature extraction combined with classifier models for a VSD diagnosis system, *Expert Systems with Applications*, 2014, 41(4): 1769-1780.
- [23] Peter Libby MD, Robert O., Bonow MD, Douglas L., Mann MD FACC, Douglas P., Zipes MD, Braunwald's Heart Disease: A Textbook of Cardiovascular Medicine, 2007, p:1583.
- [24] Samjin Choi, Detection of valvular heart disorders using wavelet packet decomposition and support vector machine, *Expert System with Applications* 2008, 35(4): 1679-1687.
- [25] M. Nilsson, P. Funk, E.M. Olsson, B. vonSchele, N. Xiong, Clinical decision-support for diagnosing stress-related disorders by applying psychophysiological medical knowledge to an instance-based learning system, *Artificial Intelligence in Medicine* , 2006, 36 : 159-176.
- [26] Donna Giri^a, U. Rajendra Achary^{a b,c,*}, Roshan Joy Martis ^b, S. Vinitha Sree ^d, Teik-Cheng Lim^a, Thajudin Ahamed VI^e, Jasjit S. Suri^{f,1}, Automated diagnosis of Coronary Artery Disease affected patients using LDA, PCA, ICA and Discrete Wavelet Transform, *Knowledge-Based Systems*, 2013, 37: 274-282.
- [27] T. Sawayama, Auscultation training by CD: Heart Sound, Publisher of Nankodo, 1994 (in Japan).
- [28] K. Nakao, Online Bed Side Learning: Heart Sound Auscultation, available at, <http://www.medic.mie-u.ac.jp/student/sinnzou.html> (in Japan). Accessed June 14, 2014.
- [29] V. Nivitha Varghees*, K.I. Ramachandran*, A novel heart sound activity detection framework for automated heart sound analysis. *Biomedical Signal Processing and Control* 13 (2014) 174-188.
- [30] F. Kova'csa,* , N.Kersnera, K.Ka'da'rb, G.Hosszu'c, Computer method for perinatal screening of cardiac murmur using fetal phonocardiography. *Computers in Biology and Medicine* 39 (2009) 1130-1136.
- [31] Shuping Sun*, An innovative intelligent system based on automatic diagnostic feature extraction

- for diagnosing heart diseases. *Knowledge-Based Systems* 75 (2015) 224-238.
- [32] Samjin Choi^{a,b,c,*}, Gyeong Bok Jung^{a,b}, Hun-Kuk Park^{a,b,c}, A novel cardiac spectral segmentation based on a multi-Gaussian fitting method for regurgitation murmur identification. *Signal Processing* 104 (2014) 339-345.
- [33] Samjin Choi^{a,*}, Si-Hyung Cho^b, Chan-Won Park^b, Jae-Ho Shin^{c,*}, A novel cardiac spectral envelope extraction algorithm using a single-degree-of-freedom vibration model. *Biomedical Signal Processing and Control* 18 (2015) 169-173.
- [34] Chia-Hsuan Shen^{a,*}, FredK.Choy^b, YuerongChen^b, ShengyongWang^b, A modular approach to computer-aided auscultation: Analysis and parametric characterization of murmur acoustic qualities. *Computers in Biology and Medicine* 43 (2013) 798-805.
- [35] S.E. Schmidt^{a,*}, M. Graebe^b, E. Toft^c, J.J. Struijk^a, No evidence of nonlinear or chaotic behavior of cardiovascular murmurs. *Biomedical Signal Processing and Control* 6 (2011) 157-163.
- [36] Samjin Choi^{a,b,c}, ZhongweiJiang^{c,*}, Cardiac sound murmurs classification with autoregressive spectral analysis and multi-support vector machine technique. *Computers in Biology and Medicine* 40 (2010) 8-20.
- [37] Zhonghong Yan^{a,*}, Zhongwei Jiang^{b,1}, Ayaho Miyamoto^b, YunlongWei^a, The moment segmentation analysis of heart sound pattern. *Computer Methods and Programs in Biomedicine* 98 (2010) 140-150.
- [38] Shuping Sun, Zhongwei Jiang, Haibin Wang, Yu Fang, Automatic moment segmentation and peak detection analysis of heart sound pattern via short-time modified Hilbert transform. *Computers in Biology and Medicine* 114(2014) 219-230.

Chapter 2

Clinical Heart Sound Acquisition

The stethoscope [1-3], which has been invented more than few hundred years ago, is one of the oldest medical diagnosis instruments, and a lot of researchers on the stethoscopic signal analysis for diagnosis of the cardiac conditions were continued for a number of decades. In the recent year, the high concern about health management and medical instruments for health care and diagnosis in daily life. Stethoscope, in addition to other health care instruments such as weight scale, a clinically thermometer and a sphygmomanometer, have come into wide use for inexperienced users. Since the stethoscope could auscultate the HS, respiratory sounds, as well as lung sound, and screen the most cardiorespiratory diseases, it might become a cheap and efficient home health care instrument in the near future.

However, the auscultation of HS through either a conventional acoustic or electronic stethoscope needs a long-term practice and experience, which could take years to acquire the auscultation skills. Although the stethoscope becomes the symbol of clinicians, primary care clinicians are documented to have poor auscultatory skill to actuality. Therefore, if the HS can be recognized or diagnosed with support of the software techniques, the above problems might be taken advantage of as a high-quality home medical and health care instrument.

1. The existing heart sound acquisition system

Recent years, we are focusing on developing a single channel single acquisition system [4-9],

which is composed of an IC recorder (Olympus Voice-Trek V-51), a microphone (audio technical AT9904), a traditional chest piece (Littman, ClassicIISE), an earphone, while auscultating HS, we can also hear in the same time.

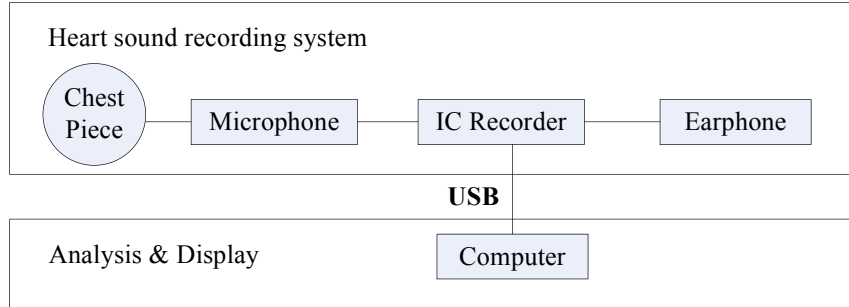


Fig. 1. Block diagram of single channel HS measurement and analysis system.

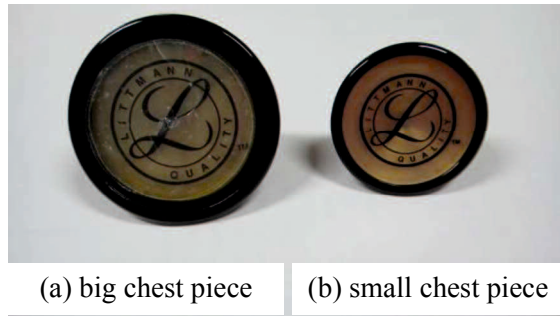


Fig. 2. Big and small chest pieces.

Table 1. Specification of the IC recorder.

IC recorder (Olympus Voice-Trek V-51)	
Sampling Frequency	44.1kHz
Frequency Band	20Hz~20kHz
Bit Rate	128kbps
Sampling Bit	16
Memory	1GB

Table 2. Specification of the microphone (audio technical®, AT805F).

Microphone (audio-technical®, AT805F)	
Frequency	30Hz~10,000Hz
Sensitivity (0dB=1V/Pa, 1kHz)	-46±3dB
Impedance	2kΩ

The system adopt the normal standard chest piece (Littman, ClassicIISE), which is used by many general doctors and is produced by America 3M company showed in Fig. 2, and the small one used for children and big one used for adults. The specifications of IC recorder and microphone are shown in Table 1~2. The HS is recorded by IC recorder and then transmitted into a computer by USB interface. And these signals will be analyzed and displayed on the computer with software MATLAB.

This single channel system is light, simple and convenient in clinic auscultation, and it realizes that HS can be recognized or diagnosed with support of the software techniques. However, there are some problems during clinical HSs acquisition with it, especially for clinical CHD HSs acquisition. Firstly, single channel system costs much more time to collect clinical HS from different positions. Furthermore, this will affect the patients to have a good rest situation. Secondly, it can not be used to acquire the multichannel signals at the same time. Lastly, the patients who suffered CHD are children or adolescents, if the child is crying, uncooperative to the examiner or breathing loudly, it is very difficult to collect high-quality clinical HSs. in order to solve the above problems, a multichannel signals acquisition system is developed, the detail will be introduced in next section.

2. Multichannel acquisition system

Multichannel measuring system with auscultation clothes and electronic stethoscope is applied to obtain the HS from patients and healthy person who has no history of heart disease. This measuring system is composed of computer, audio amplifier, and multichannel physiological signal recorder and auscultation cloth with four stethoscopes. This measuring system is also can be used for

healthy person at sports state.

So how to collect the high quality multichannel signals simultaneously is a key point for HS measuring. Because when the objects are auscultated, they are always hyperactive, uncooperative to the examiner or breathing loudly. What's more, when we are recording HS during auscultation with hands, there may be some noises from our movement or the friction between chest piece and skin. In addition, male and female's body structure are different, and the auscultation positions are always in front of the chest, the auscultation clothes made by the existing vest for male and female are showed in Fig. 3~4. Therefore, how to design the auscultation clothes for female is important for measuring system. The auscultation clothes simple graph is showed in Fig. 5. In order to keep the chest piece and auscultation positions contact closely and tightly, the elastic band is used for fixing the auscultation positions. And the clothes sample is showed in Fig. 6. This auscultation cloth has the advantages of good softness, convenient wearing, close-fitting flexibility, what's more, it's not restricted by the size of the clothes, because they are designed based on existing vest. And the auscultation effect is very good, HS sample recorded from healthy person wearing auscultation cloth showed in Fig. 7. This auscultation cloth is also can be used for healthy person at sport situation.



Fig. 3. Male vest.

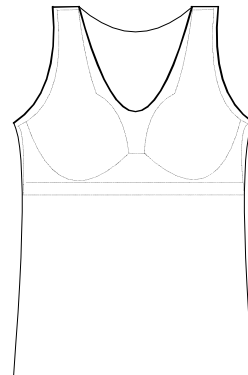


Fig. 4. Female vest.

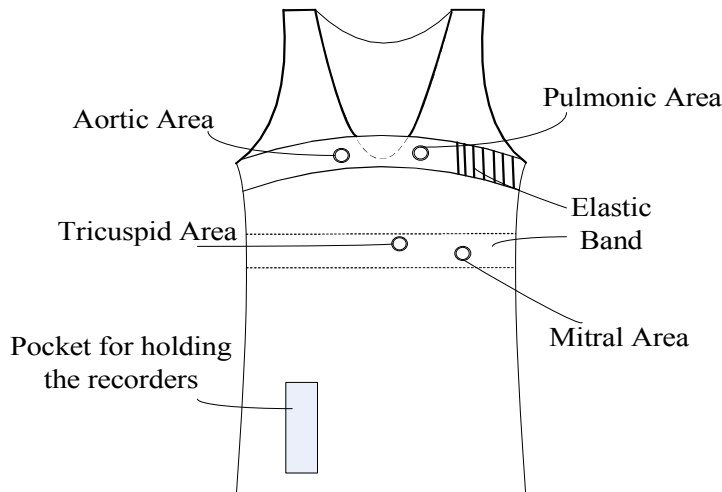


Fig. 5. Simple graph of auscultation clothes.



Fig. 6. Auscultation clothes sample.

There are two kinds of multichannel physiological signal recorders, one is BIOPAC MP150 data acquisition system, which is produced by America BIOPAC company. And the measuring system with BIOPAC showed in Fig.7.

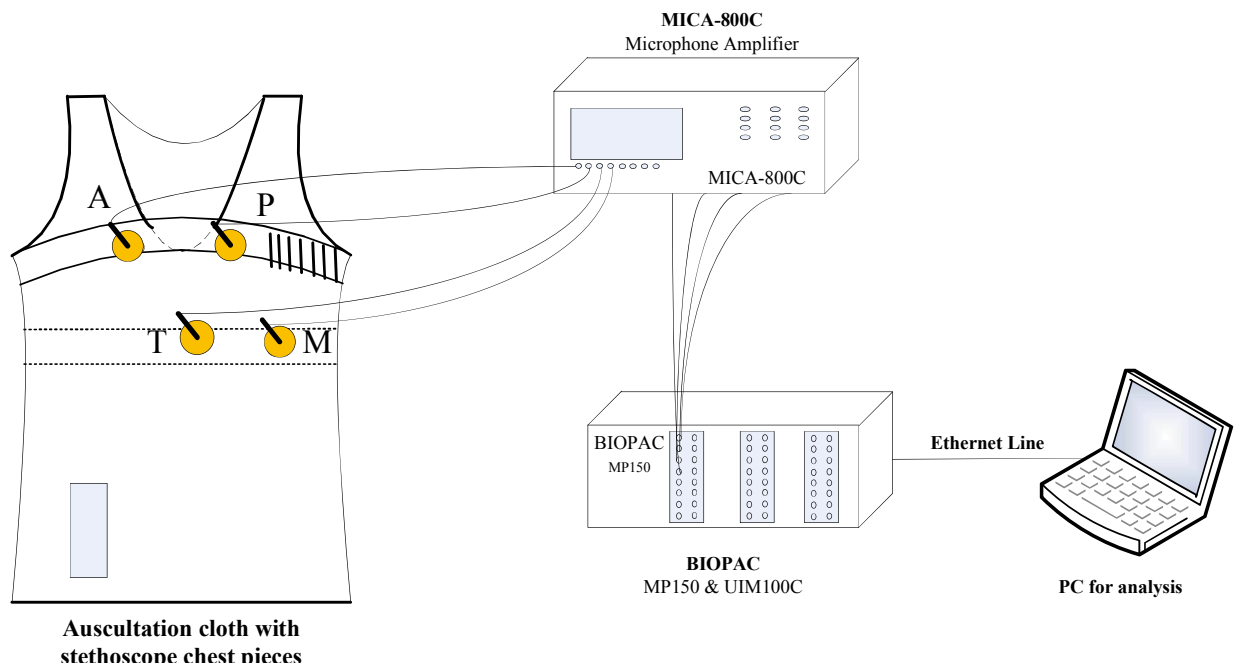


Fig. 7. Measuring system with BIOPAC.

This system offers Ethernet-ready data acquisition and analysis, and also can recorder multiple channels with different sample rates; it records at speeds up to 400 kHz (aggregate). HS recorded by the auscultation cloth with chest-pieces which are transferred to microphone amplifier, and then these signals are sent to BIOPAC MP150 data acquisition system, and sent to PC. These multichannel

signals can be displayed in PC, shown in Fig. 8(a)~(b). In this multichannel measuring system, the microphone amplifier is MICA-800C. And the clinical multichannel HS measuring is showed in Fig. 9.

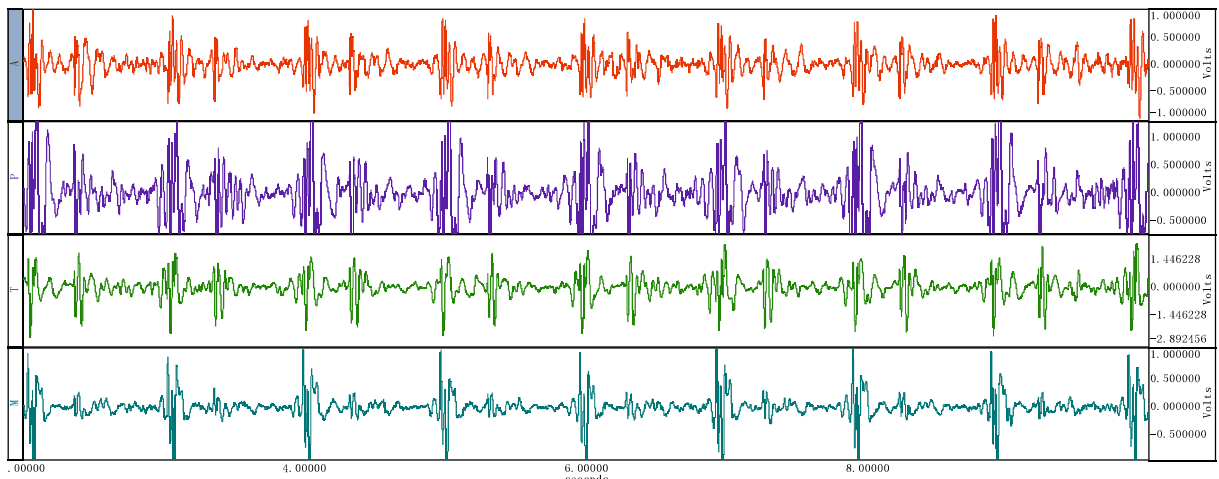


Fig.8 (a). HS real-time display graph of BIOPAC acquisition system (NHS).

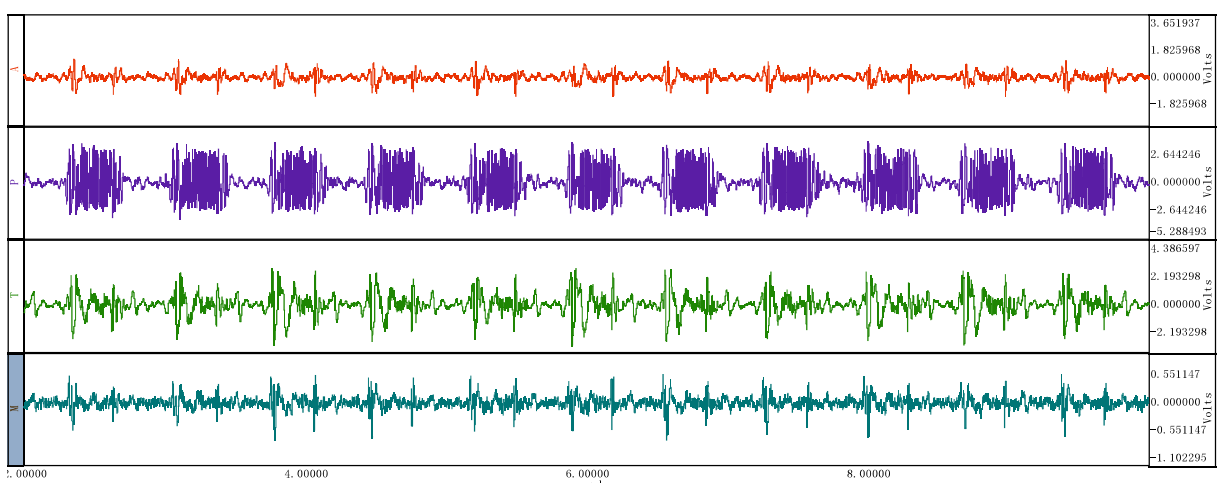


Fig.8 (b). HS real-time display graph of BIOPAC acquisition system (VSD).



Fig. 9. Measuring system with BIOPAC for clinical HS recording.

However, as shown in Fig.9, the BIOPAC multichannel measuring system is too heavy to take to different places, furthermore, it is very expensive for healthcare at hospital and at home. Therefore, the other multichannel physiological signal recorder which is composed with two IC recorders fixed with a light plastic case, shown in Fig. 10(a)~(c). the specification of IC recorders and microphones are the same with single channel system, which are given in table 1~2. This physiological signal recorder is much more simple operation, portable. The linical measuring system is showed in Fig.11-12.

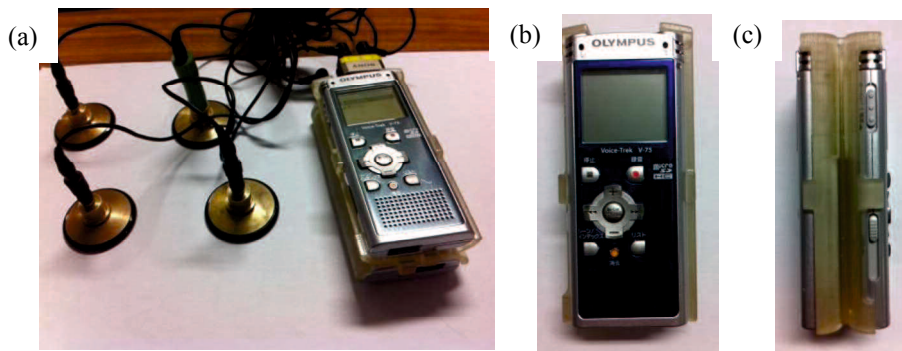


Fig. 10. Measuring system with IC recorders fixed by plastic case for clinical HS recording,
(a) Measuring system with IC recorders (b)~(c) IC recorders fixed by plastic case(front~side).

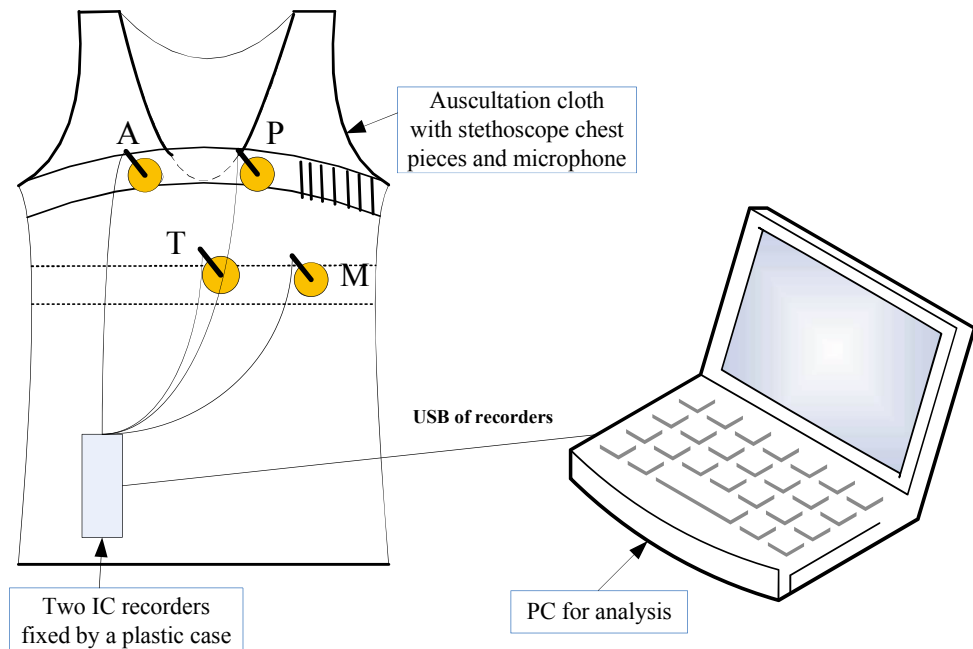


Fig. 11. Measuring system with IC recorders.

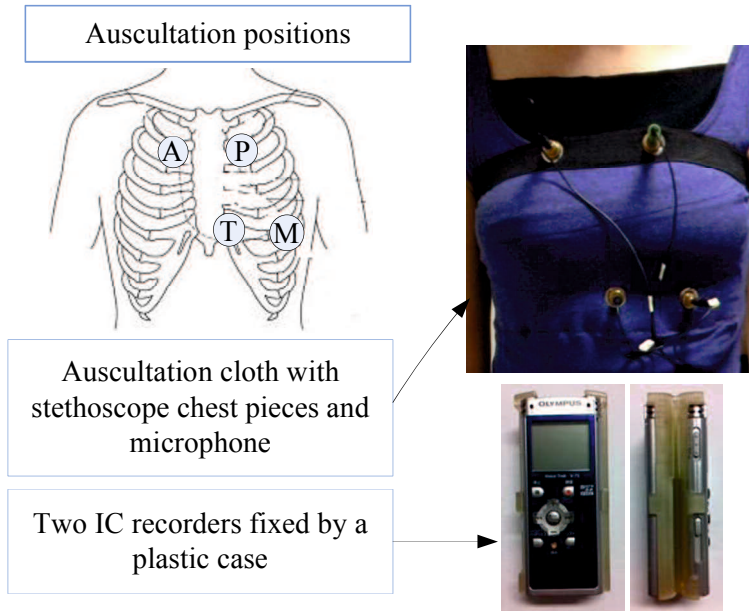


Fig. 12. Multichannel signals measuring system.

The clinical HSs, which collected by IC recorders multichannel signals measuring system, were showed in Fig.13~16. The NHS multichannel signals from A, P, T and M, which is showed in Fig. 13, show the basic HSs clearly, the CHD multichannel signals in Fig.14~16, show the strong murmurs at P positions, which are systolic murmurs,

In clinical, the doctor may hear HSs or murmurs from some different sites in front of the chest or from the back with a stethoscope. Because the defects can be located in different places on the atrial, ventricular or valves. So if we can obtain the multichannel signals synchronously, much more pathology and corresponding positions information can be collected and maybe great significance in clinical diagnosis and in-home heart healthcare. There are the four channels clinical HSs of NHS, ASD, VSD and TOF from clinic showed in Fig. 14~16, respectively. These clinical HSs show that this multichannel measuring system is effective for clinical acquisition.

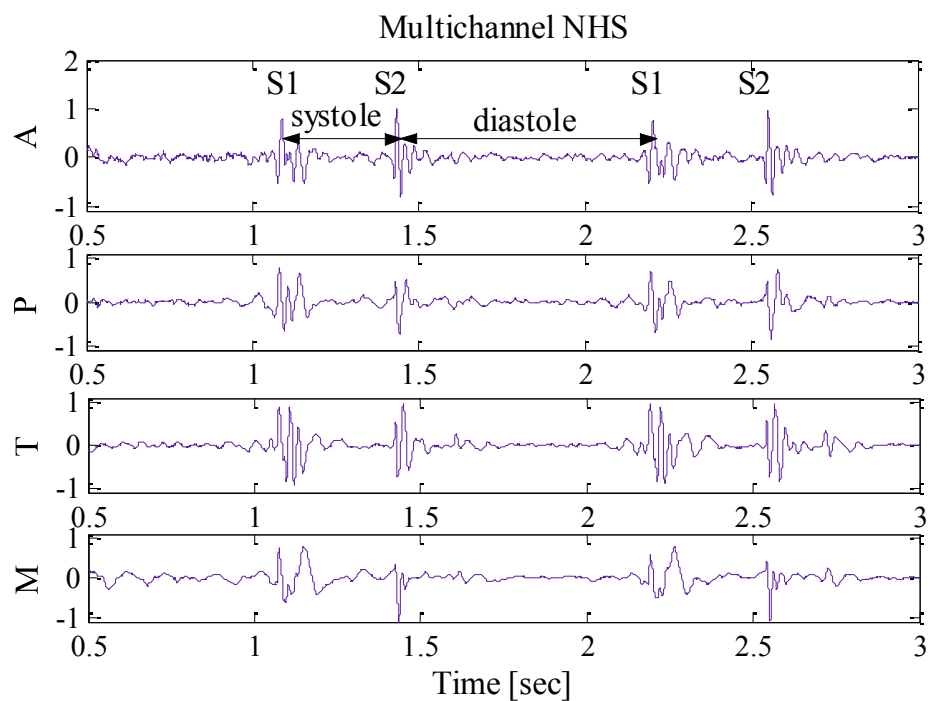


Fig. 13. Multichannel NHS.

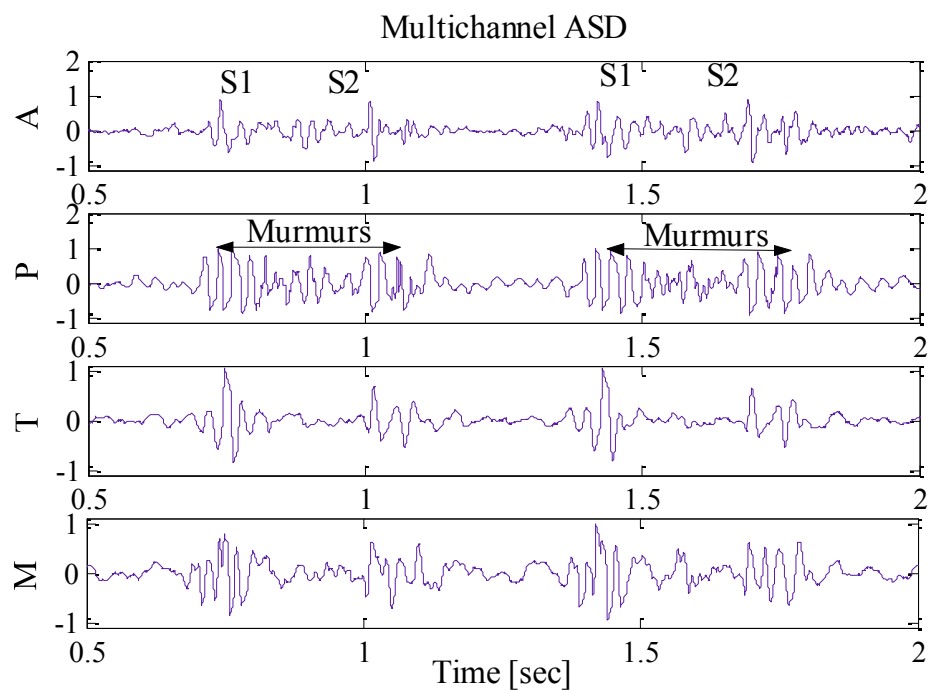


Fig. 14. Multichannel ASD signals.

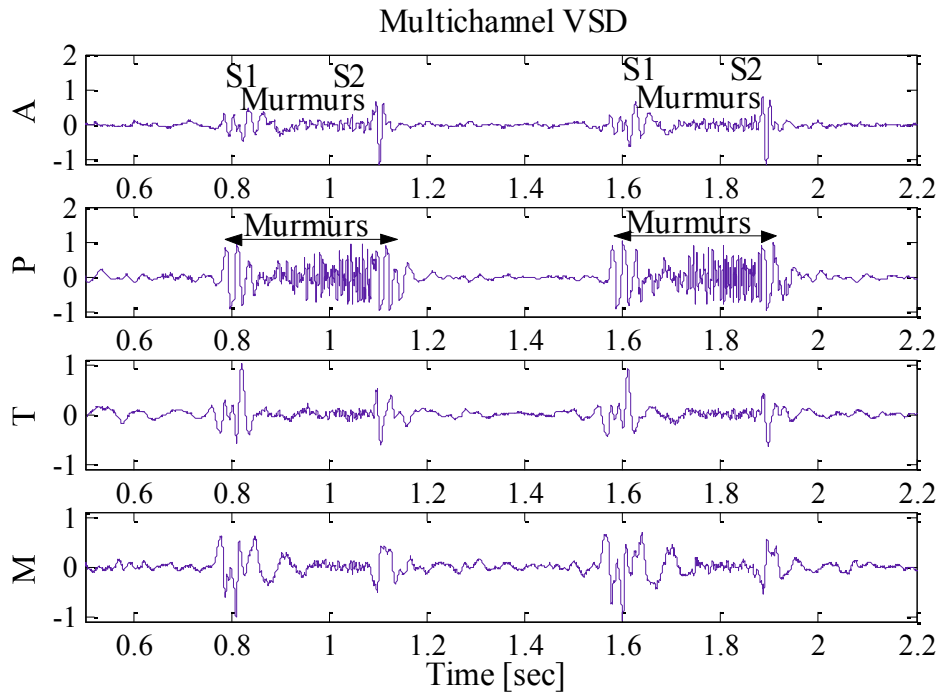


Fig. 15. Multichannel VSD signals.

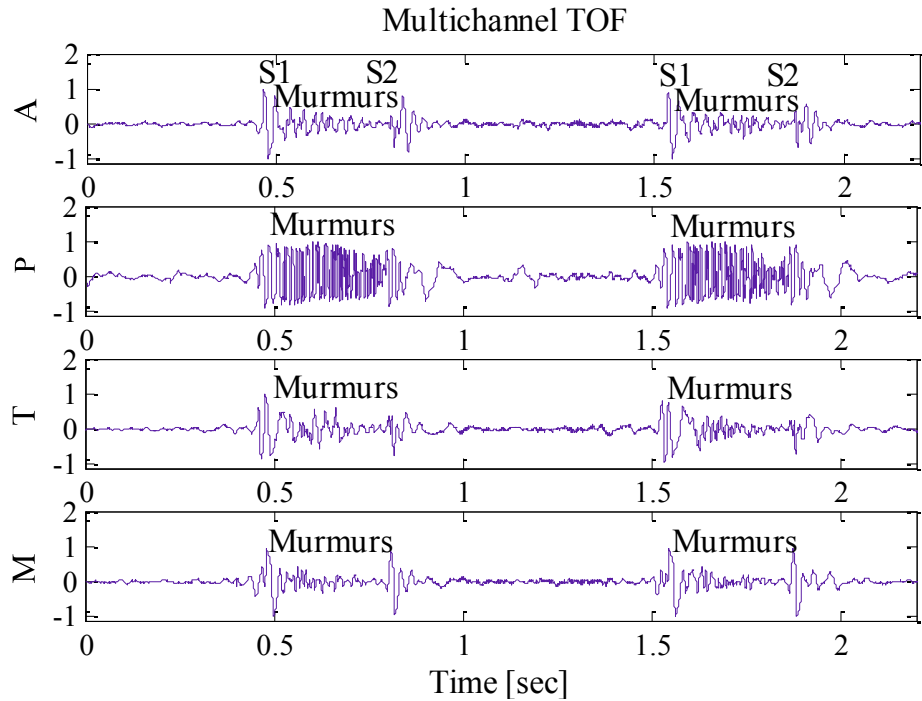


Fig. 16. Multichannel TOF signals.

HS signals contain much more important physiological and pathological information, especially, the signals from different positions reflect different turbulence conditions created when the heart valves snap shut. Furthermore, for clinical HS long-term monitoring and comprehensive analysis, it

is necessary to develop a much more convenient and effective measuring system.

From these original clinical HSs, we can see the CHD (ASD, VSD and TOF) sounds contain much more information about systolic murmurs, splitting sounds, and so on, which can be seen in Fig. 14~16. And as for different diseases, the signals from these four channels are different, for example, for NHS, the foundational S1 and S2 can be recognized clearly of the cycle. For ASD, we can find there are heart murmurs in the signals of A and P areas, and there maybe S2 splitting sounds. For VSD, the holosystolic crescendo murmur from P area can be seen clearly. And for TOF, the holosystolic murmur from P area can be seen clearly, because of its complexity, there also some decrescendo murmurs from A, T and M areas.

3. Clinical HS data statistics

Clinical HS from patients who suffer cardiac diseases are mixed with many kinds of heart murmurs and noises from various sources contaminate HS signals. Therefore, the clinical HS complexity is much more than the pure HS from standard HS database. In recent, the standard HS databases, such as 3M Littman database, which are aimed at single disease, and the quantity is small, this situation can not meet the needs of the clinical HS research with diversity and complexity. Furthermore, abundance and diversity clinical HS data provide rich data resource for clinical analysis, and lay a foundation for comparison, optimization and verity of software algorithm.

In view of these current situations, from the year 2007 to 2014, we have collected lots of clinical HSs from college students and patients who have signed informed consents. There are 101 cases NHSs from college students who have no heart disease history, and there are 206 cases abnormal heart sounds (AHS) from Chengdu Military General Hospital of People's Liberation Army, Cardiothoracic Surgery, in AHS, there are 87 cases which are common CHDs (ASD, VSD and TOF). This system is used for the multichannel visual auscultation from A, P, T and M positions, for obtaining high-quality clinical HS, it provides reliable data source for further clinical HS analysis.

4. Summary

This chapter introduced the development of two electric stethoscope devices for easy operation

in home health care. Firstly, the existing single channel acquisition system consists of an IC recorder, a microphone, a traditional chest piece, an earphone and a computer for analysis and display was introduced. However, in order to collect the multichannel signals at the same time, we also design the auscultation clothing. And the multichannel acquisition system which is composed of computer, audio amplifier, and multichannel physiological signal recorder and auscultation cloth with four stethoscopes was introduced. While there are two kinds of multichannel physiological signal recorders, one is BIOPAC MP150 signal recorder and the other is two IC recorders fixed with a plastic case, considering the simplicity and convenience, the multichannel physiological signal recorders which consist of two IC recorders fixed with a plastic case is recommended to use. Finally, the clinical HS data statistics is implemented. These HS data are used in the next chapters, and provide very valuable resource for our next research.

References

- [1] Zhongwei Jiang*, Samjin Chio, A cardiac sound characteristic waveform method for in-home heart disorder monitoring with electric stethoscope. *Expert System with Application* 31(2006) 286-298.
- [2] Ting Tao, Zhongwei Jiang, Haibin Wang, Shuping Sun, Yu Fang. Analysis of Congenital Heart Sound Based on Envelope Waveform in Time-domain. ICIARE2013, P: 82-85.
- [3] Shuping SUN, Haibin WANG, Zhongwei JIANG, Yu FANG, Ting TAO. Segmentation-based heart sound feature extraction combined with classifier models for a VSD diagnosis system[J], *Expert Systems with Applications*, Vol 41, Issue 4, Part 2, March 2014, pp 1769-1780.
- [4] Lihan Liu, Haibin Wang, Yan Wang, Ting Tao, Jinbao Zhang. Feature Analysis of Heart Sound Based on the Improved Hilbert-Huang Transform. IEEE International Conference on Computer Science and Information Technology (ICCSIT), Vol.6, P:378-381.
- [5] Ting Tao, Haibin Wang, Yu Fang, Jinqun Liu, Xiaochen Wu. A Method based on Wavelet Packet Decomposition and Memory Antibody Clone Hybrid Clustering for Diagnosis of Clinical Heart Disorders. IEEE International Conference on Computer Science and Information Technology (ICCSIT), Vol.9, P: 70-74.
- [6] Ting Tao, Haibin Wang, Xiaochen Wu, Zhongwei Jiang, Shuping Sun. Study on cardiac murmurs evaluation based on wavelet packet energy distribution. The 3rd International

Symposium on Digital Manufacturing , P: 159-164.

- [7] Jinqun Liu, Haibin Wang, Wuchang Liu, Ting Tao, Jinbao Zhang. A novel envelope extraction method for multichannel heart sounds signal detection, Proceedings of 2011 4th IEEE International Conference on Computer Science and Information Technology, Vol.10, Pages 140-145.
- [8] Yu Fang, Zhongwei Jiang, Haibin Wang, Shuping Sun, Ting Tao. Diagnosis of Ventricular Septal Defect Based on Mel Frequency Cepstrum Analysis. International Conference on Innovative Application Research and Education (ICIARE), P: 78-81.
- [9] Zhongwei Jiang¹, Ting Tao¹, Haibin Wang². New Approach on Analysis of Pathologic Cardiac Murmurs Based on WPD Energy Distribution[J], *Journal of Healthcare Engineering*, Vol 5, No.4, 2014, pp375-392.
- [10]Ting Tao¹, Zhongwei Jiang¹, Yu Fang¹, Haibin Wang². Multichannel Cardiac Sounds In-home Measuring System for Monitoring Children's Congenital Heart Disease, Evaluation of a Magnetic-Geared Induction Motor (MAGDA) , 2014, pp.343-348

Chapter 3

Multichannel Cardiac Murmurs Analysis Method and Murmurs Indexes

CHDs are problems with the heart's structure or function that is formed before birth [1], with a rate of eight out of every 1,000 newborns. It is known that this kind of defects can be cured with a high probability if the diseases could be detected in an early stage. Therefore, the research on the early detection of CHDs is one of the most important medical research areas [2]. There are many types of CHDs. Some are simple and some are more complex. ASD is one of the CHDs, a hole in the part of the septum that separates the atria. The hole makes oxygen-rich blood from the left atrium to flow into the right atrium, instead of flowing into the left ventricle as it should. ASDs can be small, medium, or large. Medium and large ASDs allow more blood to leak from one atrium to the other. VSD is another type of CHD, with a hole in the part of the septum that separates the ventricles. Small VSDs do not cause problems and may close on their own. However, large VSDs allow much blood to flow from the left ventricle to the right ventricle. As a result, the left side of the heart must work harder than normal and extra blood flow increases blood pressure in the right side of the heart and the lungs. Furthermore, the most common complex heart defect is TOF, which is a combination of four defects: Pulmonary valve stenosis, a large VSD, an overriding aorta and right ventricular hypertrophy. ASD, VSD and TOF account for the majority of the CHD [3].

Heart murmurs are pathological sounds produced by turbulent blood flow due to certain cardiac defects, and they are the most common reasons for referral to the pediatric cardiologist. In children,

about 50-70% of these murmurs are clinically insignificant [4], but if the child is crying, uncooperative to the examiner or breathing loudly, some other murmurs may occur. Because of the difficulty of mastering auscultation skills, innocent and organic heart murmurs cannot be readily distinguished. Therefore, the study of computer-aided cardiac murmurs analysis is very important for CHD diagnosis. Furthermore, without professional medical knowledge and skills, HS auscultation of HS is difficult. Therefore, HS and murmurs analysis with computer-aid become more and more important. And murmurs intensity, frequency character, the murmurs occurrence periods and murmurs time duration are the important points for clinical HS auscultation, so how to make these murmurs characters not only for doctors but also be used for general user are the aim of murmurs analysis. While, as we summarized from previous research, most of the research focus on HS or murmurs feature extraction and diseases classification by qualitative analysis, the quantitative analysis of clinical multichannel cardiac murmurs has not been pay attention to, therefore, in this thesis, in order to evaluate the clinical CHD murmurs quantitatively, the murmur index extraction methods based on murmur energy and heart vibration state are implemented in Chapter 3.

In this chapter, the murmur methods of multichannel heart murmur analysis are introduced. Firstly, the pre-processing is introduced in section 1. And then index extraction based on murmur energy analysis by wavelet packet decomposition (WPD) technique is proposed in section 2. Furthermore, in section3, the murmur index extraction based on cardiac vibration states is proposed. At last, the summary of this chapter is presented.

1. Pre-processing

In this chapter, the original HS signal $x(t)$ recorded by measuring system with 16-bit accuracy and 20kHz or 40kHz sampling frequency. Firstly, the recorded signal was converted into 20 kHz. Next, Daubechies10 (DB10) wavelet was used as a mother wavelet for the wavelet decomposition. In order to evaluate the murmur at different frequency ranges, the resulting signals with band limit of 5-1250 Hz were reconstructed by the components from d11 to d4. At last, the normalization was applied by setting the variance of the signal within a value of 1.0, and the resultant signals can be expressed as $s(t)$.

2. Murmurs indexes extraction based on energy analysis

Heart murmurs are pathological sounds produced by turbulent blood flow due to cardiac defects. In order to quantitatively analyze cardiac murmurs, the murmurs index extraction methods based on murmurs energy analysis was proposed [5-7]. Firstly, In order to extract the murmurs indexes for analyzing the entire cardiac murmurs at different frequency bands, the approach on analysis of the pathologic cardiac murmurs based on the wavelet packet decomposition technique were described. The HS signals were divided into five bands and the energy ratios at each frequency band were calculated and compared. Based on the analysis of clinic HSs data, three evaluation ICM were proposed for the analysis of the pathologic murmurs. Finally, the threshold values between the innocent and pathologic murmurs were determined based on the statistical results of the normal HSs. The statistic results showed that ICM of multichannel signals not only evaluated the murmurs quantitatively, but also revealed the murmurs generating reason by analyzing signals from four positions simultaneously.

The cardiac murmurs for different heart defects usually contain different frequency components. If the sound signal can be decomposed in different requested frequency ranges in a suitable way, the corresponding energy intensities can be evaluated quantitatively. In this study, the cardiac signal is decomposed and reconstructed at each requested frequency band by the WPD technique and their murmurs energy intensities are calculated and used for the cardiac murmurs evaluation. a block diagram of the study on cardiac murmurs evaluation based on the wavelet packet (WP) technique for assessing the murmurs distribution and levels is depicted in Fig.1.

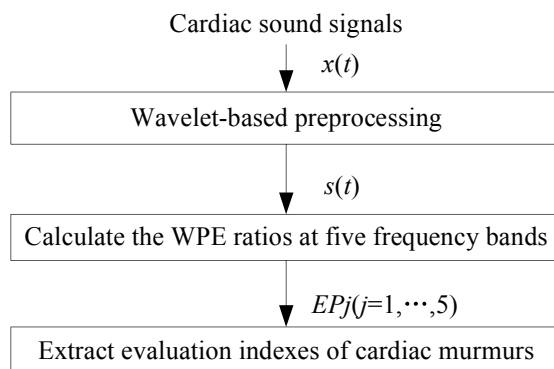


Fig. 1. A block diagram of the study on cardiac murmurs evaluation based on the WP technique

2.1 Frequency band definition

By considering the frequency ranges of the innocent and pathologic murmurs in the frequency domain, in this study, the wavelet packet decomposition at level 11 is employed to split frequency bandwidths of HS signals. Through clinical auscultation observation and energy intensities analysis at each level ($d_{11}\sim d_4$), the interested parts and useful combinations are implemented, and five frequency bands are defined and shown in Table 1, they are named as very low frequency (VLF), standard frequency (SF), low frequency (LF), middle frequency (MF) and high frequency (HF). Their corresponding wavelet detail coefficient levels, center frequencies and energy ratios are represented in Table 1.

Table 1. Murmurs frequency bands definition.

Frequency band number (j)	1	2	3	4	5
Frequency band	VLF	SF	LF	MF	HF
Wavelet detail coefficients	$d_{11}+d_{10}$	d_9+d_8	d_7	d_6	d_5+d_4
Frequency band corresponded to sampling frequency (Hz)	4.88-19.53	19.53-78.1	78.1-156.25	156.25-312.5	312.5-1250

2.2 Murmurs index evaluation based on wavelet packet energy

The wavelet packet analysis is an extension of the DWT and is one of the most efficient decomposition that could be performed on the signal. Daubechies type wavelet (DB10) is used to build a wavelet filter [6]. Further the reconstructed signals at each decomposition level are applied by FFT. Fig.1 shows the plots of some typical HSs treated by WP analysis method. Fig.2(a)-(d) are the examples of NHS, ASD, VSD and TOF signals obtained by reconstruction of the components at VLF, SF, LF, MF and HF band as defined in Table 1. A simple sum of all the VLF, SF, LF, MF and HF components represent the original HS signal.

The NHS signal plots at each frequency band show the 1st and 2nd sounds clearly and the energy is mainly distributed at the SF band. As for ASD, the signal plots show that the murmurs appeared mainly at LF and MF bands. As for VSD and TOF, the murmurs have stronger energy distributions at

MF and HF frequency bands.

Fig.2 (a)-(d) show that the energy of all types of HS signals is mainly concentrated at SF band. Further, compared to NHS, CHD signals have higher energy intensities at the higher frequency bands. To quantify the cardiac murmurs, WP energy ratio $EP(j)$ is proposed and defined as the following:

$$EP(j) = \sum_i^N |s(i)|^2 / \sum_{j=1}^5 (\sum_i^N |s(i)|^2) \quad (1)$$

$s(i)$ is the reconstructed signal at the corresponding frequency band j , N is the signal length and $j = 1, 2, 3, 4, 5$ are corresponding to frequency bands VLF, SF, LF, MF and HF respectively.

The energy distributions for these four conditions (NHS, ASD, VSD and TOF) are calculated at each frequency band defined in Table 1. The energy distribution histograms at SF, LF, MF and HF frequency bands are plotted in Fig.3 to Fig.7, the observed are from the pulmonary area (P) position. The y-axis shows the number of samples or frequency of the observations in the interval and the x-axis is the energy ratio $EP(j)$ in percentage. There are about 40% to 90% energy distributed at SF frequency band, 5% to 20% at LF band, 1% to 15% at MF and 0.1% to 3% at HF band.

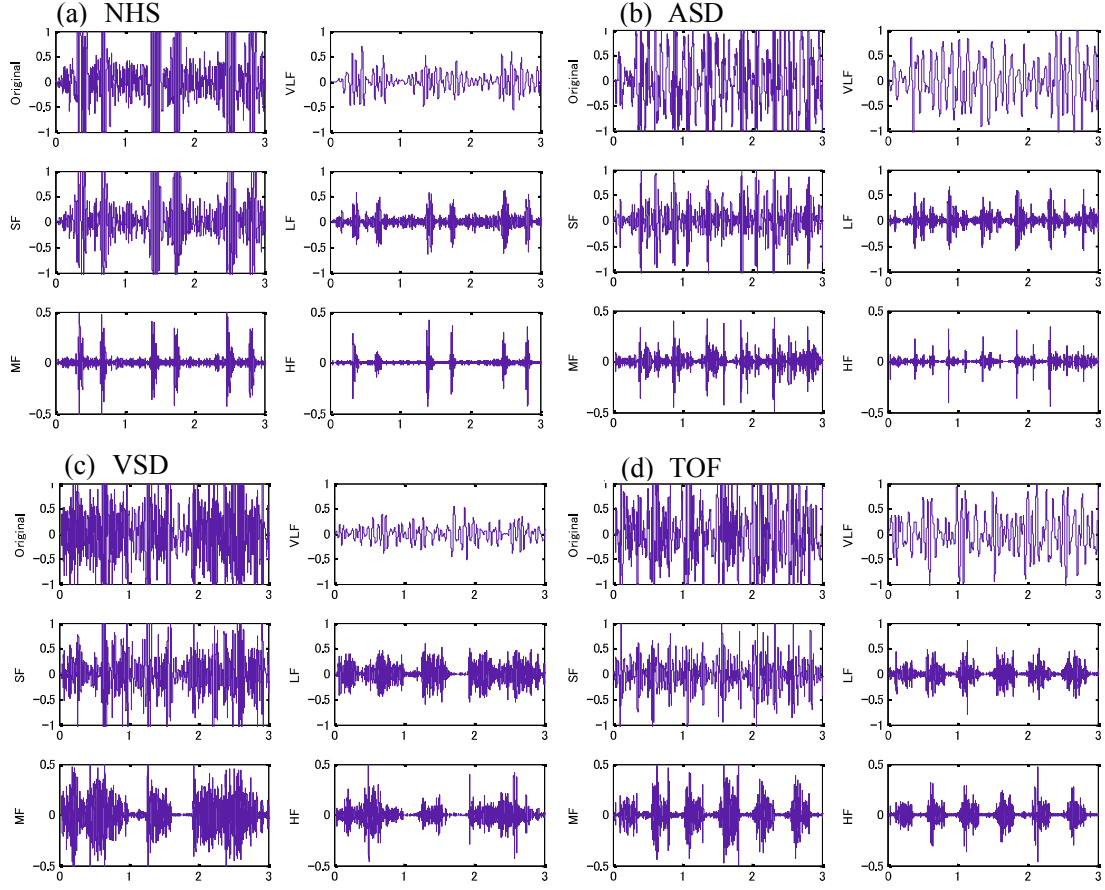


Fig.2. HS signal examples of NHS, ASD, VSD, TOF and their reconstructed signals at different corresponding frequency band, Original, VLF, SF, LF, MF and HF.

The averages and the standard deviations for these four conditions are summarized in Table 2. Statistical analysis was performed to show whether there is a significant difference in means among these four conditions (NHS, ASD, VSD and TOF) using the one-way ANOVA *F*-test. The very low *P*-values (<0.0001) were taken as statistically significant. It is obvious that the distributions of NHS are following the normal probability distribution. The energy distributions of ASD are similar to NHS. Furthermore, the energy distributions of other CHDs are spread over a wide range and the energies maintain higher values at MF and HF bands compared to those in NHS.

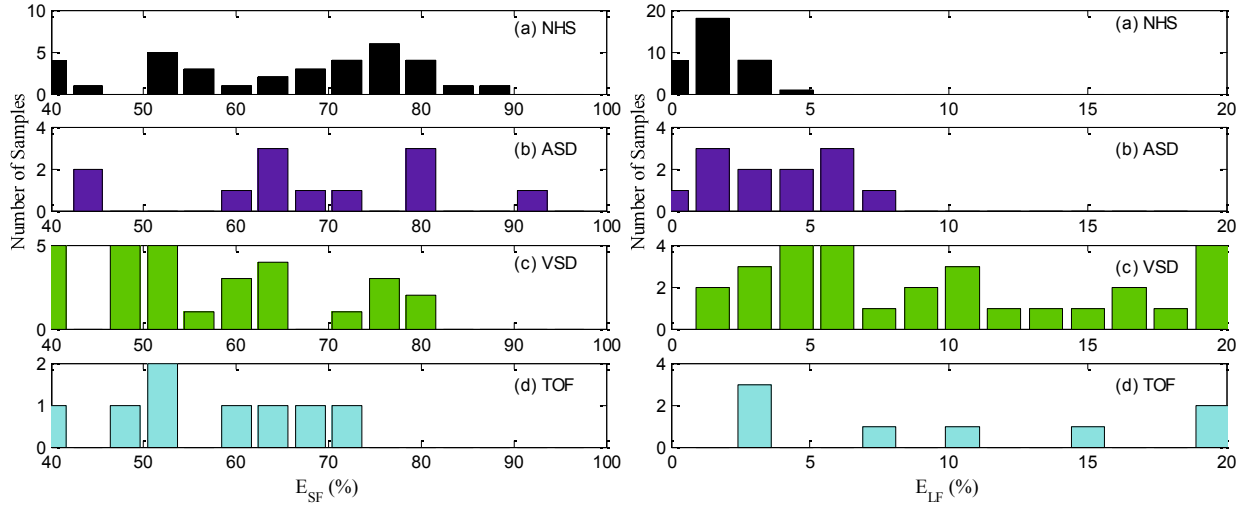


Fig. 3. Energy distribution at SF frequency.

Fig. 4. Energy distribution at LF frequency.

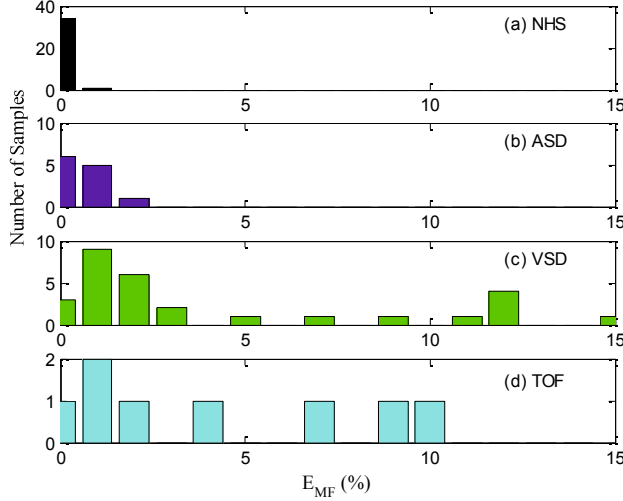


Fig. 5. Energy distribution at MF frequency.

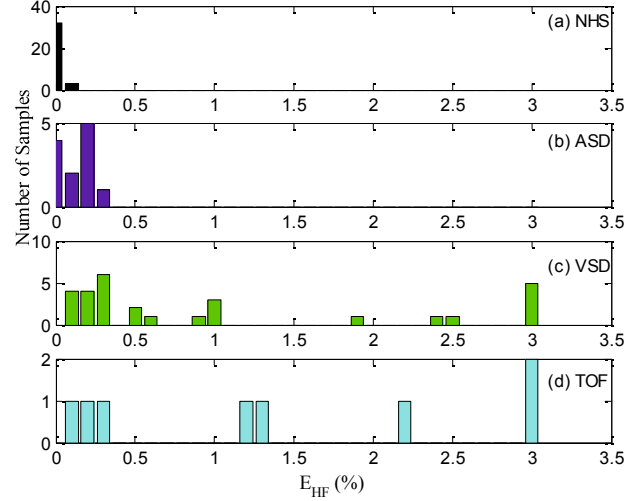


Fig. 6. Energy distribution at HF frequency.

Table 2 shows over 50% of energy in average concentrated at SF band for all conditions. This shows that the main component of HS is in the SF band. Further, Fig.3 and Table 2 indicate that the pathologic murmurs feature high energy distributions at LF, MF and HF.

Table 2. Means and variances of the energy ratios at four frequency bands.

Group ($E_{mean} \pm E_{std}$)	NHS	ASD	VSD	TOF
$E_{VLF}(\%)$	34.67 ± 17.3	27.5 ± 16.3	29.96 ± 17.9	28.38 ± 22.5
$E_{SF}(\%)$	63.58 ± 17.1	67.75 ± 15.0	55.55 ± 14.8	54.65 ± 16.9
$E_{LF}(\%)$	1.60 ± 1.0	3.90 ± 2.1	9.57 ± 6.4	10.82 ± 8.0

$E_{MF}(\%)$	0.14 ± 0.1	0.73 ± 0.6	3.57 ± 3.9	4.16 ± 3.8
$E_{HF}(\%)$	0.02 ± 0.02	0.12 ± 0.1	1.36 ± 2.5	1.99 ± 2.4

On the other hand, the energy distribution at VLF band is considered to be a vibration or systaltic movement in the body due to the heartbeat. The energy distribution histograms at VLF band are shown in Fig.7. It was found that the HSs recorded from the infant usually contain high energy components at VLF band. Because the infant has little fat, the pulsation of the heart easily leads to a movement of the whole chest region. This movement, especially due to the abnormal heart pulsation is captured by another stethoscope which shows the high energy component at VLF band. Since there are still many uncertainties for this VLF band, this study has mainly concentrated on the four bands, SF, LF, MF and HF.

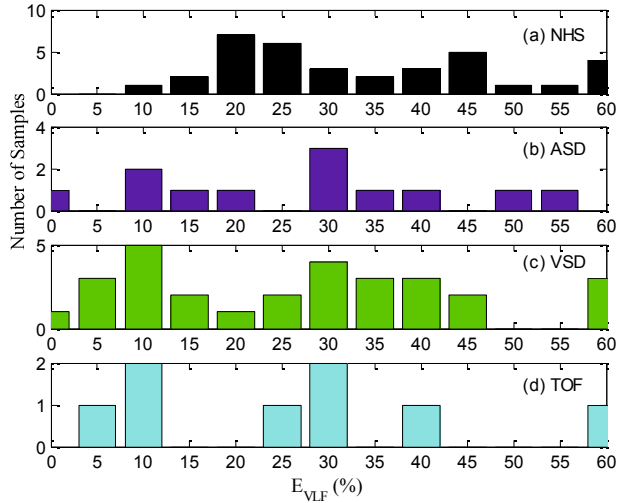


Fig. 7. Energy distribution at VLF.

2.3 Result and discussion for one channel signal

As discussed above, the main energy of HS is concentrated at SF band and the pathologic murmurs represent the high energy density at LF, MF and HF bands. Based on this fact and our investigation, the evaluation ICM are proposed and defined as the following:

$$ICM_L = \frac{E_L(\%)}{E_{SF}(\%)} \times 100\%, \quad \text{where } L = \{LF, MF, HF\} \quad (2)$$

Fig.8 shows the plots of ICM_{LF} for NHS and CHDs. The average and standard deviation of ICM_{LF} for NHS are obtained as 2.66 ± 1.95 . The threshold for cardiac murmurs (TCM) at LF band is defined by $TCM_{LF} = 2.66 + 1.95 = 4.61$, depicted as a broken line in the figure. It means that it could be diagnosed to be the pathologic murmurs if the obtained energy level is higher than this threshold TCM_{LF} . From Fig.8, it is found that four of the 12 ASD samples are below the threshold TCM_{LF} , indicating four subjects in false diagnosis. On the other hand, only two of the 27 VSD and one of the 8 TOF samples are below the threshold.

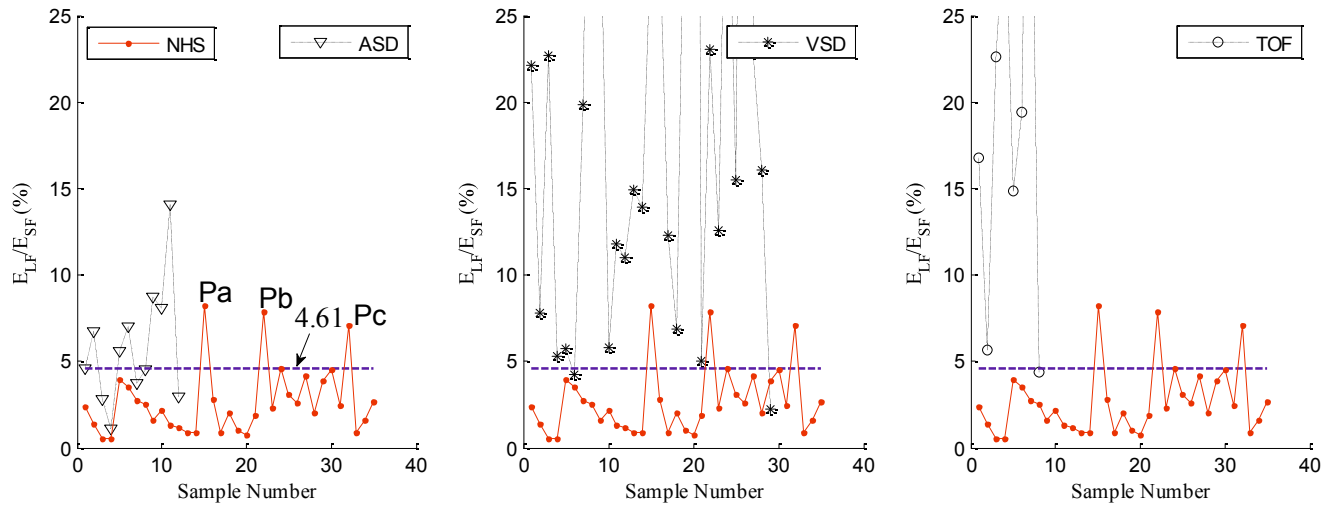


Fig. 8. Distributions of the indexes of cardiac murmurs at LF band (ICM_{LF}).

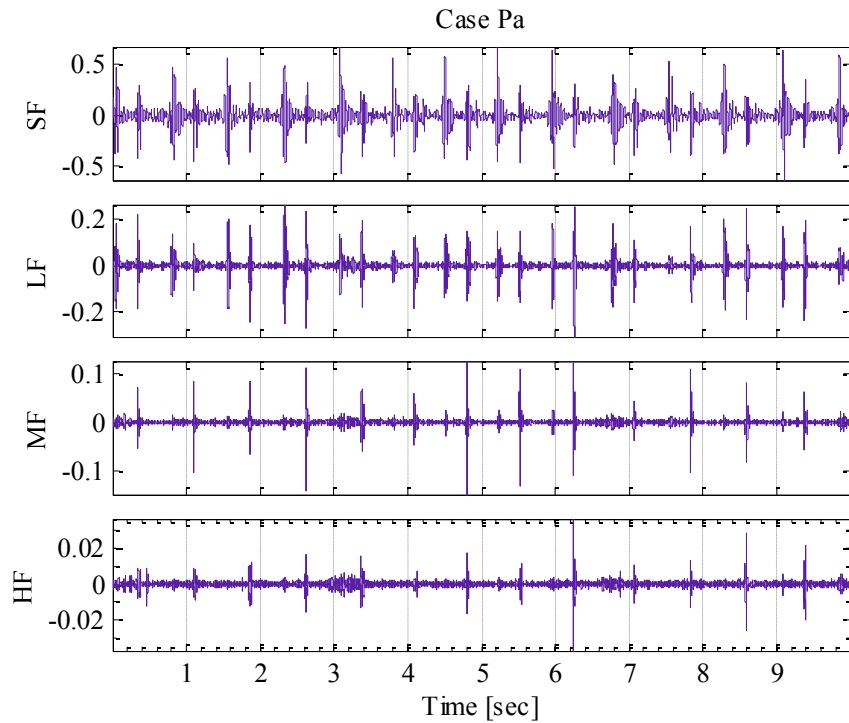


Fig. 9. Example of pulmonary sound due to a normal breath, indicated by case Pa in Fig. 8.

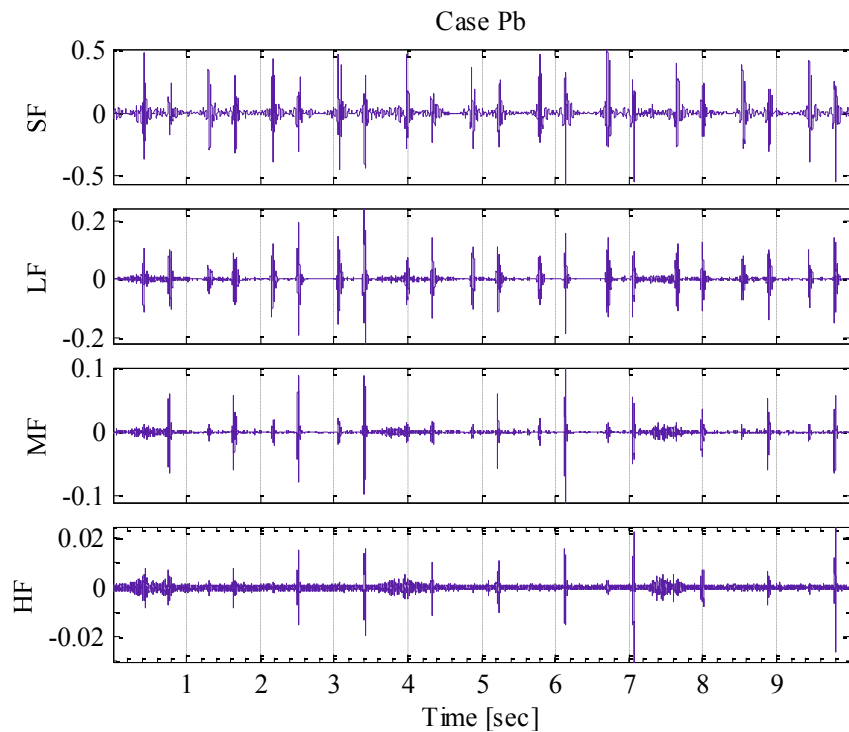


Fig. 10. Example of pulmonary sound due to a normal breath, indicated by case Pb in Fig. 8.

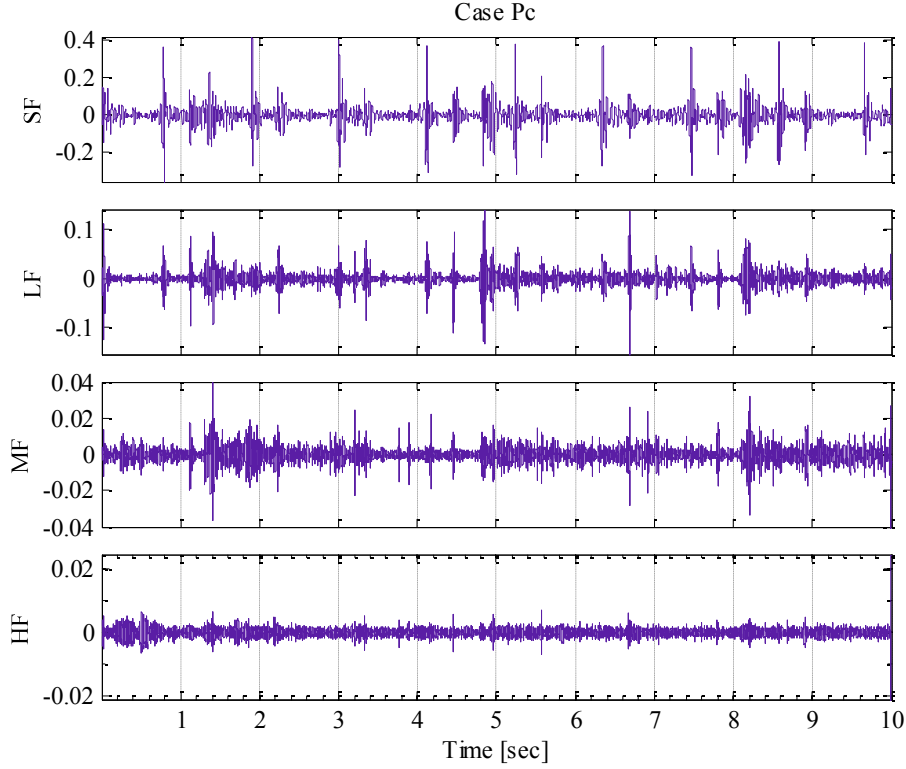


Fig. 11. Example of pulmonary sound due to a normal breath, indicated by case Pc in Fig. 8.

Points Pa~Pc in Fig.8 has the high values of ICM_{LF} in NHS at LF band, which are beyond the threshold of TCM_{LF} . These HS signals are further analysed and the results are plotted in Fig.9~11. It is confirmed that the strong energy component at LF band is the basic heart sounds (such as S1, S2). The breath component can also be found at LF band, such as case Pb, which is also have strong intensity at MF showed in Fig.12. General auscultation of HS, usually includes respiratory sound, and the pulmonary sound components are mainly distributed at LF and MF bands.

Regarding the MF band, Fig.12 shows the plots of ICM_{MF} for NHS and CHDs. The average and standard deviation of NHS's ICM_{MF} is 0.24 ± 0.19 and the threshold of the cardiac murmurs at MF band is set as $TCM_{MF} = 0.43$. It is found that there are 3 ASD, 1 VSD and no TOF samples below the level of TCM_{MF} . However, the misdiagnosed number for TOF has been improved with the comparison of the results obtained at LF band.

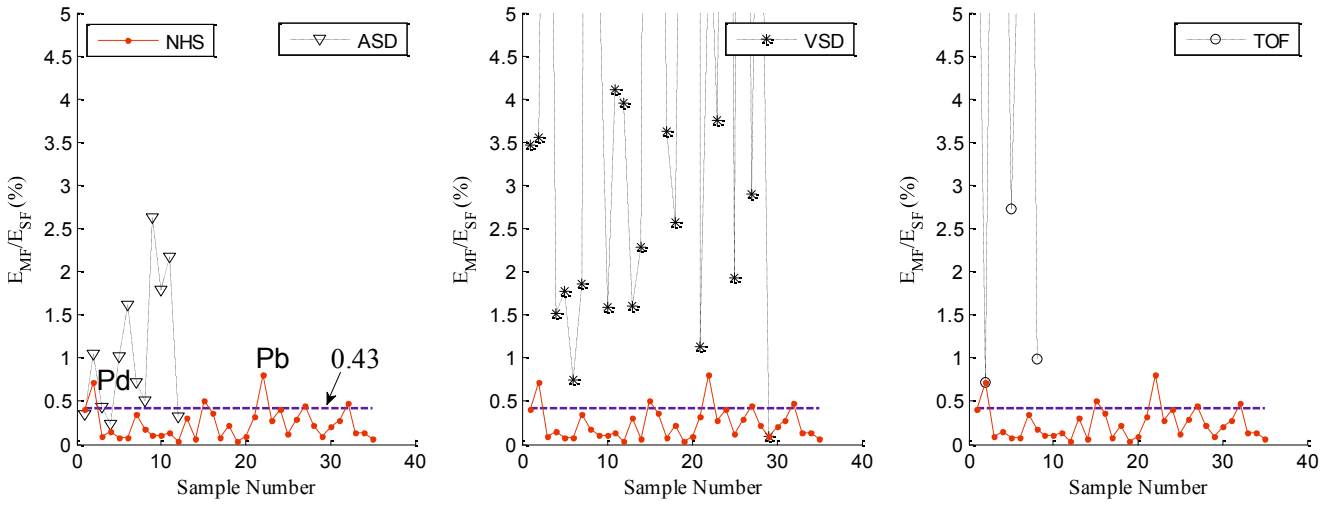


Fig. 12. Distributions of the indexes of cardiac murmurs at MF band (ICM_{MF}).

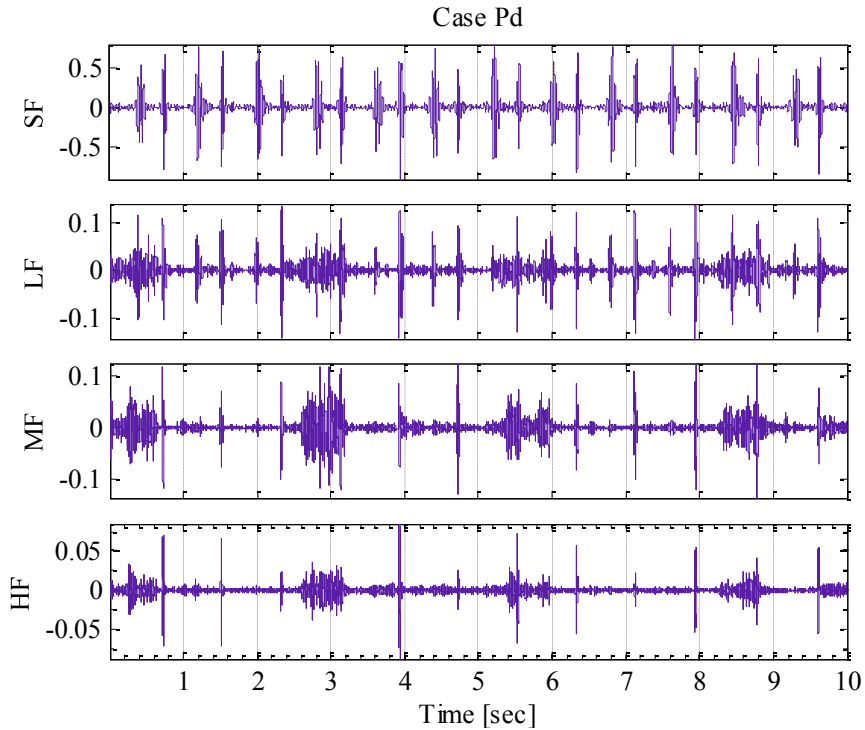


Fig. 13. Example of pulmonary sound due to a normal breath, indicated by Pd in Fig. 12.

Points Pd and Pb in Fig.12 has the high values of ICM_{MF} in NHS. Its time waveforms reconstructed at four expected frequency bands are plotted in Fig13 and Fig.10. It is clear that the breath sounds represent the strong components in LF, MF and HF bands.

The plots of ICM_{HF} are shown in Fig.14. The average and standard deviation of ICM_{HF} for NHS is 0.38 ± 0.16 and the corresponding threhold of the cardiac murmurs is given as $TCM_{HF}=0.06$. The numbers of CHD samples below the threhold TCM_{HF} are two in ASD, none in VSD and none in TOF

samples shown in Fig.14. The misdiagnosed cases are reduced significantly. This indicates that the cardiac murmurs evaluation index at HF band ICM_{HF} can be an evaluable index for quantitative diagnosis of HS murmurs. It is also evident that the diagnosis accuracy could be improved if the HS is recorded by a momentary stop of the breath, and in a quiet environment.

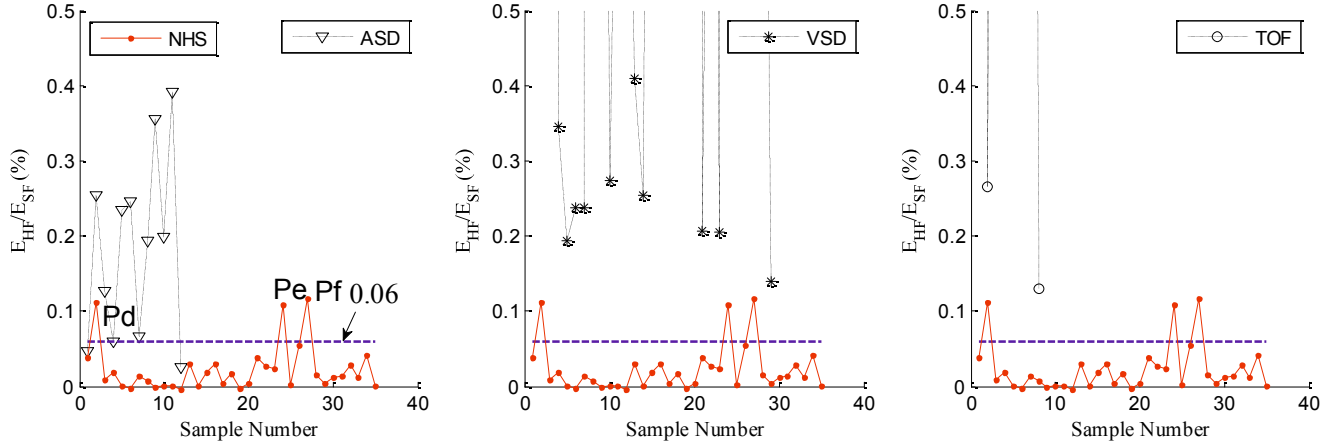


Fig. 14. Distributions of the indexes of cardiac murmurs at HF band (ICM_{HF}).

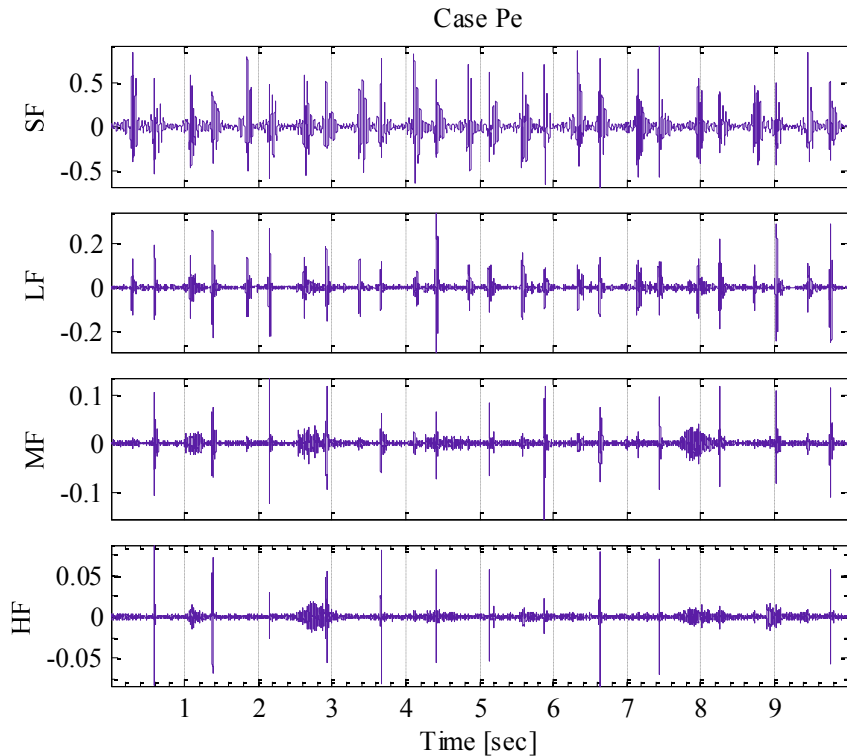


Fig. 15. Example of pulmonary sound due to a normal breath, indicated by Pe in Fig. 14.

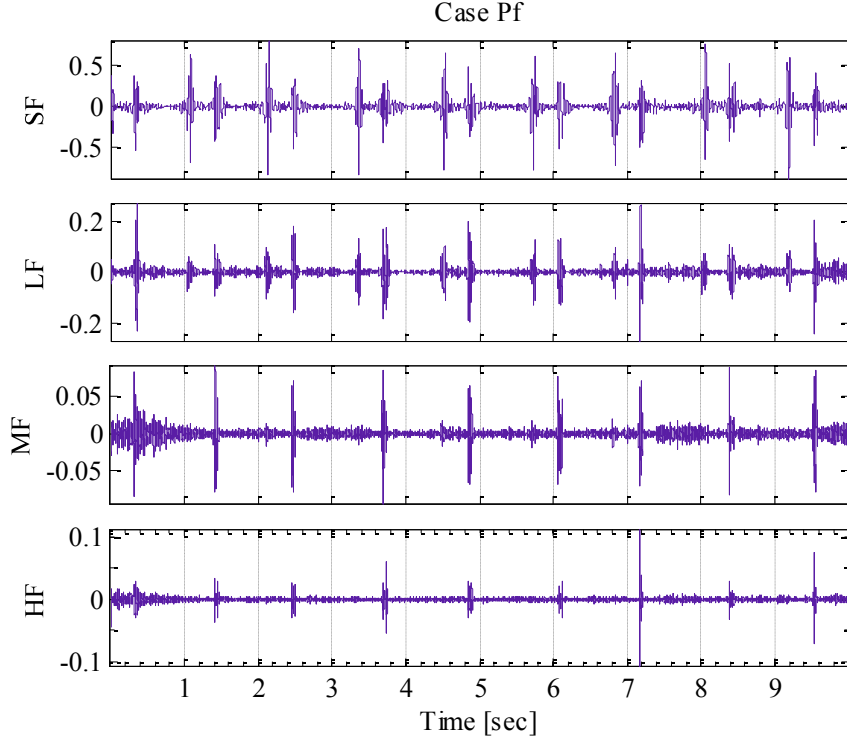


Fig. 16. Example of pulmonary sound due to a normal breath, indicated by Pf in Fig. 14.

Points Pd~Pf in Fig.14 has the high values of ICM_{HF} in NHS. Its time waveforms reconstructed at four expected frequency bands are plotted in Fig.13 and Fig.15~16. It is clear that the breath sounds represent the strong components in LF, MF and HF bands. The energy distributions of the breath component have almost the same intensity at both LF and MF frequency bands.

Based on the experimental investigation, the evaluation indexes of cardiac murmurs (ICM_{LF} , ICM_{MF} and ICM_{HF}) are discussed. Performance measures such as True Positives (TP), False Negatives (FN), True Negatives (TN), and False Positives (FP), accuracy (Acc), sensitivity (Se) and specificity (Sp) are evaluated. TN is the number of normal cases correctly identified as normal. FN is the number of CHD cases incorrectly identified as normal. TP is the number of CHD cases correctly identified as they are, and FP is the number of normal cases incorrectly identified as CHD. Sensitivity ($TP/(TP+FN)$) is the ratio of CHD samples that are correctly identified to the total CHD (congenital heart disease). Specificity ($TN/(TN+FP)$) is the ratio of normal samples are correctly identified to total normal HS. Accuracy $(TP+TN)/(TP+FN+TN+FP)$ which is the ratio of the number of correctly identified samples to total number of samples [19]. The performance measures for the evaluation indexes of cardiac murmurs are shown in Table 3. It can be seen that performance

measures of ICM_{HF} yielded the highest sensitivity of 95.7% (the correct rate of CHD cases), performance measures of ICM_{MF} yielded the highest specificity of 94.3% (the correct rate of normal cases) and accuracy of 93.9% (the correct rate of total cases), respectively, significantly better than that with ICM_{MF} and ICM_{LF} .

Table 3. TN, FN, TP, FP, sensitivity (Se), specificity (Sp) and accuracy (Acc) of evaluation indexes of cardiac murmurs ICM_L .

ICM_L	TN	FN	TP	FP	Se (%)	Sp (%)	Acc (%)
ICM_{LF}	32	7	40	3	85.1	91.4	87.8
ICM_{MF}	33	4	43	2	91.5	94.3	92.7
ICM_{HF}	32	2	45	3	95.7	91.4	93.9

As mentioned above, the energy distribution at VLF band is considered to be a vibration or systolic movement in the body due to the heartbeat shown in Fig.6. In Fig.13, the two samples below the threshold of $TCM_{HF}=0.06$ might be misdiagnosed as normal samples. Further analysis on these 2 CHD samples and comparing with NHS revealed that the energy ratios E_{VLF} of these two ASD cases are less than 34% (see Table 4). This means these two can be distinguished from NHS by $E_{VLF}(\%)$. However, based on the records of these two ASD, the patient was diagnosed as a single ostium primum atrial septal defect without mitral regurgitation or left ventricle to right atrium shunting, while the other ASD cases in this study are ostium secundum atrial septal defects. Patients with smaller ostium primum atrial septal defects (little or no mitral regurgitation or left ventricle to right atrium shunting) are usually asymptomatic [1].

Table 4. Energy ratios values at different frequency bands of CHD heart sound below the threshold TCM_{HF} .

Sample No.	$E_{VLF}(\%)$	$E_{SF}(\%)$	$E_{LF}(\%)$	$E_{MF}(\%)$	$E_{HF}(\%)$
NHS ($E_{ave}\pm E_{std}$)	34.67±17.4	63.58±17.1	1.60±1.0	0.14±0.11	0.018±0.02
ASD(1)	2.31	93.02	4.30	0.33	0.04
ASD(12)	29.35	68.37	2.04	0.22	0.01

Considering the analysis result of evaluation indexes ICM_{HF} and the two special cases of CHD (ASD) at VLF band, we can attain improved performance measures with sensitivity of 100% and accuracy of 96.3%, respectively.

2.4 Result and discussion for four channel signals

In clinical, the medical personnel may hear HSs or murmurs from some different sites in front of the chest or from the back with a stethoscope. Basically, there are four auscultation positions (A, P, T and M), which are also introduced in chapter 1 and 2. Hearing and detecting heart murmurs during a physical examination is the vital diagnosis for common clinical heart diseases, including the CHD, if the heart murmurs are detected, physicians will refer to go to a cardiologist for further diagnosis.

According to the same heart murmur evaluation method in the section 2.3, we also make the statistic data of ICM at LF, MF and HF bands. There are the four channels statistics of NHS, ASD, VSD and TOF from clinic showed in Table 5~7, respectively. And the The NHS threshold (mean+std) of TCM_{LF} , TCM_{MF} and TCM_{HF} at four positions are showed in Table.8

Table 5. Means and variances of the ICM_{LF} at four positions.

ICM_{LF} (mean±std)	A	P	T	M
NHS	2.90±2.2	2.66±2.0	1.67±1.7	4.04±2.4
ASD	4.07±2.0	5.82±3.5	5.21±4.7	5.09±3.1
VSD	9.53±7.5	15.66±10.0	9.14±7.2	9.64±7.4
TOF	9.66±7.4	20.70±14.9	13.03±9.2	6.62±3.2

Table 6. Means and variances of the ICM_{MF} at four positions.

ICM_{MF} (mean±std)	A	P	T	M
NHS	0.28±0.3	0.24±0.2	0.18±0.2	0.42±0.3
ASD	0.62±0.4	1.07±0.8	1.49±1.5	1.16±0.8
VSD	2.15±1.9	5.23±5.6	2.09±2.3	1.80±1.4
TOF	1.97±2.0	8.06±6.9	2.80±3.2	1.00±0.7

Table 7. Means and variances of the ICM_{HF} at four positions.

ICM_{HF} (mean±std)	A	P	T	M
NHS	0.04±0.04	0.03±0.03	0.04±0.06	0.09±0.1
ASD	0.25±0.3	0.18±0.1	0.63±0.7	0.37±0.3
VSD	0.67±0.6	1.49±2.0	0.75±0.7	0.79±0.6
TOF	0.45±0.4	4.26±5.1	1.66±2.9	0.83±1.4

Table 8. The threshold of TCM_{LF} , TCM_{MF} and TCM_{HF} at four positions.

TCM_L $ICM_L(\text{mean}+\text{std})$	A	P	T	M
TCM_{LF}	5.132	4.606	3.363	6.466
TCM_{MF}	0.539	0.427	0.353	0.713
TCM_{HF}	0.079	0.060	0.100	0.219

And in order to observe the comparison clearly, the histograms are drawn according to the data in Table 5~7, and showed in Fig. 17~19, respectively.

From Fig. 17~19, as for ICM at LF, MF and HF, we can find the main change trends are consistent, the ICM of CHDs are higher than NHS at differing in degree. Further, this fact shows the heart murmur evaluation parameters are effective between NHS and CHDs. Furthermore, the discussion murmur indexes at different positions of CHDs respectively in detail, based on the Fig. 17~19 and the blood flow figures which is introduced in chapter 1.

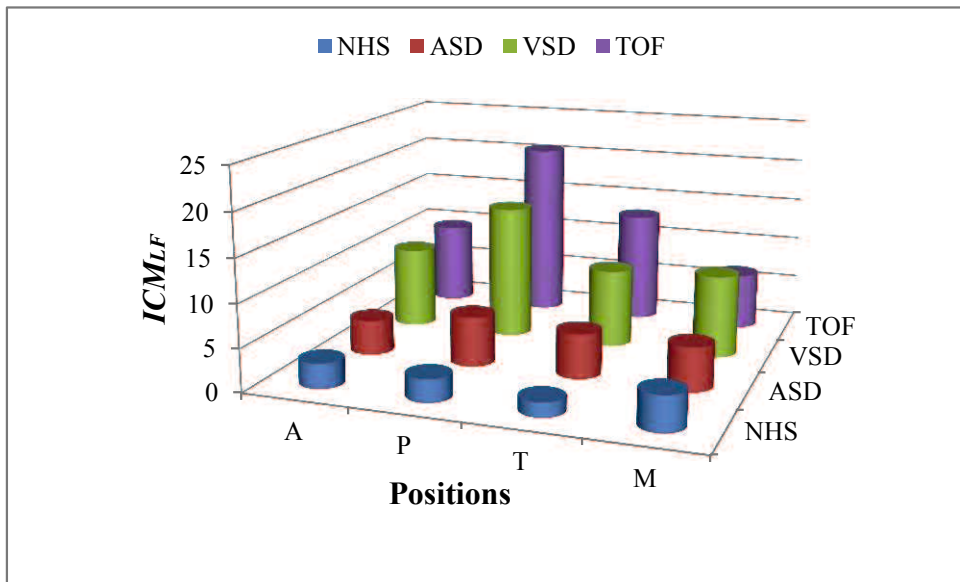


Fig. 17. Mean values of the ICM_{LF} at four positions.

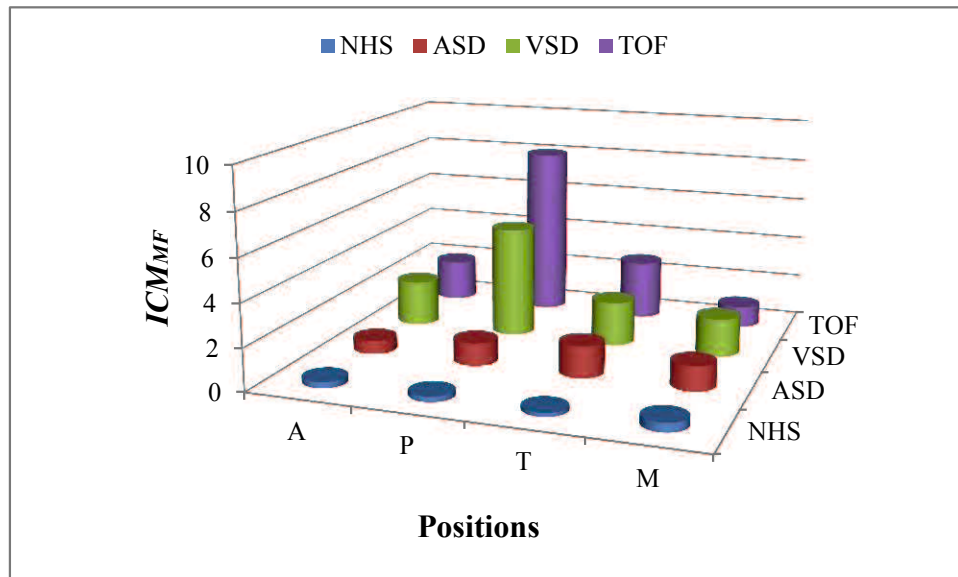


Fig. 18. Mean values of the ICM_{MF} at four positions.

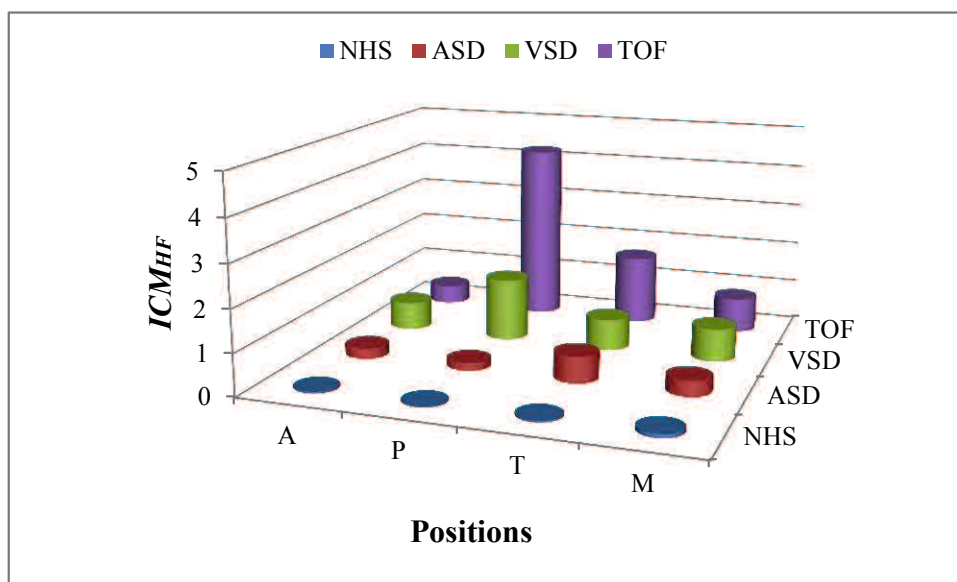


Fig. 19. Mean values of the ICM_{MF} at four positions.

As for ASD, the ICM parameters are nearest with NHS, even though, we also can find at P, T and M positions, the indexes of murmur are higher, that is because an ASD is a hole in the part of the septum that separates the atria and the upper chambers of the heart. The hole allows oxygen-rich blood from the left atrium to flow into the right atrium, instead of flowing into the left ventricle as it should, that means much more oxygen-rich blood flow through the tricuspid valve (T) to pulmonary valve (P), while less oxygenated blood flow from mitral valve (M) to aortic valve, which may cause

much more murmurs at P, T and M positions.

As for VSD, the ICM parameters are little higher than NHS at these four positions, and we also can find at P position, the index is especially higher, that is because VSD is a hole in the part of the septum that separates the ventricles-the lower chambers of the heart. The hole allows oxygen-rich blood to flow from the left ventricle into the right ventricle, instead of flowing into the aorta and out to the body as it should. This means much more mixing blood flow through the tricuspid valve (T) and mitral valve (M) to pulmonary valve (P). As a result, the left side of the heart must work harder than normal. Extra blood flow increases blood pressure in the right side of the heart and the lungs, which cause much more murmurs at P position.

As for TOF, the ICM parameters from P position data which is the highest. That is because TOF is a combination of four defects: pulmonary valve stenosis, a large VSD, an overriding aorta, and right ventricular hypertrophy. In TOF, not enough blood is able to reach the lungs to get oxygen, and oxygen-poor blood flows to the body. That because partial obstruction of right ventricular outflow and pulmonary valve (P), when the blood flow from the narrow pulmonary valve, which cause much more murmurs.

2.5 Summary

Heart murmurs are pathological sounds produced by turbulent blood flow due to cardiac defects. This section has described a new approach on analysis of the pathologic cardiac murmurs based on the wavelet packet decomposition technique which analyses both low and high frequency sub-bands of HS signals, collected from clinical subjects in general environment. The HS signal was divided into five bands and the energy intensity at each frequency band was calculated and compared. Based on the analysis of clinic HS data, three evaluation indexes for cardiac murmurs were proposed for the analysis of the pathologic murmurs.

Finally, the threshold values between the innocent and pathologic murmurs were determined based on the statistical results of the normal HSs. A pulmonary HS case study on the NHS and CHD signals was performed to validate the usefulness and performance of the proposed method. The performance measures of ICM_{HF} yielded the highest sensitivity of 95.7%, specificity of 91.4% and

accuracy of 93.9%, respectively. Furthermore, considering the analysis result of evaluation indexes ICM_{HF} at HF (312.5-1250Hz) and the two special cases at VLF band (4.88-19.53Hz), we can obtain the improved performance measures with a sensitivity of 100%, and accuracy of 96.3%, respectively.

At last, the ICM parameters are calculated with the same method. The statistic results show that ICM parameters of multichannel signals not also can evaluate the murmur quantitatively, but also reveal the murmurs generating reason by analyzing signals from four positions simultaneously.

3. Murmurs indexes extraction based on heart vibration states

In order to further quantitatively analyze the cardiac murmurs at each cardiac cycle, the murmur index extraction based on cardiac vibration state by describing the shape of different-scale window MW was proposed in this section. Firstly, the introduction of moment method is presented. And then the homomorphic segmentation of multichannel HS cycle (T) and fundamental HS (S1S2) is proposed based on homomorphic MW (HMW) extraction with window length l ($T/2$), the HS cycle and S1S2 segmentation were implemented by locating the maximum and minimum of MW respectively. Secondly, considering the segmentation points of HS S1S2 and cycle as MW centers respectively, to extract the systolic MW and diastolic MW with different window lengths ($T/8$ and $3T/8$), furthermore, extracting DWF such as SMI and DMI which were proposed based on systolic MW (SMW) and diastolic MW (DMW) with window length $T/4$. Finally, many experiments show that the murmur indexes are efficient to judge the murmur occurring periods and degree. Importantly, DMF can be computed by moment analysis very fast and simple, and therefore it's very useful to auto-diagnosis or aided-diagnosis in an artificial intelligence cardiac murmur analysis system. And the details are introduced as bellow.

The understanding of moment is derived from the image processing technology. In image processing, the moment properties are relative with the shape of object directly. The moment of signal is also relative with these properties, such as waveform, strong, weak, or other important characteristics of the signal changing. Yan [8] put forward the moment segmentation method of HSs in 2009, a lot of experimental analysis found that MW has obvious advantages, its computation is very simple, fast, and high against noise power, which usually doesn't need to do filtrating

processing.

In this section, taking the similar idea of [8], we proposed the different-scale window MW of clinical HSs on different time window sizes. However, we found some new ideas based on the reference [8].

- The homomorphic envelop waveform extraction based on multichannel signals is proposed, which is helpful to highlight the common characters of basic HSs and weaken the influence of heart murmurs or other incidental noises.
- The time window size of moment is an important parameter need to be determined, a fixed size in [8] is not easy to adapt to all situations, so we put forward the adaptive method of the time window size which is changeable with each HS cycle.
- The different time window moments of the HSs have different characteristics, these characteristics can be used to obtain the rhythm features of HSs more accurately, and we can use different-scale window MW to reveal the new feature information of clinical HSs from many clinical data.
- We also found that a new property of different-scale window MW on different time windows can realize the heart murmurs intensity evaluation.

3.1 The heart sound segmentation of multichannel signals

In this section, the HS segmentation of multichannel HSs signals is implemented based on homomorphic envelope waveform (HEM) and different-scale window MW can be expressed by the Viola integral method [9].

The original HS signals were recorded by the multichannel signals measuring system with 16-bit accuracy and different sampling frequencies (20 kHz and 40 kHz). So the resulting signals were pre-processed wavelet method introduced in section 1. At last, the normalization was applied by setting the variance of the signal within a value of 1.0. The normalization is applied and the resultant signals can be expressed as $s(t)$.

3.1.1 Envelop waveform extraction

We set a signal $s(t)$, the random noise signal as $n(t)$, and the output signal as $x(t)=s(t)+n(t)$. It is easy to express their variances by $\sigma^2(x)=\sigma^2(s)+\sigma^2(n)$, Where $\sigma(\bullet)$ denotes as the variance of a signal. The output signal $\sigma^2(s)$ is defined as envelope waveform of HSs, here we assume $\sigma^2(n)$ is only an unknown constant, and the mean is 0, and variance is 1. Therefore, output signal can be viewed as $\sigma^2(x)$. The envelop waveform (EW) of the signal was denoted as $e(t,\sigma)$, which is defined as the variance signal of actual output signal $x(t)$ and expressed as $e(t,\sigma)=\sigma^2(x)$, Where δ is neighborhood of time t , called the width δ time scale[8], and then

$$e(t, \delta) = \int_{t-\delta}^{t+\delta} (x(\tau) - \bar{x}(t))^2 d\tau \quad (5)$$

$$\bar{x}(t) = \frac{1}{2\delta} \int_{t-\delta}^{t+\delta} x(\tau) d\tau \quad (6)$$

Therefore, $e(t, \sigma)$ can be computed by

$$e(t, \delta) = \int_{t-\delta}^{t+\delta} (x(\tau))^2 d\tau - 2\delta(\bar{x}(t))^2 \quad (7)$$

And the EW of each channel is showed in Fig. 20~21. In order to test the existence of cycles and locate each of them for an approximate periodic signal, it is necessary to introduce the calculation of the multi-scales MW. For two time scales δ and l , the multi-scales moment of characteristic waveform $I(t, \delta, l)$ is defined as:

$$I(t, \delta, l) = \int_{t-l}^{t+l} (\tau - t)^2 e(\tau, \delta) d\tau \quad (8)$$

$$I(t, \delta, l) = \int_{t-l}^{t+l} \tau^2 e(\tau, \delta) d\tau - 2t \int_{t-l}^{t+l} \tau e(\tau, \delta) d\tau + t^2 \int_{t-l}^{t+l} e(\tau, \delta) d\tau \quad (9)$$

Normalization of moment calculation Eq. (8) is stated as:

$$N(t, \delta, l) = \frac{\int_{t-l}^{t+l} (\tau - t)^2 e(\tau, \delta) d\tau}{\int_{t-l}^{t+l} e(\tau, \delta) d\tau} \quad (10)$$

Here, call $I(t, \delta, l)$, $N(t, \delta, l)$ as the characteristic moment of $e(t, \sigma)$, set

$$I(t, \bar{t}, \delta, l) = \int_{t-l}^{t+l} (\tau - \bar{t})^2 e(\tau, \delta) d\tau \quad (11)$$

$$N(t, \bar{t}, \delta, l) = I(t, \bar{t}, \delta, l) / \int_{t-\delta}^{t+\delta} e(\tau, \delta) d\tau \quad (12)$$

where

$$\bar{t} = \int_{t-\delta}^{t+\delta} \tau e(\tau, \delta) d\tau / \int_{t-\delta}^{t+\delta} e(\tau, \delta) d\tau$$

3.1.2 Homomorphic envelop waveform extraction of multichannel signals

In this section, in order to highlight the common characters and weaken the influence of heart murmurs or other incidental noises at some channels to obtain the segmentation much more accurately, the HEW extraction method is proposed. The HEW is obtained from multichannel signals, and it is expressed as:

$$he(t, \delta) = \sqrt[i]{e_1(t, \delta) \cdot e_2(t, \delta) \cdots e_i(t, \delta)}, \text{ and } i = 4 \quad (13)$$

where $\delta=0.05$ [8], and the plots of HEW are shown in Fig.20~21.

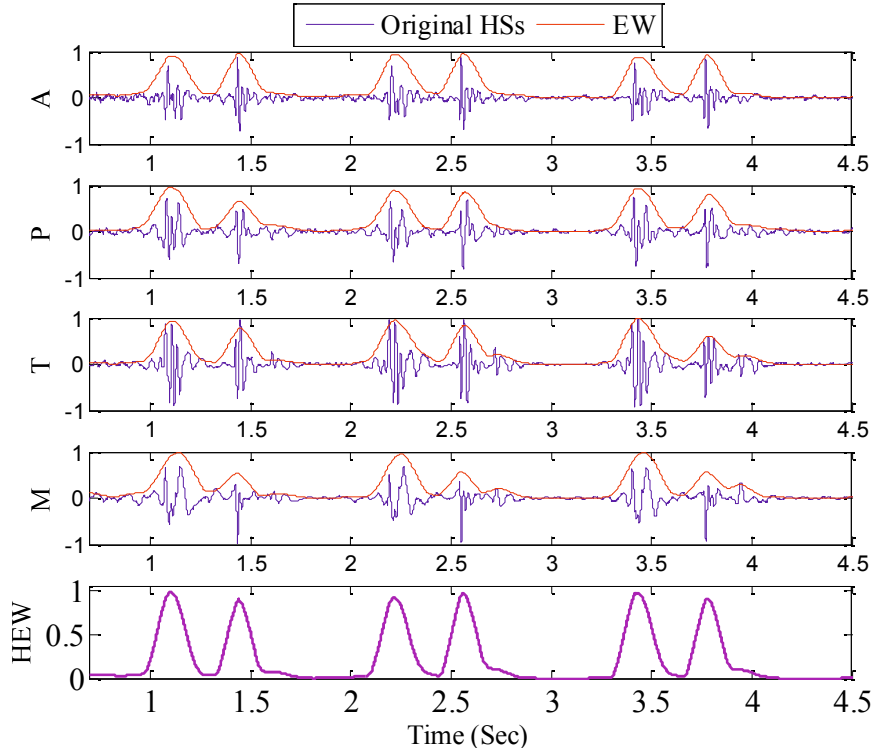


Fig. 20. Original multichannel signals, each EW and HEW of NHS.

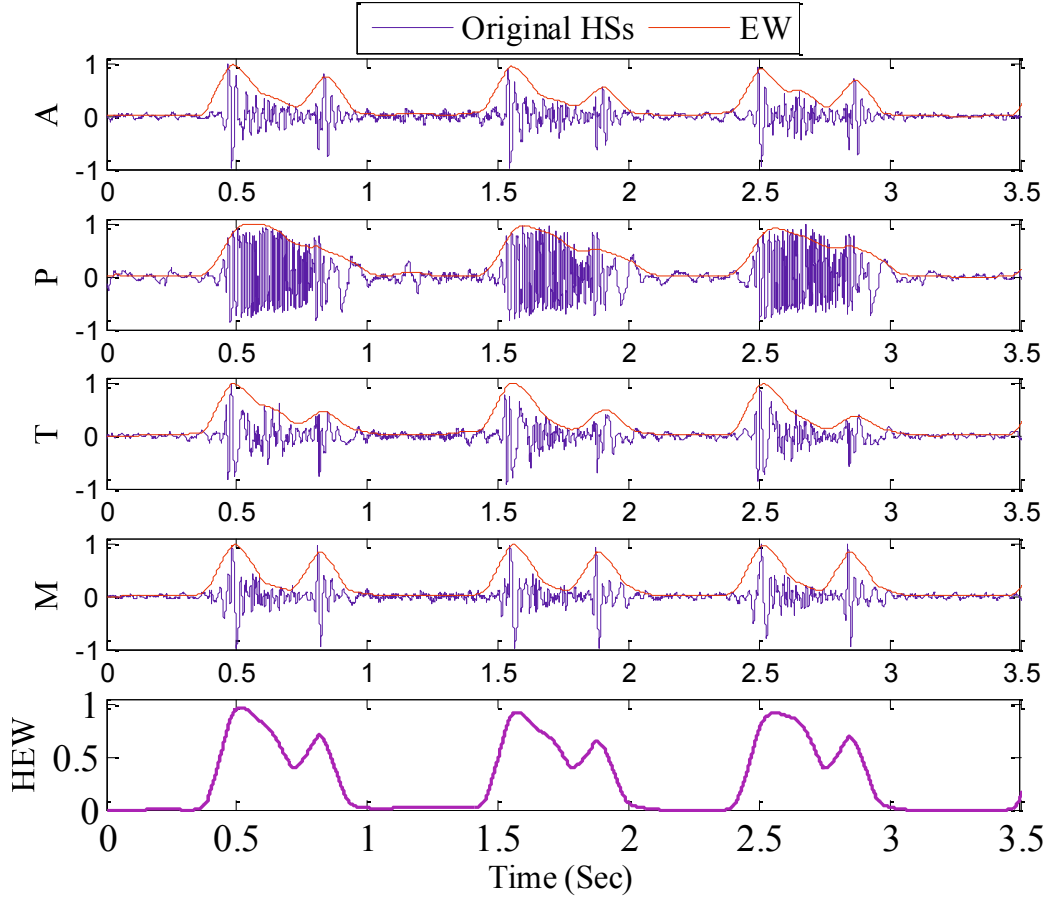


Fig. 21. Original multichannel signals, each EW and HEW of abnormal HS (TOF).

3.1.3 Moment waveform extraction based on homomorphic envelop waveform

The MW extraction of $he(t, \sigma)$ is expressed as:

$$HI(t, \bar{t}, \delta, l) = \int_{t-l}^{t+l} (\tau - \bar{t})^2 he(t, \delta) d\tau \quad (14)$$

$$HN(t, \bar{t}, \delta, l) = I(t, \bar{t}, \delta, l) / \int_{t-\delta}^{t+\delta} he(t, \delta) d\tau \quad (15)$$

Where

$$\bar{t} = \int_{t-\delta}^{t+\delta} \tau he(t, \delta) d\tau / \int_{t-\delta}^{t+\delta} he(t, \delta) d\tau$$

Based on the experimental data, in this study, $\delta=0.05$, we usually assume an initial time window size $l = 0.45$ [8]. And get a preliminary MW, then to calculate the main frequency of the waveform using *FFT* to obtain the cycle time (T), and then the window size l can be determined as the half period of the cycle to obtain the MW ($l = T/2$). and the MW extractions are showed in Fig. 24~25(b).

From these plots, we can find that the HEW extraction method successfully obtain a homomorphic envelop from these four channels, which highlight the basic HS components (S1 and S2) and the major murmurs from four channels, while the incidental noises which occurred can be weakened. The MW based on HEW extraction is helpful for improving accuracy rating of cycle and HS segmentation.

3.1.4 Calculate heart rate with FFT analysis

The normal resting adult human heart rate (HR) ranges from 60-100 bpm. Tachycardia is a fast HR, defined as above 100 bpm at rest. Bradycardia is a slow HR, defined as below 60 bpm at rest. During sleep a slow heartbeat with rates around 40-50 bpm is common and is considered normal. When the heart is not beating in a regular pattern, this is referred to as an arrhythmia. These abnormalities of heart rate sometimes indicate disease [10] .

As discussed above, the HR can be calculated based on homomorphic moment segmentation accurately. And $\delta=0.05$, $l=0.45$. Hence, $F_{max}=max(fft(HN(t,\delta,l)))$, and $HR=60*F_{max}$.

3.1.5 Calculation of heart sound cycle and heart sound segmentation

The HS segmentation including cycle segmentation and HS rhythms (S1S2) segmentation based on MW with window lengths l which is determined as the half period of the cycle (T) ($l=T/2$). According to the characteristics of moment, the HSs cycle calculation are determined by the maximum points of MW, while, the HS rhythms (S1S2) segmentations are determined by the minimum points which between in one HS cycle, they are showed in Fig. 22~23 (b), and the green lines are the cycle segmentation, the blue lines are the HS rhythms (S1S2) segmentation. Both the cardiac cycle segmentation and basic HS segmentation are performed accurately between NHS and abnormal HS cases. The homomorphic segmentation method improves the segmentation accuracy greatly. And the statistic results will be introduced as bellows.

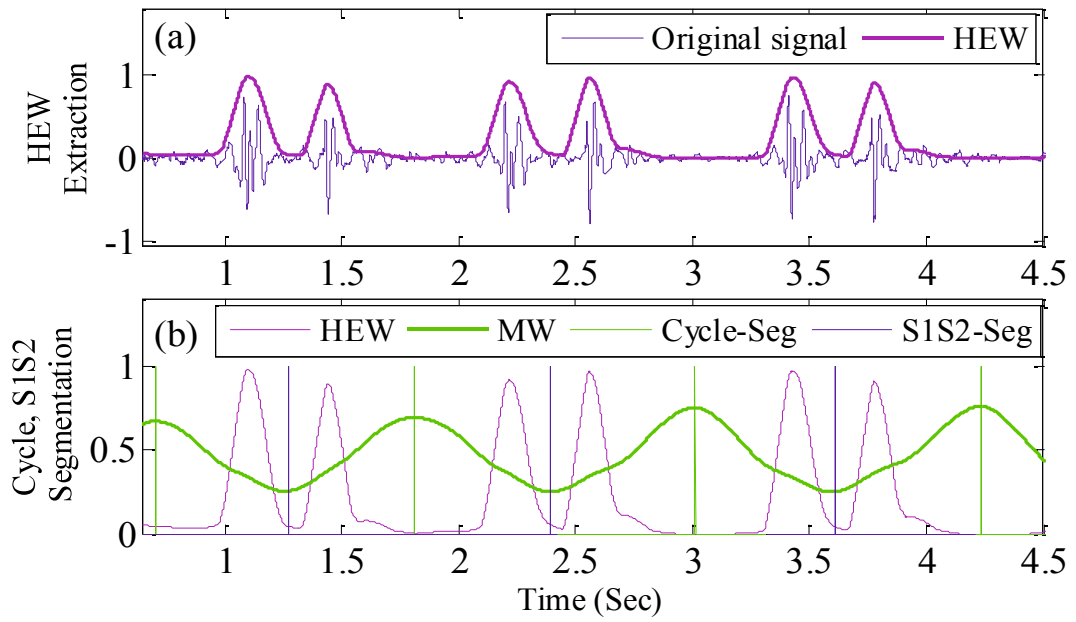


Fig. 22. HEW extraction and homomorphic segmentations based on HEW of NHS.

(a) HEW extraction (b) cycle, S1S2 segmentation based on MW ($l=T/2$).

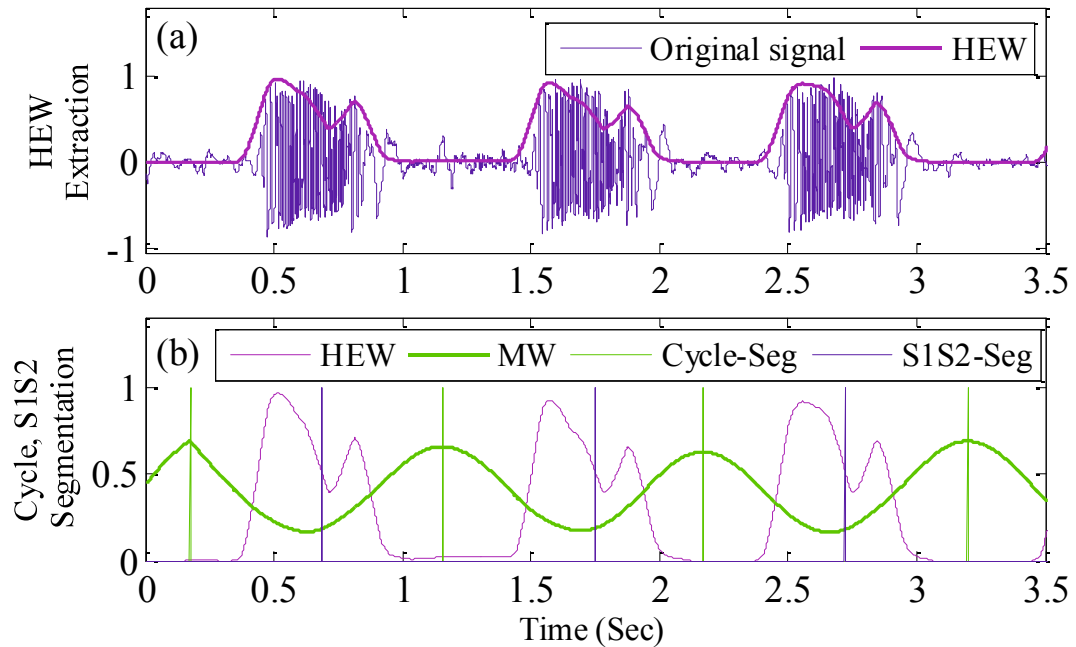


Fig. 23. HEW extraction and homomorphic segmentations based on HEW of abnormal HS (TOF).

(b) HEW extraction (b) cycle, S1S2 segmentation based on MW ($l=T/2$).

The homomorphic segmentation flow chart is showed in Fig. 24.

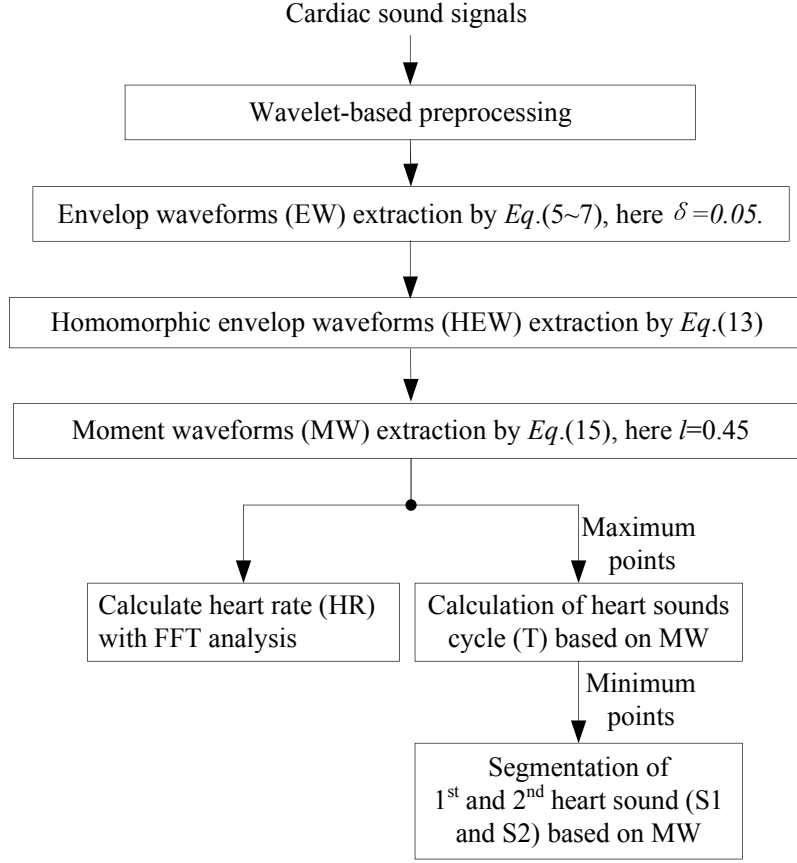


Fig. 24. The HS segmentation flow chart.

3.2 Murmurs indexes extraction based on dual moment features

Using *Eqs. (5~12)*, the moment extraction are implemented. Based on *Eq. (10)*, the systolic and diastolic MW are can be expressed as

$$SN(t, \delta) = N\left(t, \delta, \frac{T}{8}\right) \quad (16)$$

$$DN(t, \delta) = N\left(t, \delta, \frac{3T}{8}\right) \quad (17)$$

Where for systolic MW, $l=T/8$, and for diastolic MW, $l=3T/8$. And the MW extractions are showed in Fig. 25~26 (c~d). The different window length moments have different characteristics, these characteristics can be used to obtain the systolic and diastolic features of HSs more accurately, at systole and diastole of one heart cycle, the MW shape are showed in Fig. 27~28 (b~c) in detail. And the shapes of these parts which are marked in the dotted boxes are similar with the Gaussian distribution of the signals.

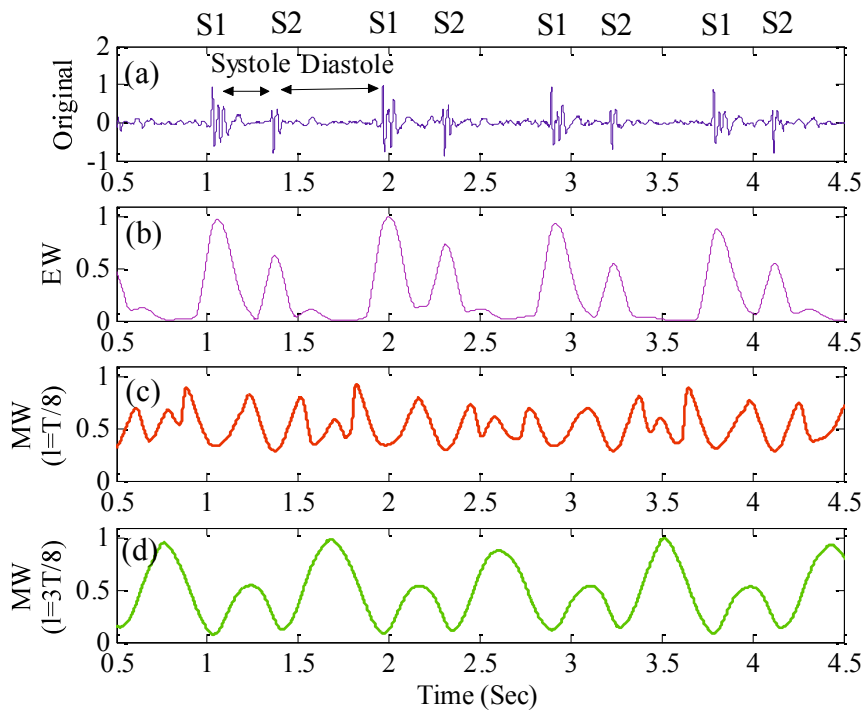


Fig. 25. Systolic and diastolic MW of NHS with different window lengths
 (a)Original NHS, (b) HEW extraction, (c) MW($l = T/8$), (d) MW($l = 3T/8$).

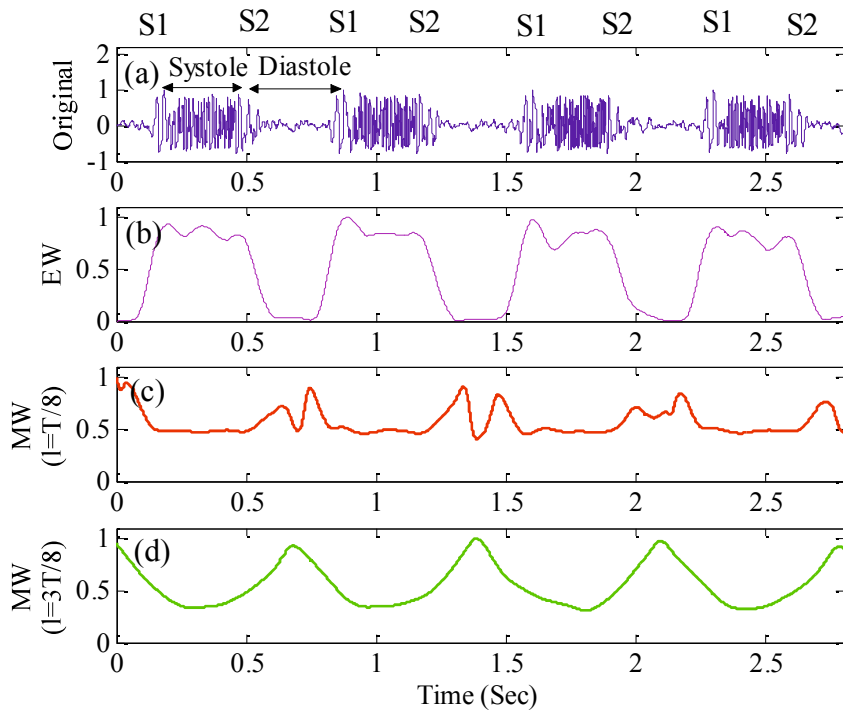


Fig. 26. Systolic and diastolic MW of VSD with different window lengths
 (a)Original VSD signal, (b) HEW extraction, (c) MW($l = T/8$), (d) MW($l = 3T/8$).

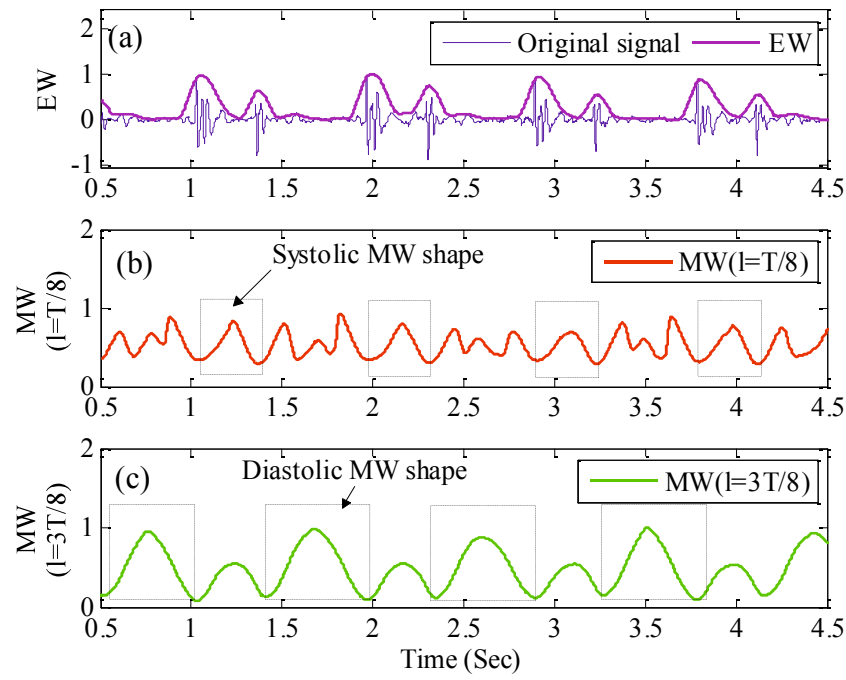


Fig. 27. Systolic and diastolic MW of NHS with different window lengths

(a) EW extraction, (b) $MW(l = T/8)$, dotted box shown the systolic MW shape,

(c) $MW(l = 3T/8)$, dotted box shown the systolic MW shape.

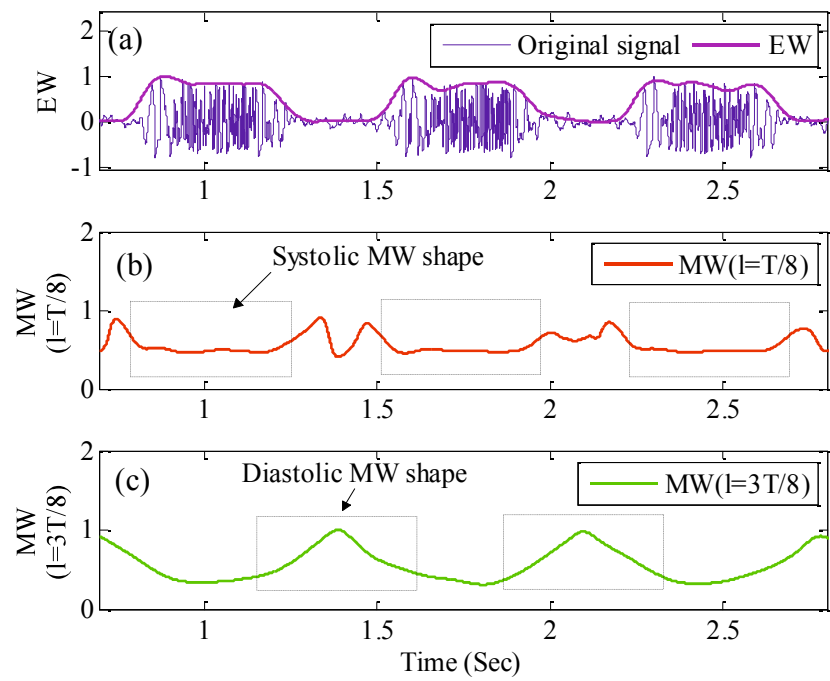


Fig. 28. Systolic and diastolic MW of VSD with different window lengths

(a)EW extraction, (b) $MW(l = T/8)$, dotted box shown the systolic MW shape,

(c) $MW(l = 3T/8)$, dotted box shown the systolic MW shape.

3.2.1 The introduction of moment method

Moment is the invariant features or stable features of an image, as well as moment can be the invariant features of the signal. Nevertheless, it depends on scales of the observation, the time window size is hence important to choose. Here we briefly introduce moment analysis and calculation method of [8], and we define the general p -moments of an energy limited signal $f(x)$ of a real variable about a value t as

$$u_p = \int_{-\infty}^{\infty} (x - t)^p f(x) dx \quad (18)$$

Where the normalization from is expressed $u_p = \frac{\int_{-\infty}^{\infty} (x-t)^p |f(x)|^2 dx}{\int_{-\infty}^{\infty} |f(x)|^2 dx}$, and $t = \frac{1}{\|f\|_2^2} \int_{-\infty}^{\infty} x |f(x)|^2 dx$

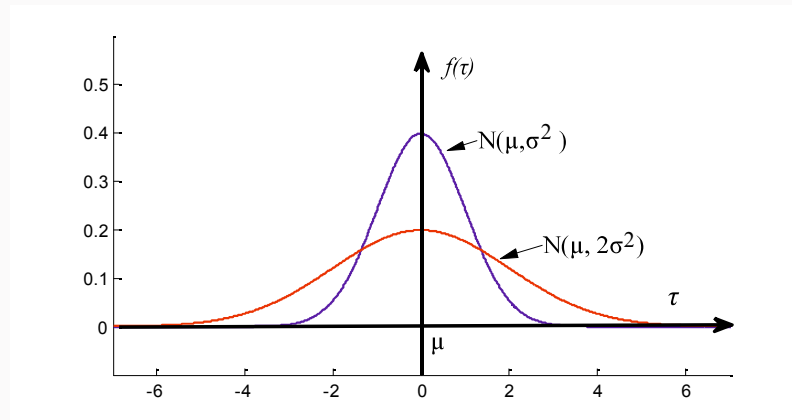


Fig. 29. Schematic diagram of signal moment

The Gaussian signal $f(\tau) = \frac{1}{\sqrt{2\pi}\sigma} e^{-\frac{(\tau-\mu)^2}{2\sigma^2}}$, $\tau \in (-\infty, +\infty)$ is shown in Fig.29, and $\sigma^2 = \int_{-\infty}^{\infty} (\tau - \mu)^2 f(\tau) d\tau$. Therefore, when $p = 2$, $u_2 = \sigma^2$. Note that the signal is viewed as one component on $\tau \in (-\infty, +\infty)$ and the moment $u_2 = \sigma^2$, makes a good description to the shape of Gaussian curve. However, in the HS analysis, the ever-changing HSs in a long duration must contain many components in HS cycles. Obviously, only one moment parameter on whole duration may not reveal the physiological and pathological information fully during the cardiac vibration. Yan [8] introduced a move time window to observe the different moment characteristics, different-scale MW can be effectively used to analyze the features of HSs, due to the fact that different time window

moment has different characteristics, and these characteristics have relative stability, as shown in Fig.27(c~d) and Fig.28(c~d) very clearly.

and t is taken as the center of the window. So there is the following moment form:

$$u_p = \frac{\int_{t-l}^{t+l} (\tau-t)^p |f(\tau)|^2 d\tau}{\int_{t-l}^{t+l} |f(\tau)|^2 d\tau} \quad (19)$$

Where we only use $p = 2$. u_2 is the different-scale MW signal on a time window l -length.

3.2.2 Murmurs indexes extraction

Furthermore, Different signals show different MW, which are show in Fig. 30, in Fig.30, when there are strong systolic murmurs from P position, and there are a certain degree murmur existed at other three channels. The MW shapes, which are marked with dotted boxes, are showed in Fig.30. the shape from P position is different with other three channels (A, T and M) signals, meanwhile, the MW shapes of the other three channels signals are similar with each other, while, with the difference of the murmurs (A, T and M) intensity, the shapes are a little different.

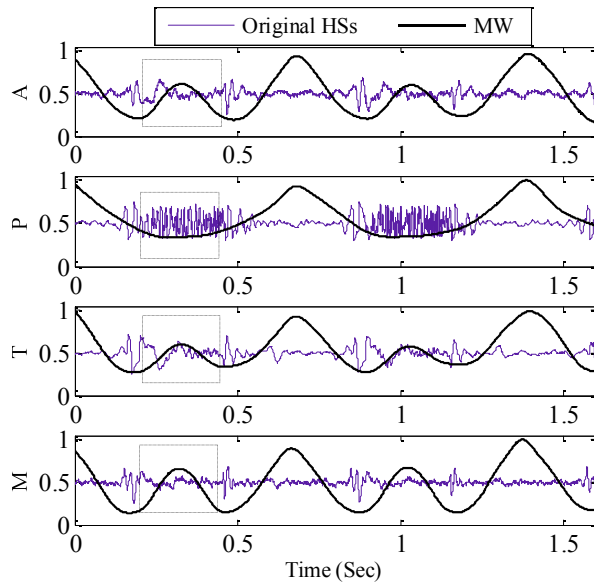


Fig. 30. The four-channel VSD original sound signals and their MW.

According to this property, we find that the shape of MW could be used to judge presence of heart murmurs or ambient noises, murmur intensity at each HS cycle. So if there is no too much interference of noise in signal, the shape of the moment waveform can detect the existence of the heart murmurs effectively. We hence defined the SMI and DMI by dual moment features of the signals. For SMI, the S1S2-Seg points are considered as the time centers which are called t_i . And for DMI, the Cycle-Seg points are considered as time centers which are called t_j , which are showed in Fig.31.

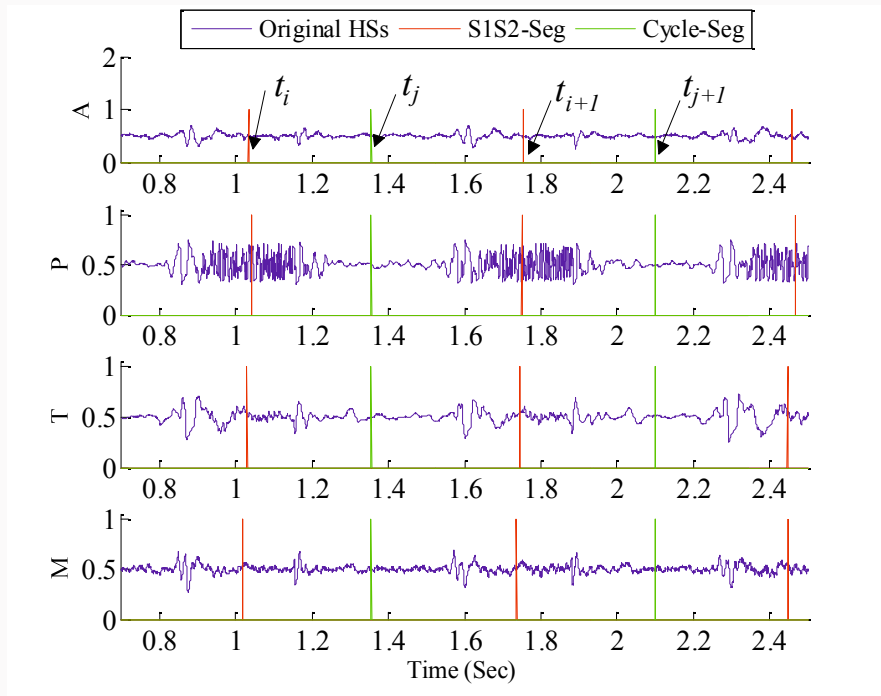


Fig.31. S1S2 and cycle segmentation points as the time centers (t_i, t_j).

Therefore, based on the systolic MW, $SN(t, \delta)$, and the diastolic MW $DN(t, \delta)$. The time centers are showed in Fig.32. The SMI and DMI are expressed as

$$SMI(t, \delta, l1) = \frac{\int_{t_i-l1}^{t_i+l1} (\tau-t_i)^2 SN(t, \delta)^2 d\tau}{l * \left(\int_{t_i-l1}^{t_i+l1} SN(t, \delta)^2 d\tau \right)} \quad (20)$$

Where $l1=T/4$, $i = (1 \sim N)$, N is the number of the HS cycles. t_i is the time centers of systolic MW.

$$DMI(t, \delta, l1) = \frac{\int_{t_j-l1}^{t_j+l1} (\tau-t_j)^2 DN(t, \delta)^2 d\tau}{l * \left(\int_{t_j-l1}^{t_j+l1} DN(t, \delta)^2 d\tau \right)} \quad (21)$$

And, $l1=T/4$, $j = (1 \sim N)$, N is the number of the HS cycles. t_j is the time centers of diastolic MW.

A block diagram of the proposed murmurs index of multichannel HSs based on cardiac vibration state describing by DMF with different window lengths is presented in Fig.32.

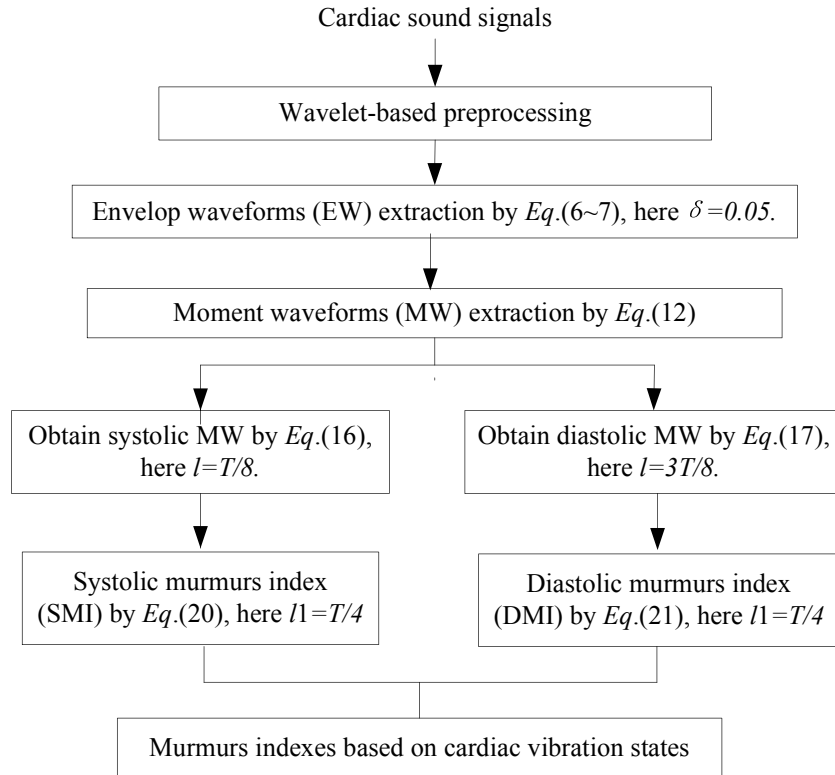


Fig. 32. A block diagram of murmurs indexes based on cardiac vibration states

3.3 Result and discussion

In this study, the multichannel the HS data were collected from 82 test subjects who have signed an informed consent. The subjects included 35 healthy young students and 47 clinical CHD patients (3 month to 10 years old, several are 24~27 years old), and the clinical CHS subjects are including 12 ASD, 27 VSD and 8 TOF. Moreover, the data are from four auscultation sites, so there are 140 normal samples, and 168 CHD samples.

3.3.1 Heart rate of clinical four channel signals

HR, or heart pulse, is the speed of the heartbeat measured by the number of contractions of the heart per unit of time typically beats per minute (bpm). The HR can vary according to the body's physical needs, including the need to absorb oxygen and excrete carbon dioxide. Activities that can provoke change include physical exercise, sleep, anxiety, stress, illness, ingesting, and drugs.

From Table 9 and Fig.33, we can find that the RH of NHS is from 60-78 bpm, which meet the normal human RH standard, and the RH of CHD subject are higher than NHS, meanwhile, the varying range are greater than NHS. The patients who suffered CHD can not absorb oxygen and excrete carbon dioxide smoothly, further causing arrhythmia and other cardiac abnormalities. Therefore, HR is a useful diagnostic feature.

Table 9. Means and variances of the HR between NHS and CHD

Subjects	NHS	ASD	VSD	TOF
$HR(bpm)$ (mean±std)	69±9	88±16	94±14	90±23

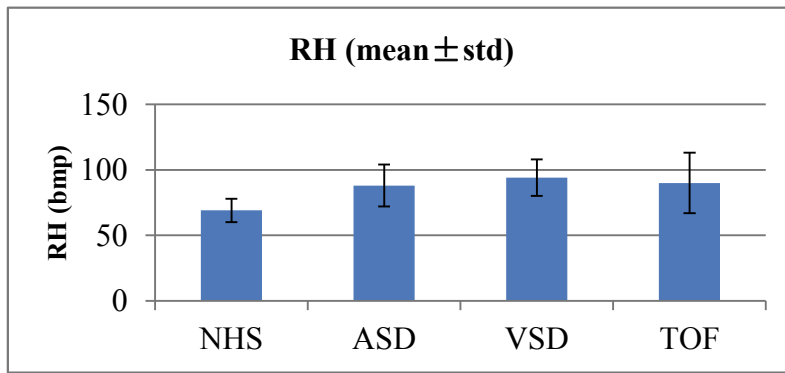


Fig.33. RH of NHS and CHDs

3.3.2 Homomorphic segmentation of clinical four channels signals

As for the ASD cases, there is one case which is collected from a two years old child. The original multichannel signals are showed in Fig.34. Because the ASD patient is too young, it is difficult to collect the clinical data successfully. And also, there are strong breath sounds and noise which may be from the pediatric physical movement, showed at the A, P and T in Fig.34, and the signal from M position is very weak which is not collected well. There are some fault homomorphic cycle and HS segmentations of this ASD case. As a result, this ASD case is deleted from the segmentation accuracy statistic.

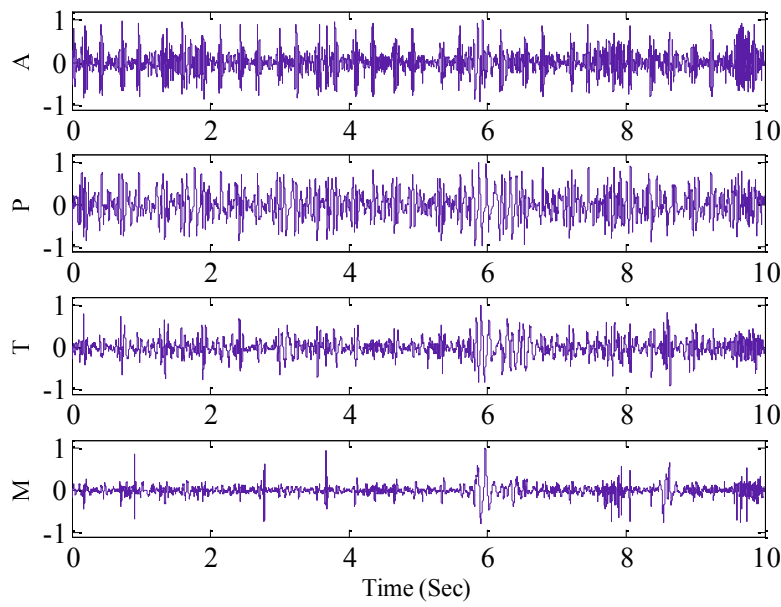


Fig.34. The original of the multichannel ASD signals (deleted sample)

The automatic cycle segmentation and S1S2 segmentation accuracy are calculated and summarized in Table 10~11. From table 10~11, we can find that the clinical multichannel automatic segmentation accuracies are very high.

Table 10. The statistic of cycle automatic segmentation accuracy

Cases	Subject data	Cycle data	Error cycle data	Correct cycle data	Automatic Segmentation accuracy
NHS	35	284	0	284	100%
ASD	11	120	0	120	100%
VSD	27	323	5	318	98.1%
TOF	8	78	0	78	100%

Table 11. The statistic of S1S2 automatic segmentation accuracy

Cases	Subject data	Cycle data	Error cycle data	Correct cycle data	Automatic Segmentation accuracy
NHS	35	284	0	284	100%
ASD	11	120	0	120	100%
VSD	27	323	8	315	97.5%
TOF	8	78	0	78	100%

There are several error cycle and S1S2 automatic segmentations of two VSD cases. The detail discussion will be introduced as bellows.

The first VSD case is from a patient who is 5 years old and suffered perimembranous type VSD. The homomorphic cycle (green bar) and S1S2 (red bar) segmentation of this multichannel VSD (case 1) signals is showed in Fig.35~36, the part in the black dotted box is error segmentation of cycle or S1S2. Fig.36 shows the homomorphic cycle segmentation of this VSD signals, the part in the red dotted box is strong body movement noise which influence the extreme points searching, and further cause the error homomorphic cycle segmentation. Fig.36 shows the homomorphic S1S2 segmentation of this VSD signals, the part in the black dotted box is strong breath sounds which influence the extreme points searching, and further cause the error homomorphic S1S2 segmentation.

The second VSD case is from a patient who is 3 years old and suffered basilar type VSD. Fig.37~38 shows the homomorphic cycle and S1S2 segmentation of this VSD signals, respectively, the part in the dotted box is strong friction sound from the auscultation head and body, also there are electronic interference which influence the extreme points searching, and further cause the error homomorphic cycle and S1S2 segmentation.

In this section, the automatic moment segmentation method is implemented, and the statistic results showed the high segmentation accuracy, shown in Table 10~11, the NHS, ASD and TOF segmentation accuracy are 100%. Because of the noise from the clinical collection of multichannel HS and some electronic interference, which we should improve in the clinical HS skill, that will decrease the error segmentations.

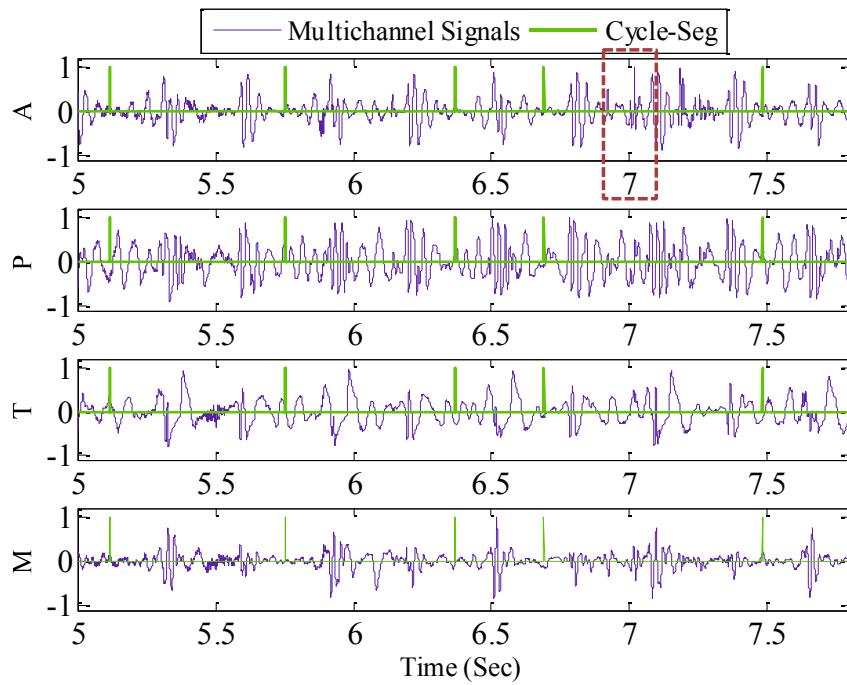


Fig. 35. The homomorphic cycle segmentation of multichannel VSD (case 1) signals, the part in the red dotted box is noise which influence the homomorphic cycle segmentation

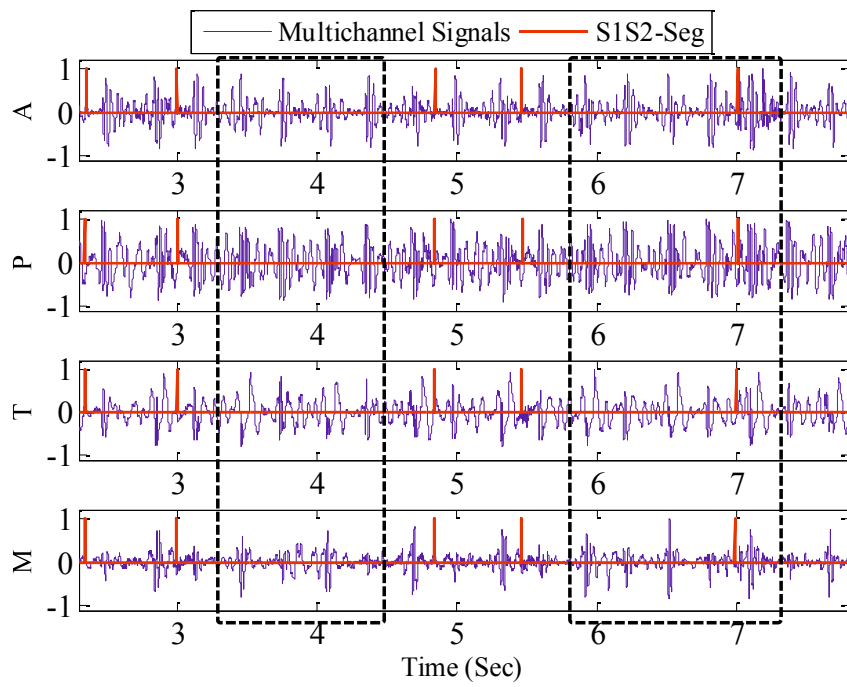


Fig.36. The homomorphic S1S2 segmentation of multichannel VSD (case 1) signals, the part in the black dotted box is error segmentation of S1S2

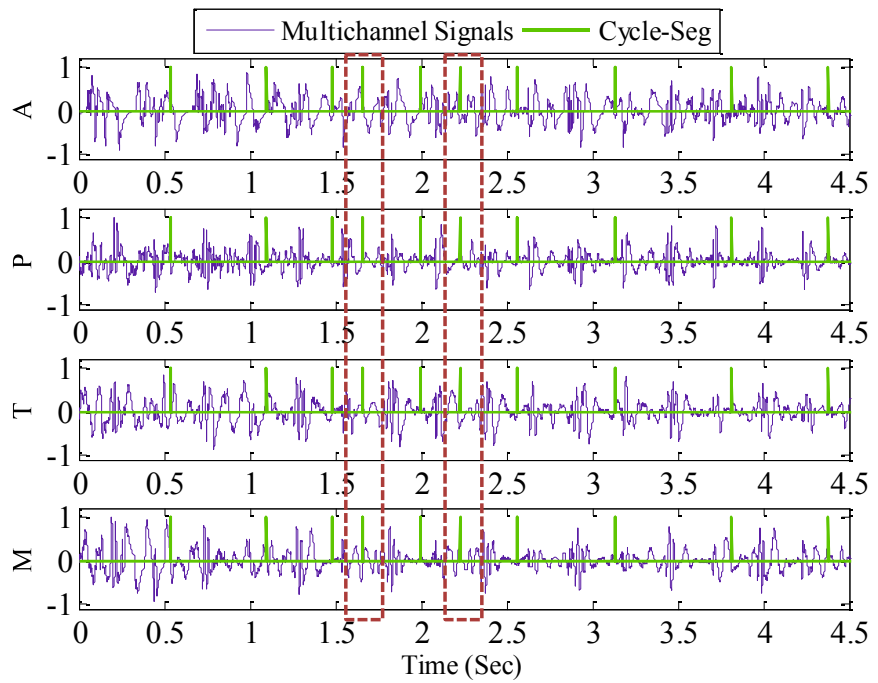


Fig.37. The homomorphic cycle segmentation of multichannel VSD (case 2) signals, the part in the dotted box is noise which influence the homomorphic cycle segmentation

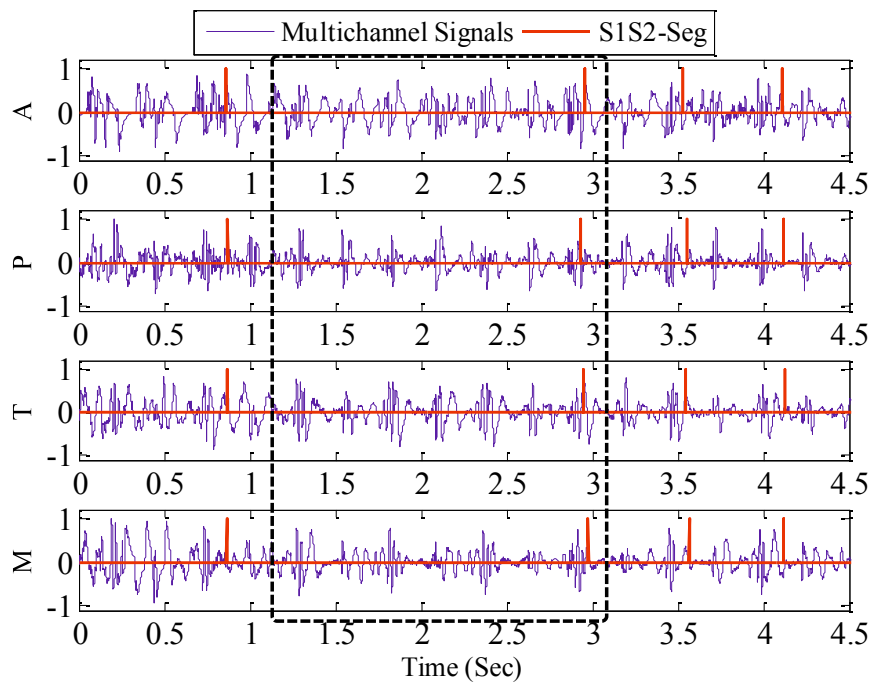


Fig.38. The homomorphic S1S2 segmentation of multichannel VSD (case 2) signals, the part in the black dotted box is error segmentation of S1S2

3.3.3 Murmurs indexes of clinical four channels signals

The systolic murmurs can be seen obviously in the CHD subjects. According to Eq.(18~19), we can compute the murmurs indexes (SMI, DMI) of systole and diastole. The mean and variance are calculated in Table 12~13. From Table 12~13 and Fig. 39~40, we can find that the murmurs indexes of CHD subjects at four positions are higher than 0.19. And the parameters in diastole are almost near with the NHS subjects, that is to say, there are no or few diastolic murmurs in the CHD subjects, from these statistic results, the murmurs existing can be judged. Furthermore, the murmurs intensity at these four positions can be evaluated by these indexes. In order to evaluate the murmurs intensity level in a simple way, the systolic and diastolic murmurs index level limit (MIL) are defined as follows

$$SMIL = \overline{SMI} + \overline{\sigma_{SMI}} \quad (20)$$

$$DMIL = \overline{DMI} + \overline{\sigma_{DMI}} \quad (21)$$

Where σ_{SMI} and σ_{DMI} are the standard deviations of SMI and DMI, \overline{SMI} , \overline{DMI} , $\overline{\sigma_{SMI}}$, $\overline{\sigma_{DMI}}$ are the mean values of SMI, DMI, and σ_{SMI} , σ_{DMI} at four positions. The statistic results are showed in Table 14~15.

Table 12. The murmurs indexes in systole ($SMI \pm \sigma_{SMI}$).

SMI (mean±std)	A	P	T	M
NHS	0.17±0.02	0.15±0.02	0.15±0.02	0.16±0.02
ASD	0.21±0.03	0.19±0.03	0.19±0.02	0.20±0.02
VSD	0.21±0.04	0.23±0.04	0.21±0.04	0.21±0.03
TOF	0.24±0.04	0.26±0.05	0.23±0.04	0.23±0.04

Table 13. The murmurs indexes in diastole ($DMI \pm \sigma_{DMI}$).

DMI (mean±std)	A	P	T	M
NHS	0.17±0.03	0.17±0.03	0.16±0.02	0.17±0.02
ASD	0.17±0.01	0.16±0.02	0.15±0.01	0.15±0.01
VSD	0.17±0.02	0.18±0.03	0.17±0.02	0.17±0.02
TOF	0.17±0.02	0.19±0.03	0.17±0.02	0.17±0.03

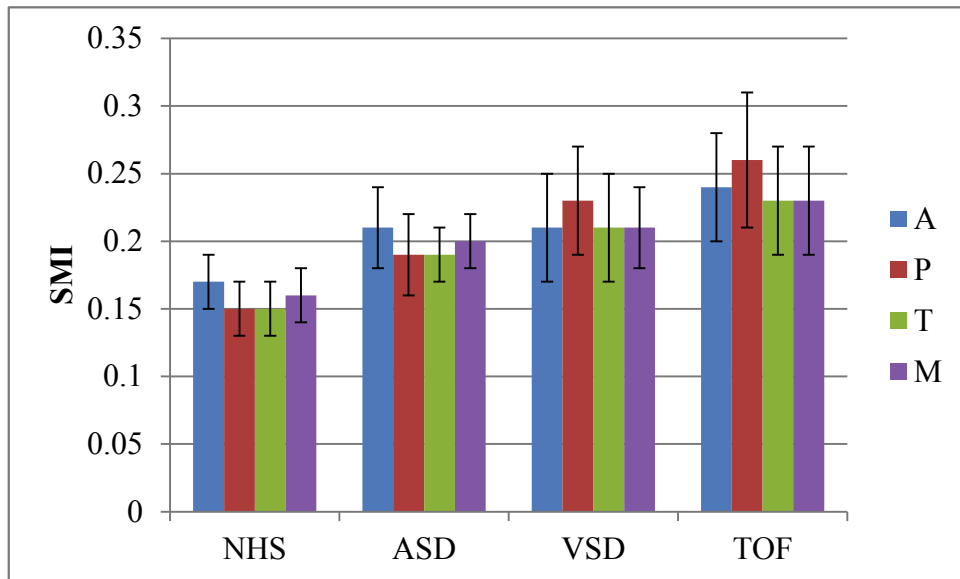


Fig. 39. The histogram statistics of double moment feature values in systole

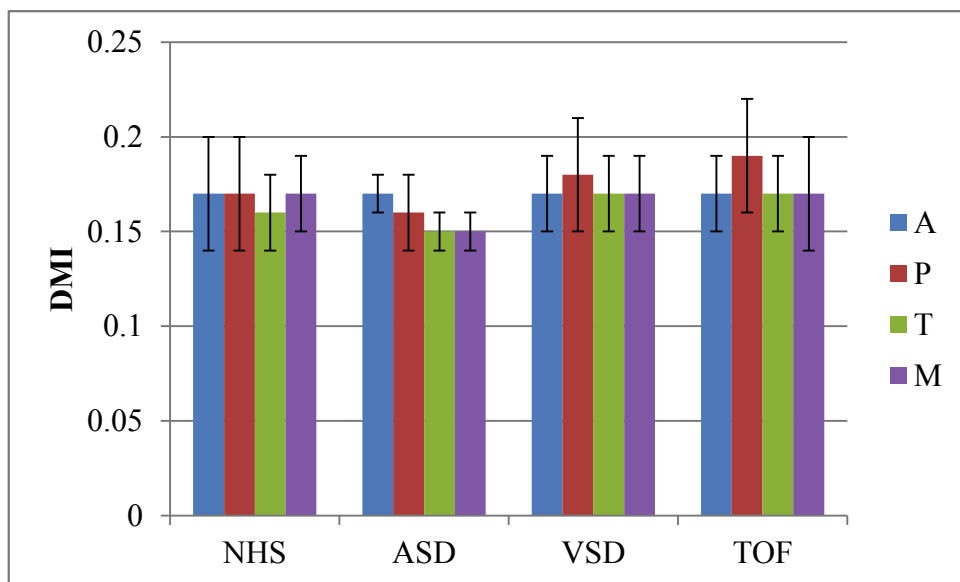


Fig. 40. The histogram statistics of double moment feature values in diastole

Table 14. The MIL of systole (SMI) and diastole (DMI).

Parameters	SMI	$\overline{\sigma_{SMI}}$	SMIL	DMI	$\overline{\sigma_{DMI}}$	DMIL
NHS	0.158	0.020	0.18	0.168	0.025	0.19
ASD	0.198	0.025	0.22	0.158	0.0125	0.17
VSD	0.215	0.038	0.25	0.173	0.0225	0.20
TOF	0.240	0.043	0.28	0.175	0.025	0.20

Table 15. the MIL definition of systole and diastole.

MIL	No murmur level 0	level 1	level 2	level 3
MIL	0~0.20	0.20~0.25	0.25~0.30	Over 0.30

3.4 Summary

In order to further quantitatively analyze the cardiac murmurs at each cardiac cycle, the murmur index extraction based on cardiac vibration state by describing the shape of different-scale window MW was proposed in this section. Firstly, the homomorphic segmentation of multichannel HS cycle (T) and fundamental HS (S1S2) is proposed based on homomorphic MW extraction with window length l ($l=T/2$), the HS cycle and S1S2 segmentation were implemented by locating the maximum and minimum of MW respectively, and the HR was also calculated, the cycle automatic segmentation accuracy yielded the highest of 100%, the lowest accuracy was even up to 98.1%. Meanwhile, the S1S2 segmentation accuracy yielded the highest of 100%, the lowest accuracy was even up to 97.5%.

Secondly, considering the segmentation points of HS S1S2 and cycle as MW centers respectively, to extract the systolic MW and diastolic MW with different window lengths ($T/8$ and $3T/8$), furthermore, extracting DWF such as SMI and DMI which were proposed based on systolic and diastolic MW with window length $T/4$. And many experiments showed that the original clinical HS signal included more murmur components when the DMF was high and its value over 0.20. The MIL was defined to evaluate murmur quantitatively, MIL which is less than 0.20, it is defined that there is no murmur, and MIL is belong to 0.20~0.25, it is murmur level 1, and belong to 0.25~0.30, it means murmur level 2, and If MIL is more than 0.30, it is defined that the murmur level is 3. These simple evaluation limits are used to estimate the clinical CHD murmur quantitatively.

Finally, many experiments show that the murmur indexes are efficient to judge the murmur occurring periods and degree. Importantly, DMF can be computed by moment analysis very fast and simple, and therefore it's very useful to auto-diagnosis or aided-diagnosis in an artificial intelligence cardiac murmur analysis system.

References

- [1] Patient, 1978. <http://patient.info/doctor/heart-murmurs-in-children>. Accessed June 14, 2015.
- [2] Valafar H., Valafar F., Darvill A., Albersheim P., Kutlar A., Woods K.F., Hardin J., Predicting the effectiveness of hydroxyurea in individual sickle cell anemia patients, *Artificial Intelligence in Medicine*, 2000, 18(2): 133-148.
- [3] CONGENITAL HEART DISEASE, 2011. <http://www.pted.org/?id=list#1>. Accessed July 28, 2014.
- [4] Amer Abdullah Lardhi, Prevalence and clinical significance of heart murmurs detected in routine neonatal examination, *Journal of the Saudi Heart Association*, 2010, 22(1): 25-27.
- [5] Ting Tao, Haibin Wang, Xiaochen Wu, Zhongwei Jiang, Shuping Sun. Study on cardiac murmurs evaluation based on wavelet packet energy distribution. The 3rd International Symposium on Digital Manufacturing , pp: 159-164.
- [6] Zhongwei Jiang¹, Ting Tao¹, Haibin Wang². New Approach on Analysis of Pathologic Cardiac Murmurs Based on WPD Energy Distribution, *Journal of Healthcare Engineering*, Vol 5, No.4, 2014, pp375-392.
- [7] Ting Tao¹, Zhongwei Jiang¹, Yu Fang¹, Haibin Wang². Multichannel Cardiac Sounds In-home Measuring System for Monitoring Children's Congenital Heart Disease, Evaluation of a Magnetic-Geared Induction Motor (MAGDA), 2014, pp.343-348
- [8] Zhonghong Yan^{a,*}, Zhongwei Jiang^{b,1}, Ayaho Miyamoto^b, YunlongWei^a, The moment segmentation analysis of heart sound pattern. *Computer Methods and Programs in Biomedicine* 98 (2010) 140-150.
- [9] P.Viola, M.Jones, Robust real-time object detection, Technical Report, COMPAQ Cambridge Research Laboratory, 2001.
- [10] Target Heart Rates. American Heart Association. 4 Apr 2014. Retrieved 21 May 2014.

Chapter 4

Unexpected Noise Reduction for Improvement of Auscultation

The medical automatic diagnosis based on the mobile platform or home health care will become more and more widely acknowledge. The heart disease is yet one of the most important causes of death in the world population. Therefore, more attention has been paid to an artificial intelligence PCG analysis system on computer or mobile platform. Heart auscultation is a simple, non-invasive and cost-effective technique to provide an important source of clinical information related to heart mechanical action. PCG records HS which contain two main components S1and S2, and murmurs by electronic stethoscope on chest skin can be used to detect heart diseases with high accuracy.

1. Unexpected noise problems of clinical heart sound

In a PCG automatic diagnostic system, the main obstacle is the PCG signal noise [1-3]. The noises coming from various sources contaminate HS signals and affect heart disease detection. The noises mainly include two groups, external factor and internal factor [2]. The external disturbances, shown in Fig.1~2, include a wide frequency and intensity spectrum of signal from ambient noise in surrounding environment, noise of contact between stethoscope diaphragm and skin, device power interference, and its distortion. Whereas, the internal disturbances, shown in Fig.3~4, consists of mainly signals caused by digestive and respiratory processes, such as sounds from internal organs, respiratory or lung sounds, and skin movements. Moreover, there are many other types of noises, such as vocal, physiological, sensor and so on. While, some HS signals which also have similar character to noise may indicate the occurrence of heart diseases, and affect the effect of auscultation

seriously [3]. Therefore, noise reduction method development is of great importance and it is the research subject of many research fields.

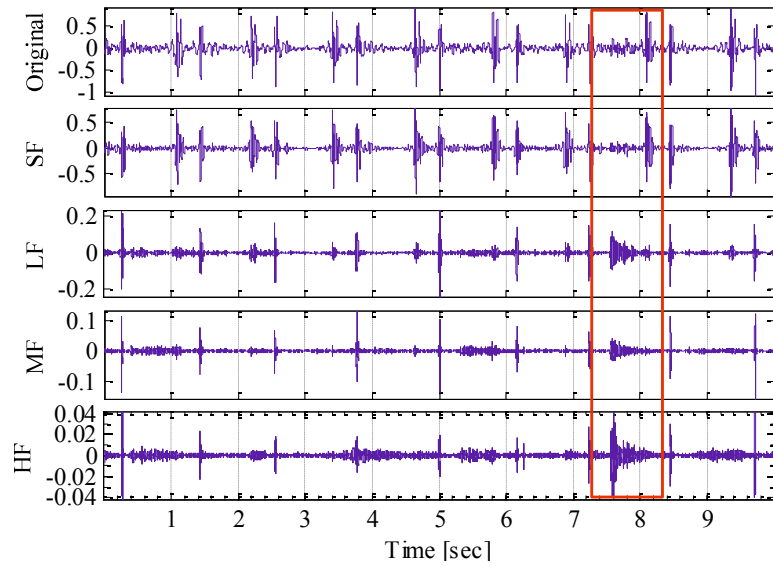


Fig.1. Original Normal HS and the signals at different frequency bands (SF, LF, MF, HF), the door slam noises shown in red box

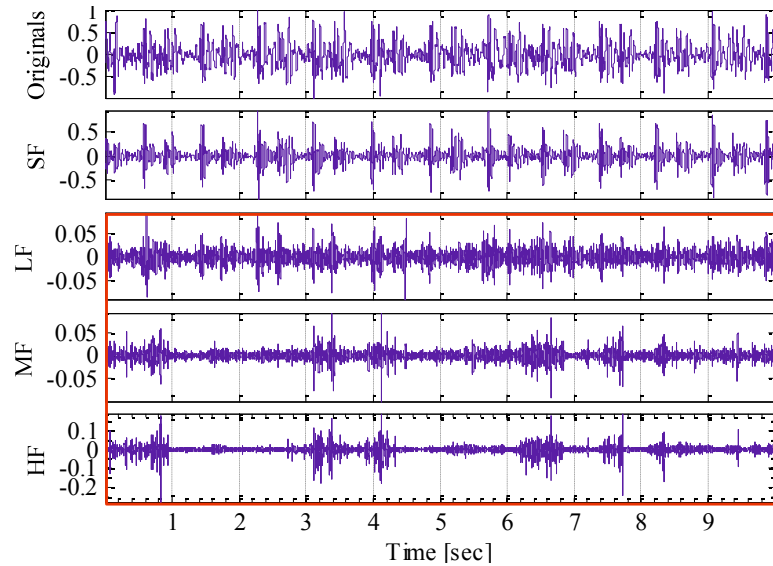


Fig.2. Original CHD HS and the signals at different frequency bands (SF, LF, MF, HF), the electronic noise and car horns noise shown in red box

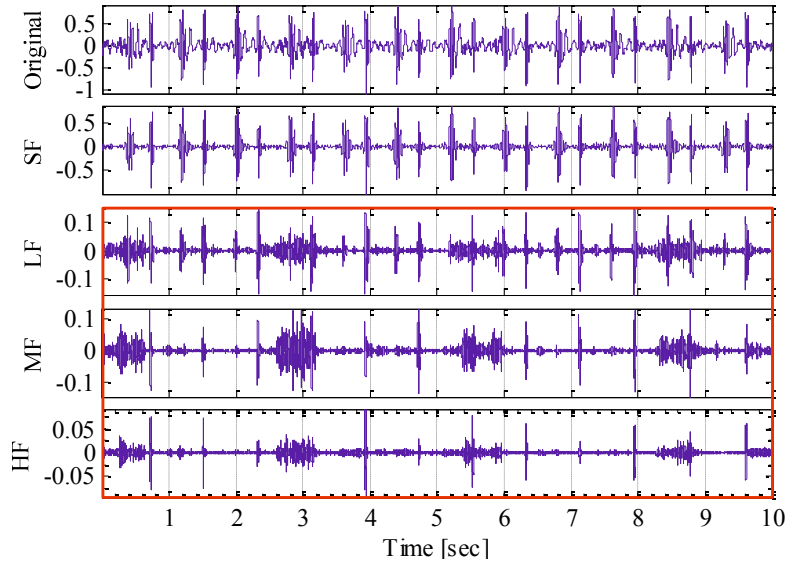


Fig.3. Original Normal HS and the signals at different frequency bands (SF, LF, MF, HF), the strong breath sounds shown in red box

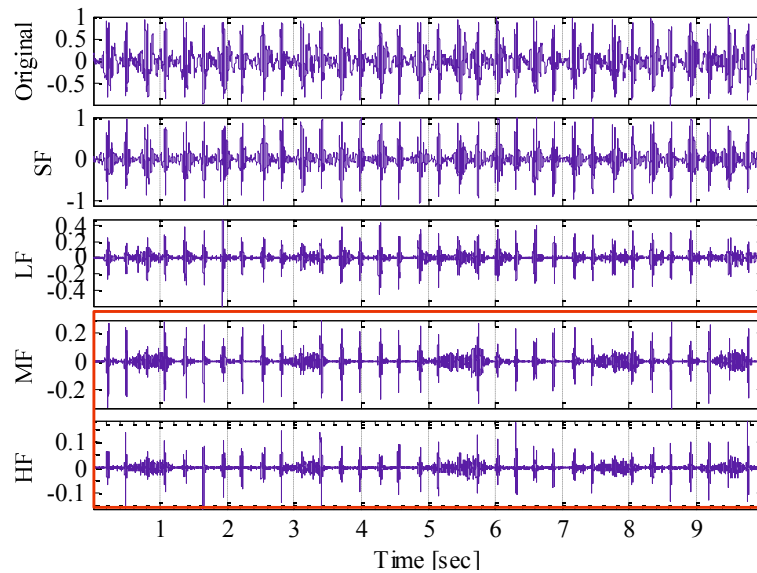


Fig.4. Original CHD HS and the signals at different frequency bands (SF, LF, MF, HF), the strong breath sounds shown in red box

2. Reviews of noise reduction methods

The most common methods of noise reduction can be summarized into two categories. One is filtrating in time domain, the other is in frequency domain. Recently, to cancel these unwanted components, the DWT or continuous wavelet transform, tunable-Q wavelet transform etc. are used to filtrate noise due to the fact wavelet transform can provide good resolution or localization in both time and frequency domains [3-11]. However, the artificially designed center frequency of this wavelet transform may not adaptive to a signal; this is a common problem in wavelet transform. The

characteristics of a mother wavelet function always affect the performance of time-frequency analysis, and its optimal wavelet parameter is not easy to choose. On the other hand, generally, wavelet-based noise cancellation will damage the original signal because HS signal often includes many different frequency components at the same time or many different time components in same (or close) frequency. In fact, all of the existing wavelet transforms use multiple-levels decomposition to realize frequency subdivision, but it is regretted that the designed frequency subdivision always make the original signal fragmentation. Recent years, TVD method is also used in HS analysis [18], but TVD is much more suitable to ‘block wave’ situations [16-18]. Fortunately, FSWT can provide more and better control in time and frequency domains [12-15].

The filtering properties of FSWT are presented in our study. According to the real power spectral density of a signal, the center frequency of a signal is easy to implant in FSWT directly, therefore the frequency slice processing of signal is an important idea, and noise reduction of clinical HS signal become the main focus in this paper. FSWT is first used to get the TFR of PCG signal, and then an image process method of TFR is proposed to solve our problem.

2.1 *Introduction of frequency slice wavelet transform method*

In our study [12-15], FSWT is defined as a new kind of TFR of a signal. For any $f(t) \in L^2(R)$, the FT of a window function $p(t)$ exists, and the FSWT is simplified as:

$$W_f(t, \omega, \sigma) = \frac{1}{2\pi} \int_{-\infty}^{\infty} \hat{f}(u) \hat{p}^*(\frac{u-\omega}{\sigma}) e^{iut} dt \quad (1)$$

Where, the scale $\sigma \neq 0$ is a constant or a function of ω and t , and the star ‘*’ means the conjugate of a function (the following is same). Here we call ω and t as the observed frequency and time, and u is the assessed frequency. $\hat{p}(\omega)$ is also called frequency slice function. And FSWT has inverse transformation. If the $\hat{p}(\omega)$ satisfies $\hat{p}(0) = 1$, then the original signal $f(t)$ can be reconstructed by,

$$f(t) = \frac{1}{2\pi} \int_{-\infty}^{\infty} \int_{-\infty}^{\infty} W_f(\tau, \omega, \sigma) e^{i\omega(t-\tau)} d\tau d\omega \quad (2)$$

FSWT has many better properties [12] than traditional wavelet transform, such as symmetry,

controllability, easy-to-design, dynamic scale, filter, and the reconstruction independency etc. Due to these new features, FSWT is more flexible to fit ever-changing signals than the classical methods.

HS de-noise is the main task in this paper, but we do not directly design any filter even if the original signal includes high noise. As a new filter method of FSWT application recommended in this paper, the image process idea of TFR is introduced to implement the signal filter in time-frequency domain directly, where we only need to choose a simple parameter to control the filter processing.

2.2 A natural assumption

The time or frequency components of a PCG signal are usually overlap and its noise will aggravate the situation. One way to detect these complexities presented in a PCG signal is to study the time-frequency relationship. We have a sample assumption about these time or frequency components as following. Assumption: Each of time-frequency components of PCG are connected at local area on its TFR image.

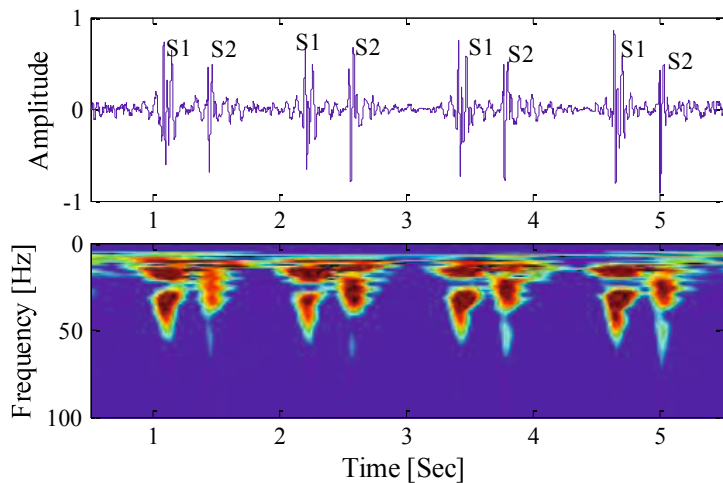


Fig. 5. The original clinical normal HS signal and its time-frequency representation (TFR) image with real-life noise.

Fig. 5 shows the connected time-frequency components of each S1 and S2 of a normal clinical HS signal clearly. The ambient noises are usually presented in extensive frequency bands randomly and in low energy state on TFR plane, and this character is used to signal filtrating significantly in this paper.

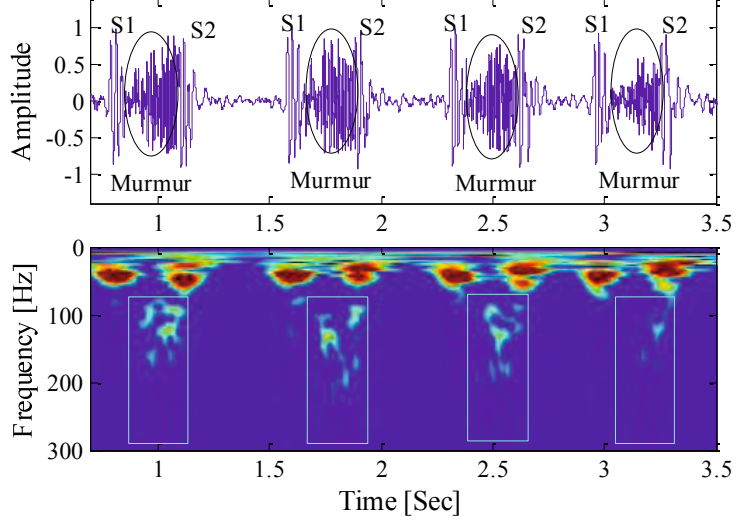


Fig. 6. The original clinical abnormal HS signal and its time-frequency representation (TFR) image of ventricular septal defect with real-life noise.

Fig. 6 shows the S1 and S2 of an abnormal HS signal for each high energy area with frequency band from 20 Hz to 80 Hz. The heart murmurs mainly distribute in high frequency bands, and the low frequency bands are probable the background or device noise. The different connect types of TFR image are clear to show the different clinical information of HS signals.

3. Noise reduction methods

3.1 Noise reduction by discrete wavelet transform method

Wavelet analysis provides both time and frequency localization and the resultant wavelet coefficients can be used as features in classifiers. The wavelet representation of a signal is sparse compared to time domain representation due to energy compaction property of wavelet transform. In order to decompose the heart rate variability signal into time-frequency components, a basis function at scale a and location b is defined as

$$\varphi_{a,b}(t) = \frac{1}{\sqrt{a}} \varphi\left(\frac{t-b}{a}\right) \quad (3)$$

Eq. (3) defines continuous wavelet transform. It is sampled on a dyadic grid to obtain the DWT. The basis function of DWT at scale 2^{-m} and the time instant n is given by,

$$\varphi_{m,n}(t) = 2^{-m} \varphi(2^{-m}t - n) \quad (4)$$

Using the dyadic wavelets, and DWT of the signal $x(t)$ is given by,

$$T_{m,n} = \int_{-\infty}^{\infty} x(t) \varphi_{m,n}(t) dt \quad (5)$$

The inverse of DWT is given by,

$$x(t) = \sum_{m=-\infty}^{\infty} \sum_{n=-\infty}^{\infty} T_{m,n} \varphi_{m,n}(t) \quad (6)$$

To decompose a signal, the basis function shape must be similar to that of the signal. The HS signal is decomposed using db10 into 10 layers.

DWT have been successfully applied in many fields [3, 4, 7]. DWT can decompose the original signal into different scales components, and these decomposed components do not have same sample resolution, low frequency bands have low sample resolution. The detail algorithm of DWT noise reduction method is expressed as bellows,

- (1) Obtain the maximum value T_m of wavelet decomposition vector (T_v) according to Eq. (5).
- (2) Choose an adjustment parameter $\alpha > 0$.
- (3) Adjust the TFR image as $DWT^{adj} = T_v(1 - e^{-\alpha|T_v|/T_m})$.
- (4) Reconstruct the signal from DWT^{adj} by Eq. (6).

This property may be disadvantage to low frequency bands that may include high energy. The common filter method based on DWT used to cut or adjust the high frequency components, and then reconstruct the estimated signal by inverse DWT.

3.2 Noise reduction by total variance de-noise method

TVD is an approach for noise reduction developed so as to preserve sharp edges in the underlying signals. It is also often used for image filtering and restoration, in this study it was used to compare with the proposed method. TVD method was introduced by Rudin, Osher, and Fatemi [16], and it is an effective filtering method for recovering piecewise-constant signals [17-18]. The derivation is based on the min-max property and the majorization-minimization (MM) procedure.

TVD assumes that the noisy data $y(n)$ is of the form

$$y(n) = x(n) + w(n), \quad n = 0, \dots, N - 1 \quad (7)$$

Where $x(n)$ is a piecewise constant signal and $w(n)$ is white Gaussian noise, TVD estimates the signal $x(n)$ by solving the optimization problem:

$$\min_x \left\{ F(x) = \frac{1}{2} \sum_{n=0}^{N-1} |y(n) - x(n)|^2 + \lambda \sum_{n=1}^{N-1} |x(n) - x(n-1)| \right\} \quad (8)$$

The regularization parameter $\lambda > 0$ controls the degree of smoothing. Increasing λ gives more weight to the second term which measures the fluctuation of signal $x(n)$ [19].

TVD is a method to smooth signals based on a sparse-derivation signal model. And it is formulated as minimization of non-differentiable cost function. Unlike a conventional low-pass filter, the output of the TVD filter can only be obtained through a numerical algorithm. TVD is most appropriate for piecewise constant signals, however, it has been modified and extended so as to be effective for more general signals [19].

3.3 Noise reduction by histogram curve adjusting method

Histogram curve adjusting of an image is frequently used in image processing, and the contrast enhanced map is an often used tool that make image of interest objectives more clearly and this idea is used in this paper. HCA method is implemented to modify TFR image computed by FSWT, and de-noise the PCG signal. The histogram curves are very similar to the exponential damping curve, shown as in Fig.7: s0 is a standard NHS original signal (from 3M database), adding white noise from 10% to 50% respectively. The curve descends more slowly means it contains much more noises, this property is therefore used to noise reduction by adjusting damping speed of HCA, the detail algorithm is expressed as bellows,

- (1) Compute the maximum $M = \max_{t,\omega} |W_f(t, \omega, \sigma)|$ according to Eq. (1).
- (2) Choose an adjustment parameter $\alpha > 0$.
- (3) Adjust the TFR image as $W_f^{adj}(t, \omega, \sigma) = W_f(t, \omega, \sigma) (1 - e^{-\alpha |W_f(t, \omega, \sigma)| / M})$.
- (4) Reconstruct the signal from $W_f^{adj}(t, \omega, \sigma)$ by Eq. (2).

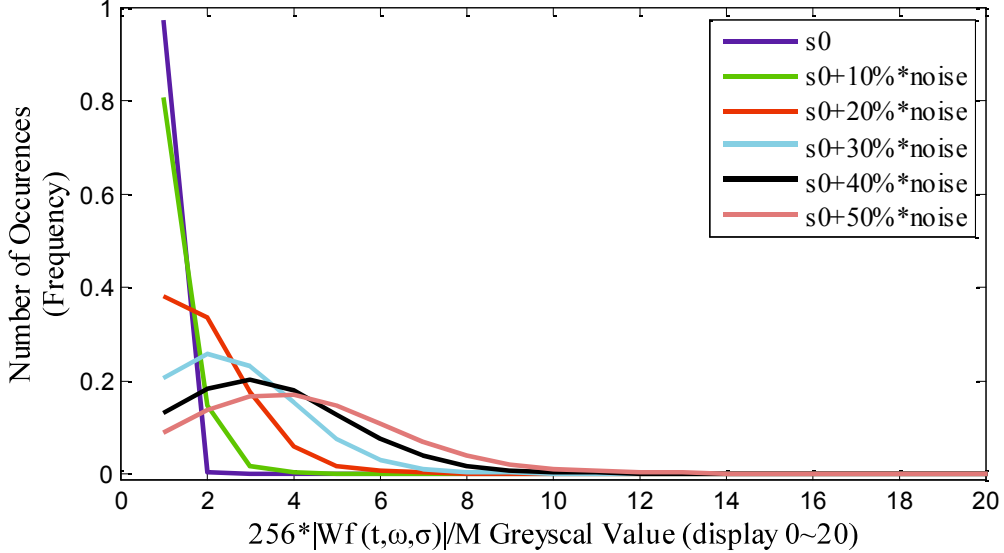


Fig. 7 Histogram curves of FSWT from a standard NHS original signal s_0 , adding white noise from 10% to 50% respectively.

From Fig.7, we can find that, the energy which is divided in to 256 parts $256 * |W_f(t, \omega, \sigma)|/M$ which expressed as greyscale values, and the y-axis means the occurring times at one energy scale.

And the validation performances are implemented in the next section, which is used to determine the optimal adjustment parameters for these three noise reduction methods.

4 Validation

In order to find the optimal adjustment parameter α and regularization parameter λ , the evaluation indicators SNR and CC of the noise reduction method are performed in this paper, SNR is defined as

$$SNR = 10 \log_{10} \left(\frac{P_{signal}}{P_{noise}} \right) \quad (9)$$

Where P_{signal} is power of original signal, P_{noise} is the power of noise signal. CC was defined as:

$$CC = \frac{\sum Y\hat{Y} - \frac{\sum Y\hat{Y}}{N}}{\sqrt{(\sum(Y)^2 - \frac{(\sum Y)^2}{N})(\sum(\hat{Y})^2 - \frac{(\sum \hat{Y})^2}{N})}} \quad (10)$$

We denote Y as the original signal, \hat{Y} as the estimated signal after de-noising by noise reduction methods, and N as the length of signal,

At last, the noise reduction methods are evaluated by MSE between the original signal Y and de-noised signal \hat{Y} , MSE is defined as

$$MSE = \frac{1}{N} \sum_N (Y - \hat{Y})^2 \quad (11)$$

5 Comparison of noise reduction methods

5.1 Comparison of standard HS noise reduction

The effects of these noise reduction methods at different noise levels are investigated to acquire the optimal de-noising information. Firstly, SNR and CC are employed to evaluate the capability of noise reduction for attenuating noise. SNR and CC variation trend for noise reduction at different noise level are shown in Fig.8~10. The optimal parameters α and λ can be also determined by searching the maximum SNR and CC at each noise level, and shown with blue star marks in Fig.8~10. Based on many experiments statistic, the appropriate parameters are recommended in a certain range (mean \pm variance) presented in Table 1 for these three methods. For α selection, which is decreasing with the increase of noise, however, λ selection is opposite. It is obvious that HCA has more robustness for the adjustment parameter α , because it changes more slowly than others in Fig. 8~10, in another word, TVD and WDT are more sensitive to their adjustment parameters than HCA.

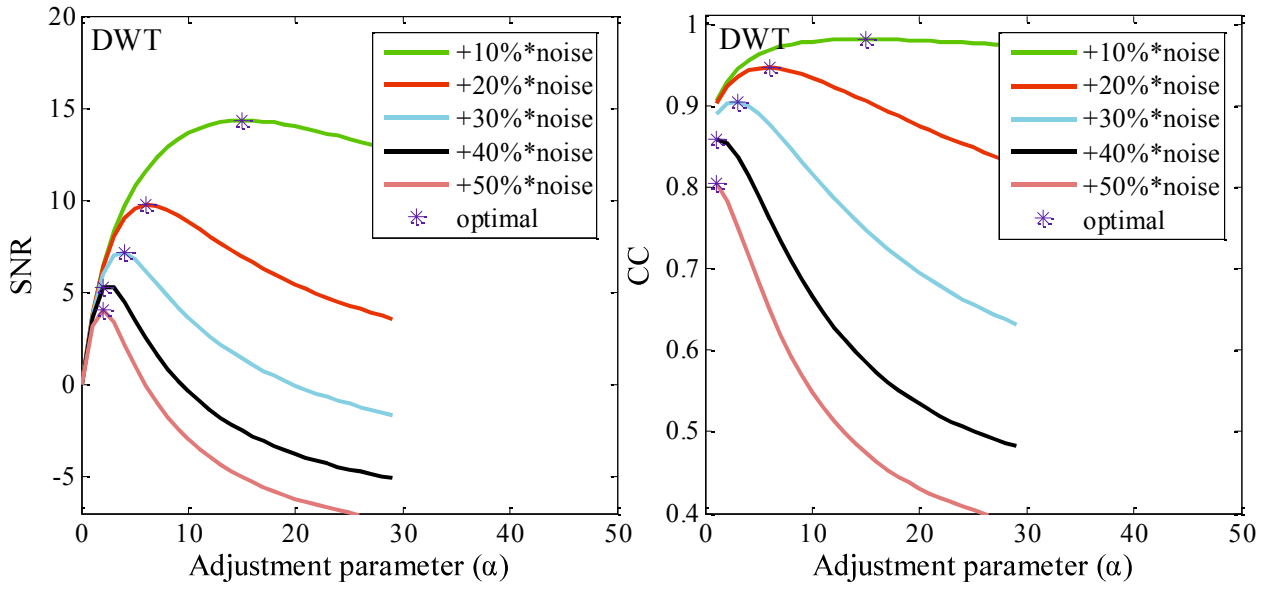


Fig.8. DWT method: SNRs and correlation coefficients tendency with different adjustment parameters for different noise levels from 10% to 50% respectively, and the blue star mark '*' is the optimal adjustment parameter at each noise level.

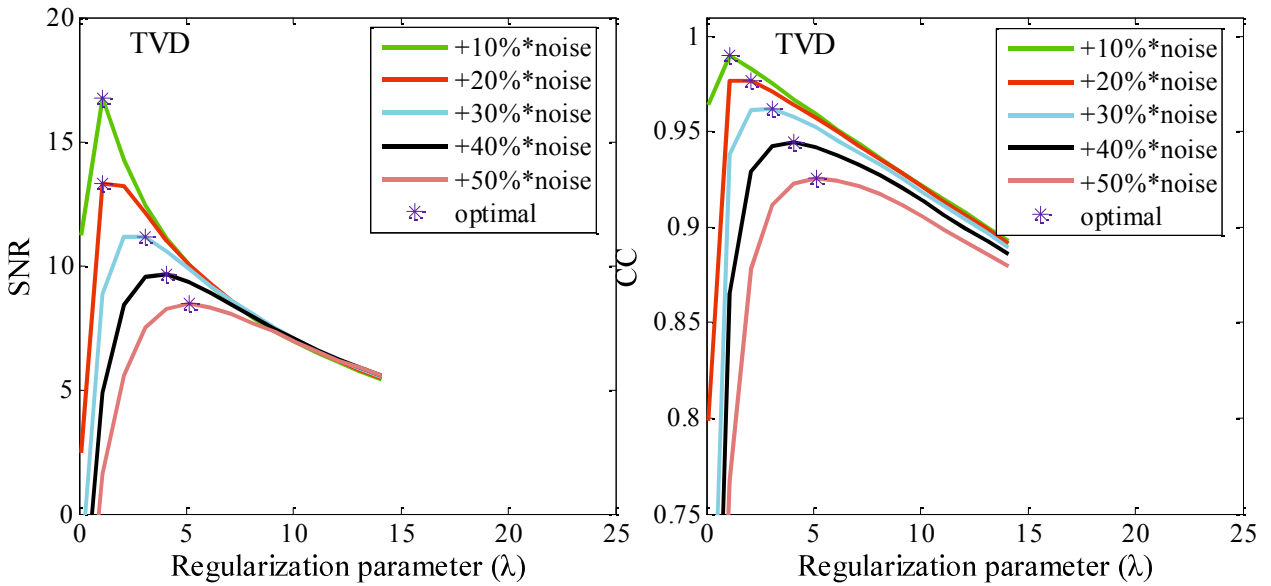


Fig. 9. TVD method: SNRs and correlation coefficients tendency with different regularization parameters for different noise levels from 10% to 50% respectively, and the blue star mark '*' is the optimal regularization parameter at each noise level.

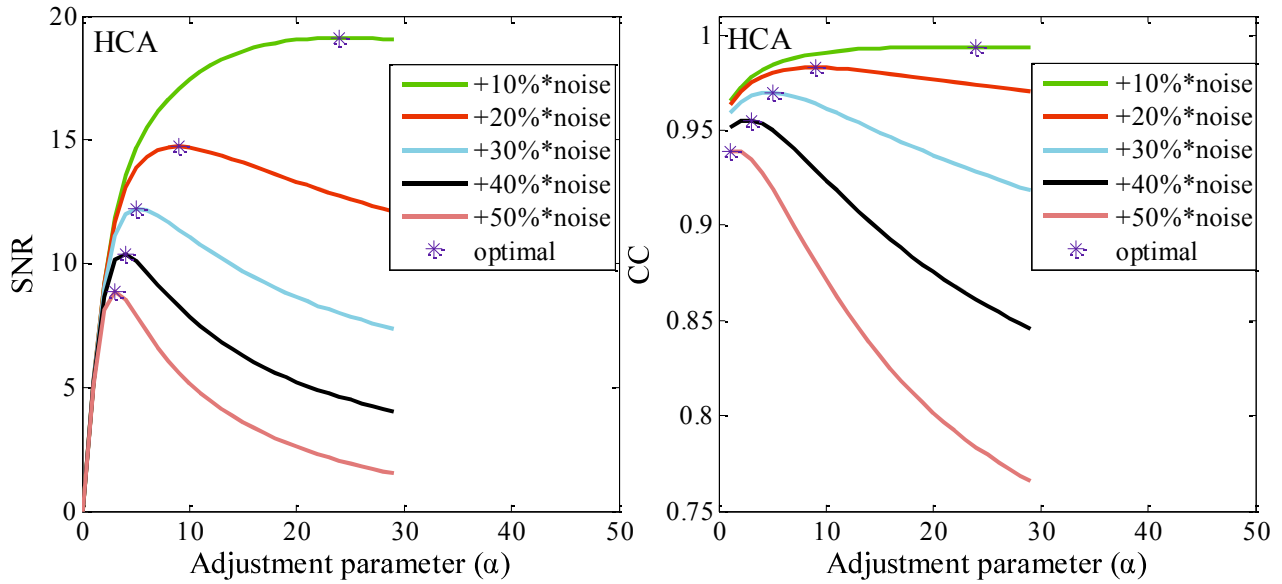


Fig. 10. HCA method: SNRs and correlation coefficients tendency with different adjustment parameters α for different noise levels from 10% to 50% respectively, and the blue '*' is the optimal adjustment parameter at each noise level.

Table1. Optimal parameters at five noise level with three de-noised methods.

Noise level	10%	20%	30%	40%	50%
α (DWT)	15.0 \pm 0.7	6.6 \pm 0.8	4.0 \pm 1.2	2.3 \pm 0.9	2.2 \pm 1.0
λ (TVD)	1.3 \pm 0.5	1.8 \pm 0.8	2.7 \pm 0.7	3.3 \pm 1.1	4.0 \pm 1.1
α (HCA)	31.1 \pm 6.8	13.2 \pm 3.9	8.0 \pm 2.7	5.8 \pm 2.1	4.6 \pm 2.1

Furthermore, the assessment parameters comparison of HCA, TVD and DWT for same signal with same noise levels from 10% to 50% respectively shown in Fig.11, the extremely improvement of performance of HCA method can be seen obviously, compare with TVD and DWT methods, HCA method further enhances the SNR and CC, and reduce the MSE. With the increase of noise level, the improvement can be seen much more obviously.

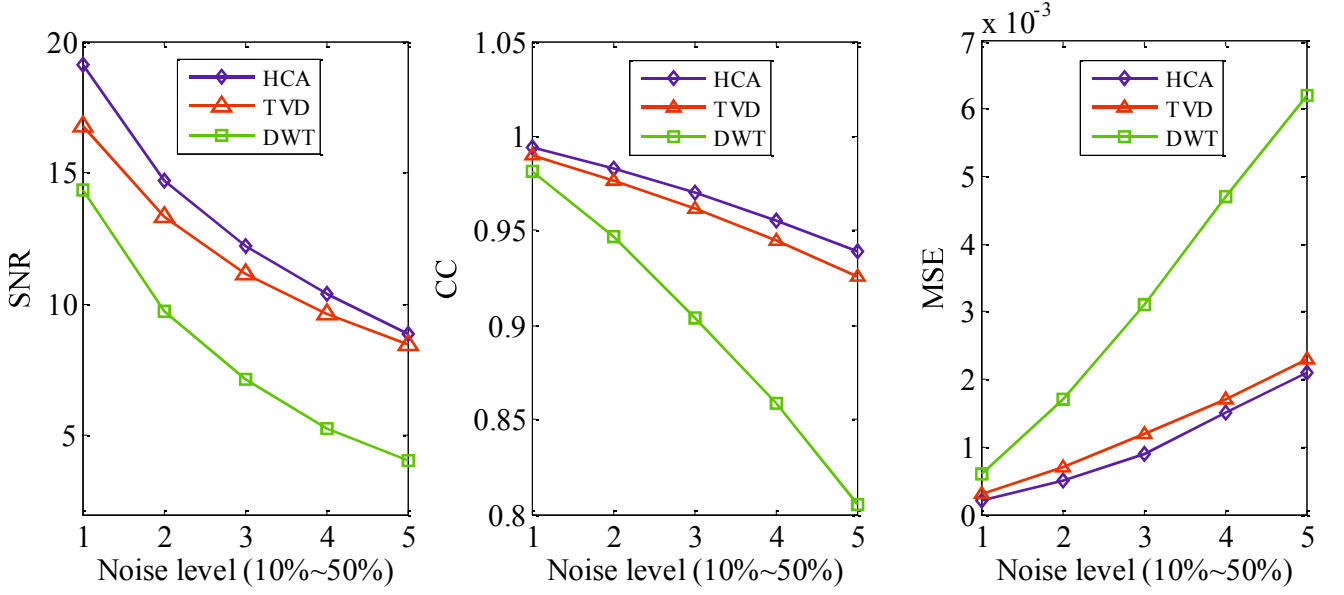


Fig.11 The SNR, CC and MSE curve at different noise levels with HCA, TVD and DWT methods.

And then, in order to show the effects of these noise reduction methods, we chose to add two noise levels (plus 10% and 30%), respectively, to normal HS (from 3M database) which has no noise, and the results showed in Fig.12. When the noise level is 10%, the effects of these three de-noised methods are almost similar from time domain waveform, shown in Fig.18 (a). While, compare to 10% noise situation, when noise level is 30%, we found there are some obvious different of these de-noised signals in Fig.12 (b), from the de-noised signal with TVD method, which seemed there are strongest correlation with the original signal especially for low frequency bands, but the peak parts of the signal were squared severely for high frequency parts. About the de-noised signal with DWT method, the waveform is kept well compared with TVD, but there are lots of residual noises. At the same time, the de-noised signal with HCA method, we also can found several residual noise parts, but from the sense of hearing, the basic HS can be heard most clearly and comfortable in three methods.

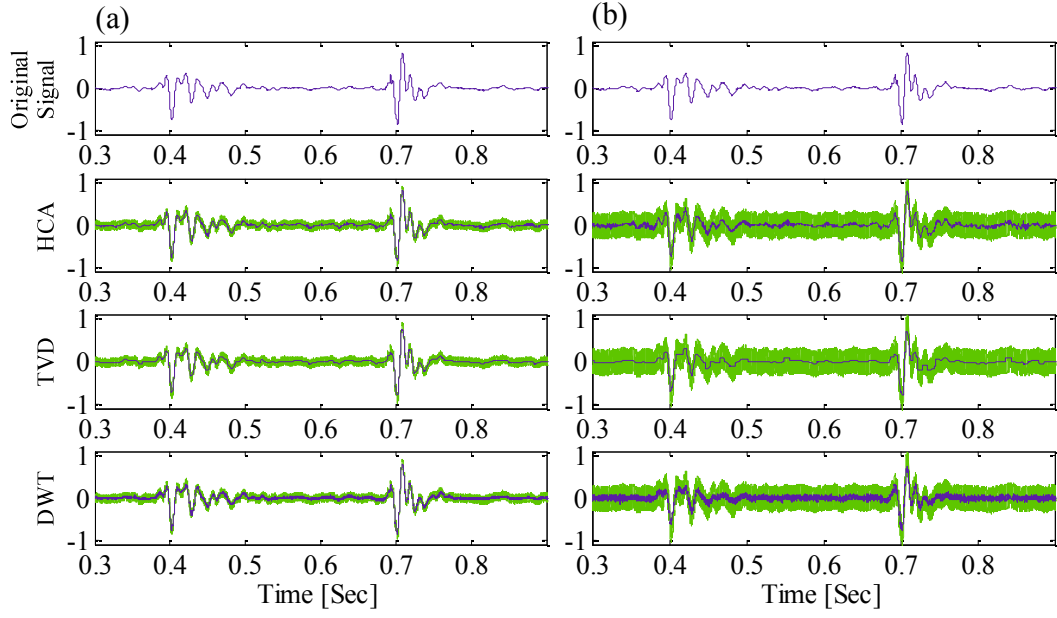


Fig.12 Time domain noised signals (green) and de-noised signals (blue) by HCA, TVD and DWT methods. (a) Plus 10%noise (b) Plus 30%noise

5.2 Comparison of clinical noise reduction

In order to further illustrate the effectiveness of the proposed HCA noise reduction method, the cases of clinical HSs which were introduced in section 1, door slam noises and strong breath sounds were verified by these three noise reduction methods in this study, shown in Fig. 13~18.

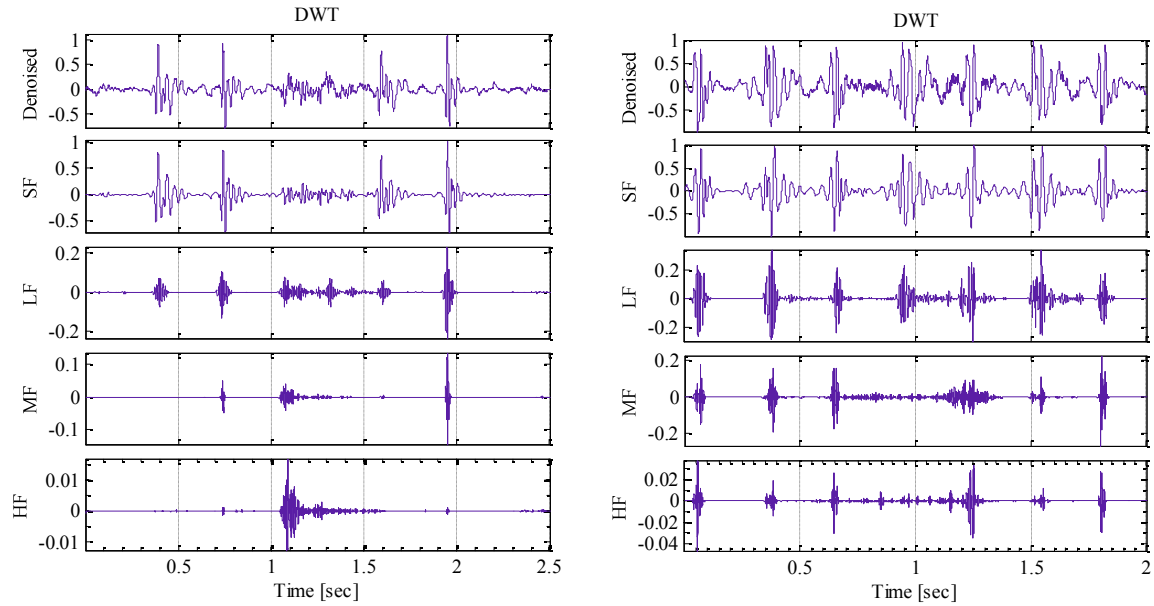


Fig. 13. Noise (in Fig.1) reduction by DWT. Fig. 14. Noise (in Fig.4) reduction by DWT.

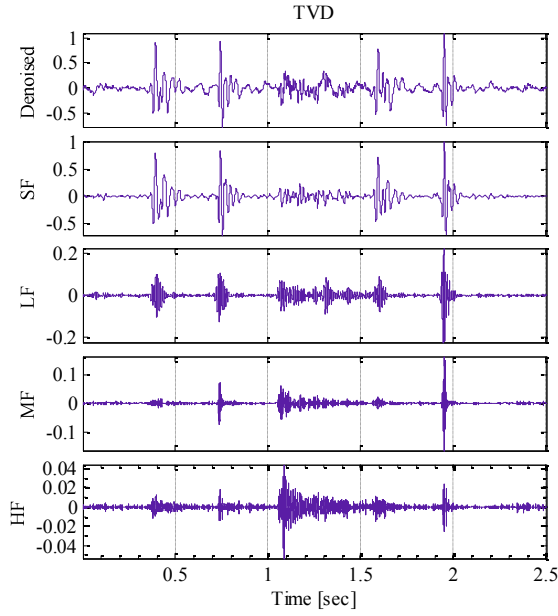


Fig. 15. Noise (in Fig.1) reduction by TVD.

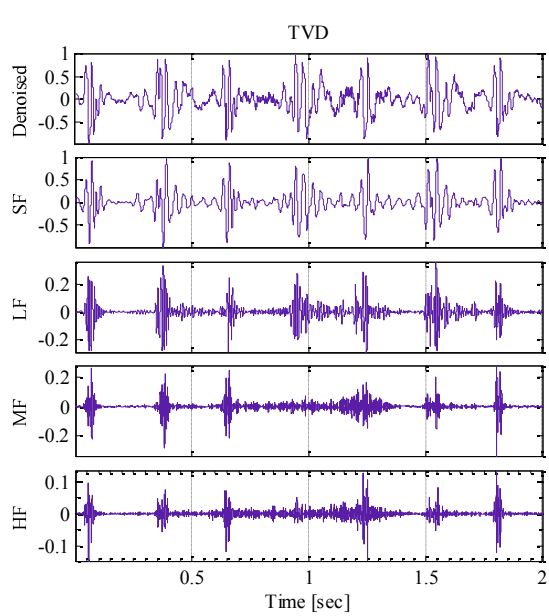


Fig. 16. Noise (in Fig.4) reduction by TVD.

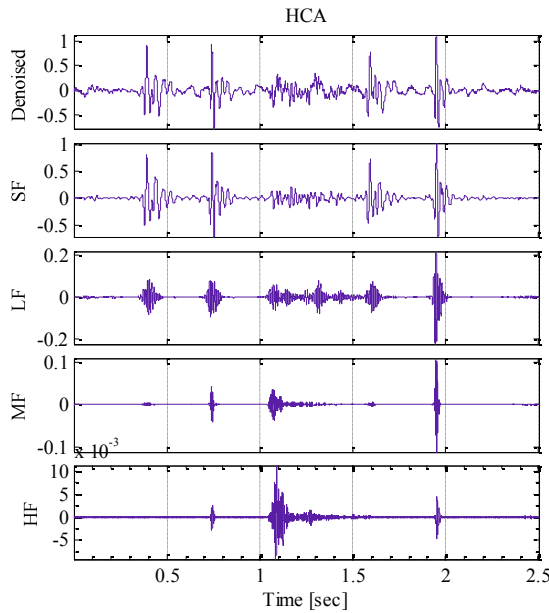


Fig.17 Noise (in Fig.1) reduction by HCA.

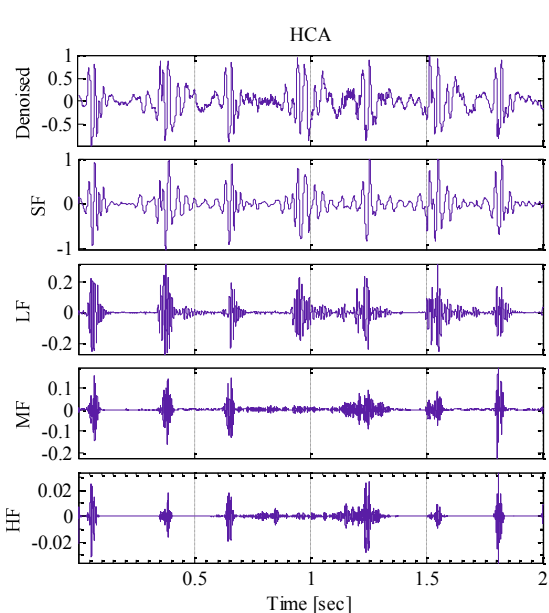


Fig.18 Noise (in Fig.4) reduction by HCA.

The noise reduction effects of door slam noise mixed in the NHS signals which showed in Fig.1, and the strong breath noise which shown in Fig. 4, are implemented by the three noise reduction methods and showed in Fig.13~18. As for the method TVD, the noises at LF, MF and HF bands are not reduced effectively, and the strong breath sounds which may affects the normal auscultation can

not be reduced efficiently. The TVD method compares to general signals, which is appropriate for those ‘block wave’ signals. As for DWT and HCA, we used the same FSWT decomposition and reconstruction techniques, the effectiveness are similar, but from the sense of hearing, the HCA method can give a good audio effect, that is because the energy distribution at LF, MF and HF bands (E_{LF} , E_{MF} , E_{HF}), which summarized in Table 2~3 showed, there noise which in high frequency bands are still remained with method DWT.

Table 2. The energy ratio at LF, MF and HF frequency bands of case 1 (door slam noise) in Fig 1.

Methods	$E_{LF}(\%)$	$E_{MF}(\%)$	$E_{HF}(\%)$
DWT	1.77	0.23	0.0027
TVD	2.45	0.46	0.0433
HCA	2.07	0.18	0.0017

Table 3. The energy ratio at LF, MF and HF frequency bands of case 2 (strong breath sounds) in Fig 2.

Methods	$E_{LF}(\%)$	$E_{MF}(\%)$	$E_{HF}(\%)$
DWT	3.11	0.58	0.0105
TVD	4.09	1.24	0.158
HCA	3.08	0.49	0.0102

Finally, in order to further illustrate the effectiveness of the proposed HCA noise reduction method, a case of clinical normal HS which was measured in a real life noisy environment was verified in this study, shown in Fig. 19~20. The noisy signals contain ambient noise, device power interference, noise of slamming the door (from 1 second to 1.5 seconds), vocal, and so on in the clinical signal. By comparing the time diagrams and phase space maps before and after noise reduction, we can find the proposed HCA method is much more effective for noise reduction and its phase space map curve is most smooth. We found the ambient noise, device power interference and vocal noises are removed clearly, and noise of slamming the door was almost reduced. It not only maintains the signal’s smooth, but also ensures the high-quality hearing effects. This effectiveness is very useful to clinical HS auscultation for medical care personnel and general users.

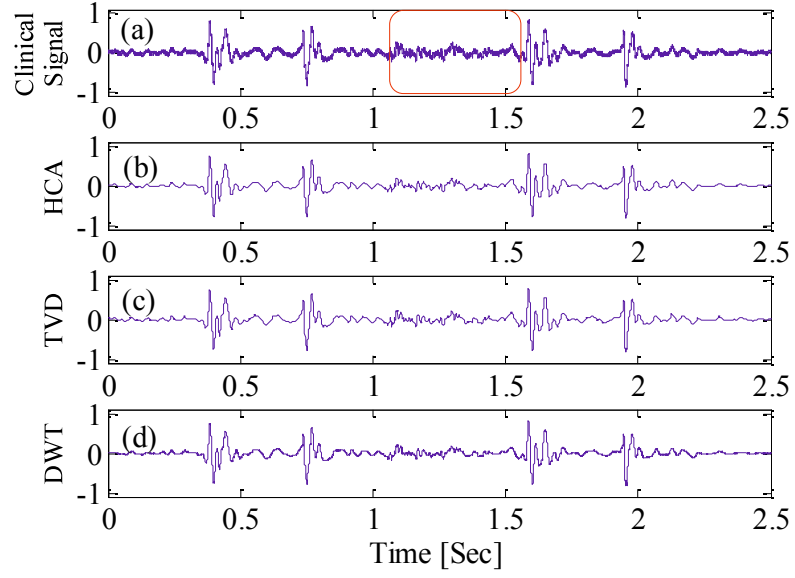


Fig.19. Time diagrams. (a) The raw clinical HS signal. (b) De-noised signal with HCA method.
(c) De-noised signal with TVD method. (D) De-noised signal with DWT method.

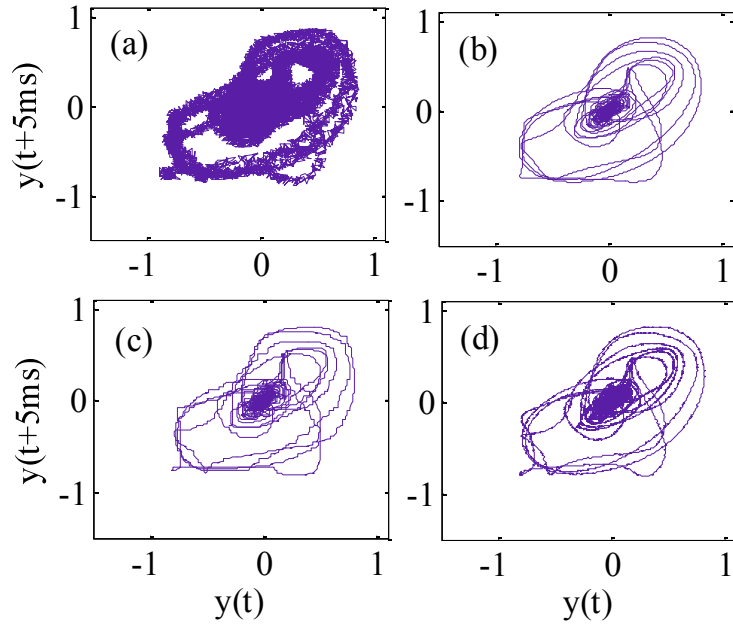


Fig.20. The phase space maps of HS signal. (a) The raw clinical HS signal. (b) De-noised signal with HCA method. (c) De-noised signal with TVD method. (D) De-noised signal with DWT method.

6 Summary

A novel noise reduction method based on FSWT that can consummate the filtrating in time and frequency domain simultaneously was proposed in this paper. The image process idea of TFR was used instead of designing filter directly. This method is assessed using SNR, CC and MSE evaluation indicators and comparing with the TVD and DWT methods, experimental results showed HCA

method is much more effective for external (ambient noise, speech noise, stethoscope device power interference) and internal (respiratory or lung sounds, and skin movements) disturbances noise reduction. Finally, a case of clinical HS is implemented to validate the proposed method can cancel the HS noise and interference adaptive, simple and correctly.

The proposed HCA noise reduction method not only maintains the signal's smooth, but also ensures the high-quality hearing effects, these performance advantages are very useful to clinical HS auscultation for medical care personnel and general users. Furthermore, it also even benefits for other physiological signal auscultation and further analysis of home medical and health care system.

References

- [1] Kehan Zeng ^{a,b*}, Mingchui Dong ^a, A novel cuboid method with particle swarm optimization for real-life noise attenuation from heart sound signals. *Expert Systems with Applications* 41 (2014) 6839-6847.
- [2] P. Varady, Wavelet-based adaptive denoising of phonocardiographic records, in: Proceedings of the 23rd Annual International Conference of the IEEE, Engineering in Medicine and Biology Society, 2001, vol. 2, <http://dx.doi.org/10.1109/IEMBS.2001.1020582>.
- [3] Dawid Gradolewski*, Grzegorz Redlarski, Wavelet-based denoising method for real phonocardiography signal recorded by mobile devices in noisy environment. *Computers in Biology and Medicine* 52 (2014) 119-129.
- [4] Henrique Mohallem Paiva ^{a,*}, Roberto Kawakami Harrop Galvao ^{b,1}, Optimized orthonormal wavelet filters with improved frequency separation. *Digital Signal Processing* 22 (2012) 622-627.
- [5] Tang, H., Li, T., Park, Y., & Qiu, T. Separation of heart sound signal from noise in joint cycle frequency-time-frequency domains based on fuzzy detection. *IEEE Transactions on Biomedical Engineering*, 57(2010), 2438-2447.
- [6] Hamed Shamsi, I. Yucel Ozbek*, Robust heart sound detection in respiratory sound using LRT with maximum a posteriori based online parameter adaptation. *Medical Engineering & Physics* 36 (2014) 1277-1287.
- [7] D S.M. Debbal*, F. Bereksi-Reguig, Automatic measure of the split in the second cardiac sound by using the wavelet transform technique. *Computers in Biology and Medicine* 37 (2007) 269-276.

- [8] Shivnarayan Patidar, Ram Bilas Pachori*, Segmentation of cardiac sound signals by removing murmurs using constrained tunable-Q wavelet transform. *Biomedical Signal Processing and Control* 8 (2013) 559-567.
- [9] Shivnarayan Patidar^a, Ram Bilas Pachori^{a*}, Niranjan Garg^b, Automatic diagnosis of septal defects based on tunable-Q wavelet transform of cardiac sound signals. *Expert Systems with Applications* 42 (2015) 3315-3326.
- [10] Shivnarayan Patidar, Ram Bilas Pachori*, Classification of cardiac sound signals using constrained tunable-Q wavelet transform. *Expert Systems with Applications* 41 (2014) 7161-7170.
- [11] Shivnarayan Patidar, Ram Bilas Pachori*, Constrained Tunable-Q wavelet Transform based Analysis of Cardiac Sound Signals. *AASRI Procedia* 4 (2013) 57-63.
- [12] Zhonghong Yan^{a,b,1}, Ayaho Miyamoto^a, Zhongwei Jiang^{a,2}, Frequency slice wavelet transform for transient vibration response analysis. *Mechanical Systems and Signal Processing* 23 (2009) 1474-1489.
- [13] Zhonghong Yan^{a,b}, Ayaho Miyamoto^{b,1}, Zhongwei Jiang^{b,2}, Xinglong Liu^{b,2}, An overall theoretical description of frequency slice wavelet transform. *Mechanical Systems and Signal Processing* 24 (2010) 491-507
- [14] Zhonghong Yan^{a,b,*1}, Ayaho Miyamoto^{b,2}, Zhongwei Jiang^{b,3}, Frequency slice algorithm for modal signal separation and damping identification. *Computers and Structures* 89 (2011) 14-26.
- [15] Zhonghong Yan^{a,*}, Zhongwei Jiang^{b,1}, Ayaho Miyamoto^b, YunlongWei^a, The moment segmentation analysis of heart sound pattern. *Computer Methods and Programs in Biomedicine* 98 (2010) 140-150.
- [16] L. Rudin, S. Osher, and E. Fatemi. Nonlinear total variation based noise removal algorithms. *Physica D* 60 (1992) 259-268.
- [17] I.W. Selesnick, I. Bayram, Total variation filtering, Technical Report, February 4, 2010.
- [18] F.I. Karahanoglu, I. Bayram, D. Van De Ville, A signal processing approach to generalized 1-D total variation, *IEEE Trans. Signal Process.* 59 (11) (2011 Nov) 5265–5274.
- [19] Ivan Selesnick, Total variation denoising (an MM algorithm), Technical Report, March 17, 2014.

Chapter 5

Multichannel Heart Murmur Monitoring System

Heart disease is the leading or the second cause of death for people in the world, according to American Heart Association report, in the United States, killing nearly 787,000 people alone in 2011, and the total cost is estimated to be 298 billion dollar [1]. 80% of the total mortality occurs in low and middle-income countries. In the recent year, the high concern about health management and medical instruments for health care and diagnosis in daily life. Due to the development of technology of medical treatment, the life duration of human beings has increased constantly and brings some new requests on in-home health care and management. The diseases CHDs are the most frequent form of major birth defects in newborns affecting close to 1% of newborn babies (8 per 1,000), CHDs are not always found during pregnancy or at birth, they also can not be cured, and they must be monitored throughout life [2]. Thus, if life-style related diseases could not be monitored continuously during a long period in the early stage, they might be difficult to be diagnosed appropriately.

A report [3] showed that among the patients who had heart murmurs and were referred by primary care physicians, just about 25% of them could be found to have pathology directly by echocardiography testing or closer examination. That means an expensive testing based on clinical assessment such as the CE, PCG, and PCI is probably not cost-efficient prior to the primary screening examination, especially in low and middle-income countries. In consequence, screening for heart diseases by clinical HS auscultation and HS analysis remain important for general daily

health care. CHD sounds including abundant helpful physiological and pathological information, especially the clinical CHD sounds. Thus, prescreening for CHD sounds will be greatly improve the prevention of clinical CHD in advance, and helpful to in the primary screening examination, and becomes stronger for the general users to perform the auscultation at home.

In this chapter, it will introduce the multichannel heart signals measuring system and Matlab GUI monitoring system. The detail content will be introduced in section 1 and section 2.

1. System design

The multichannel heart murmur monitoring system, shown in Fig.1, consists of the measuring system, shown in Fig.2, which was introduced in Chapter 2, the analysis server part and the monitoring system which will be introduced in Section 2 of this Chapter in detail.

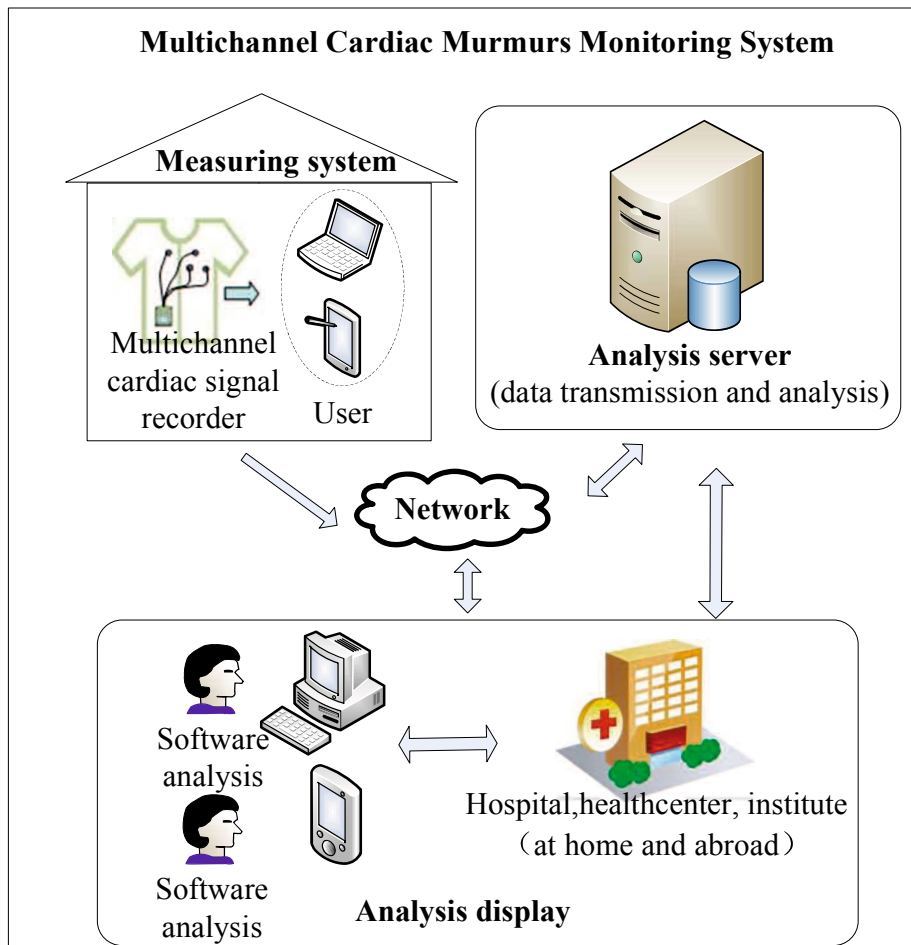


Fig.1. The multichannel heart murmur monitoring system.

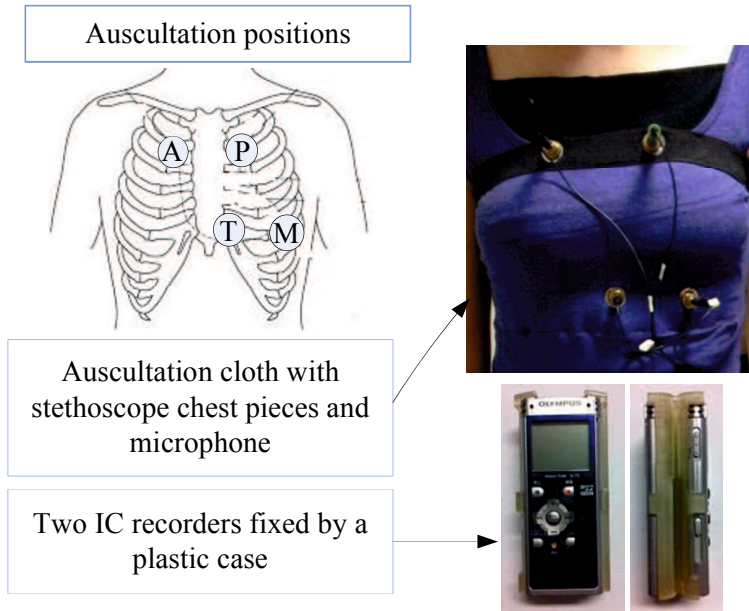


Fig. 2. Multichannel heart murmur measuring system.

2. Analysis engine

This GUI monitoring system functions showed in Fig.3, which include file reading (A), original multichannel signals display (B), each channel listening selection (C), including the original signals and de-noised signals which implemented in Chapter 3, multi-signals analysis (D) and multichannel parameters information (E). Meantime, the multi-signals parameter information (HR, DMFs, DMF_d, ICM_{LF}, ICM_{MF}, and ICM_{HF}) from four positions (A, P, T and M) can be displayed timely, it is easy and convenient to understand and use.

The four channels signals are analyzed based on analysis methodologies which were discussed in Chapter 4 in detail. In order to detect cardiac sound simple and conveniently, the mean value plus variance of feature parameters (MIL, TCM_{LF}, TCM_{MF} and TCM_{HF}) of NHS are chose as standard values. As for cardiac murmur intensity level, If DMF is less than 0.20, it means that there is no murmur, defined as level 0, and DMF is belong to 0.20~0.25, it is murmur level 1, and belong to 0.25~0.30, it means murmur level 2, and If DMF is more than 0.30, it is defined that the murmur level is 3. These simple evaluation limits are used to estimate the murmur strength quantitatively. As murmur evaluation, if the ICM values of detected signals are less than standard values (green bar in Fig.5 and Fig.7, middle column), they are considered that there may be no murmurs at these bands. However, if ICM values are more than standard values (red bar in Fig.7, middle column), they are

considered there may be murmurs at these bands. What's more, as for the NHS sample, we can see there are no significant differences between the four channel signals. Therefore, these analysis parameters may contribute to multi-channel cardiac signals' pathology analysis in our further study.

NHS and CHDs clinical signals samples will be discussion in Section 2.1~2.4 in detail, from the parameters. We can find much more information about the multi-signals from their four positions. This health care in-home system is not only suitable for doctors and parents to monitor the CHD patient's condition, but it also can be used for healthy persons to monitor their cardiac sound condition daily at home.

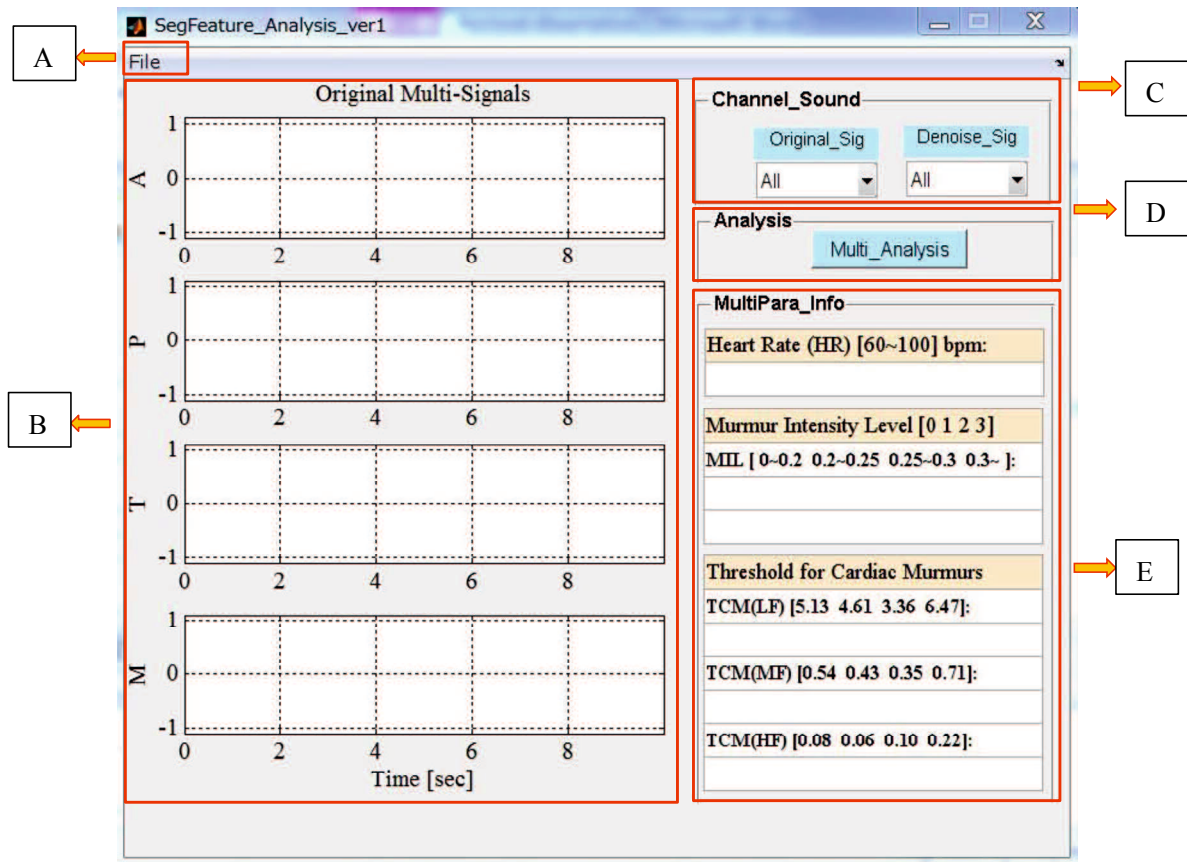


Fig.3. The GUI monitoring system.

3. Murmurs analysis indexes display

3.1 Discussion of normal heart sound (NHS) case

In this section, the cases of NHS with the GUI monitoring system will be discussed in detail. As for NHS case, which is showed in Fig.4~5, the HR is 90bpm, which is within the normal range

(60~100) bpm. The cardiac murmur evaluation parameters which showed in Fig.5 (middle column), are displayed with green bar meaning there are no murmur at these frequencies. And the murmur appearance period and intensity level parameters which showed in Fig.5 (right column), are revealed the MIL is 0 (level 0) that means there are no murmur at systolic and diastolic periods. The judgment values of the multichannel signals from the four positions are displayed in Fig.4.

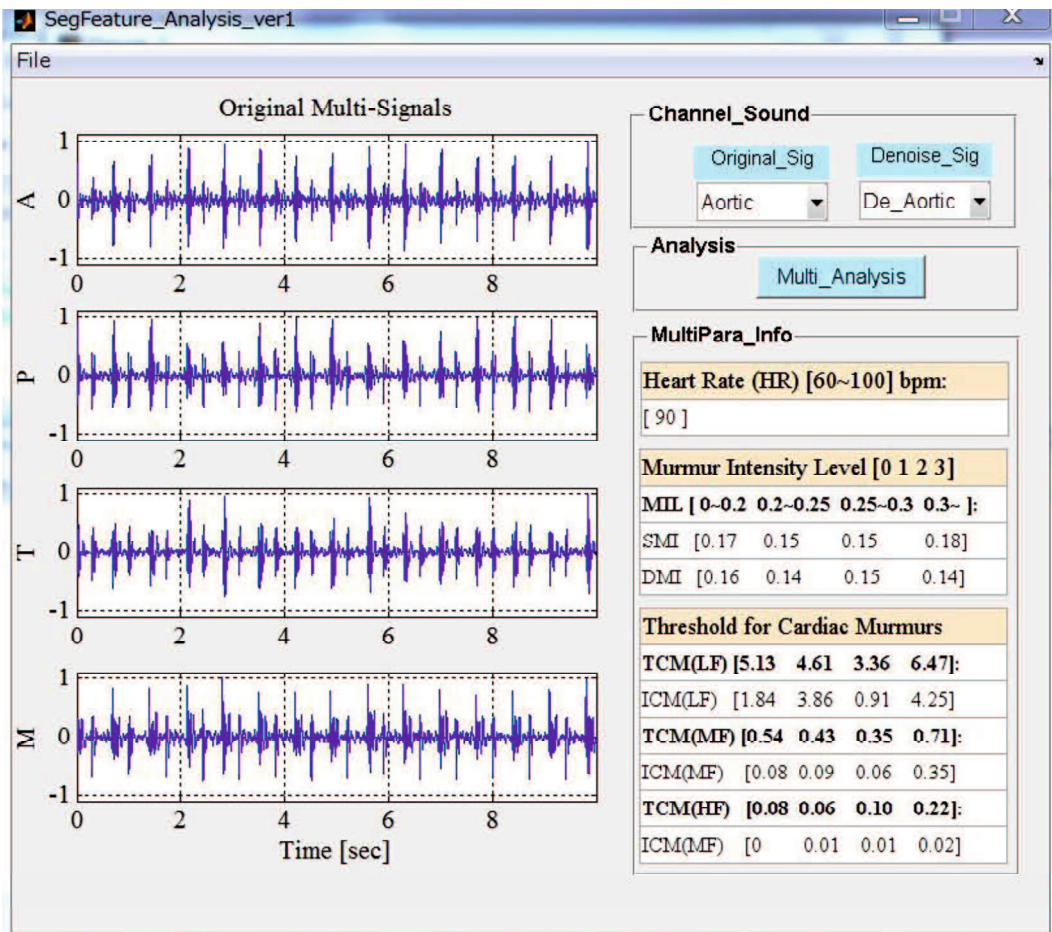


Fig.4. The GUI monitoring system of four channels NHS case (WBD).

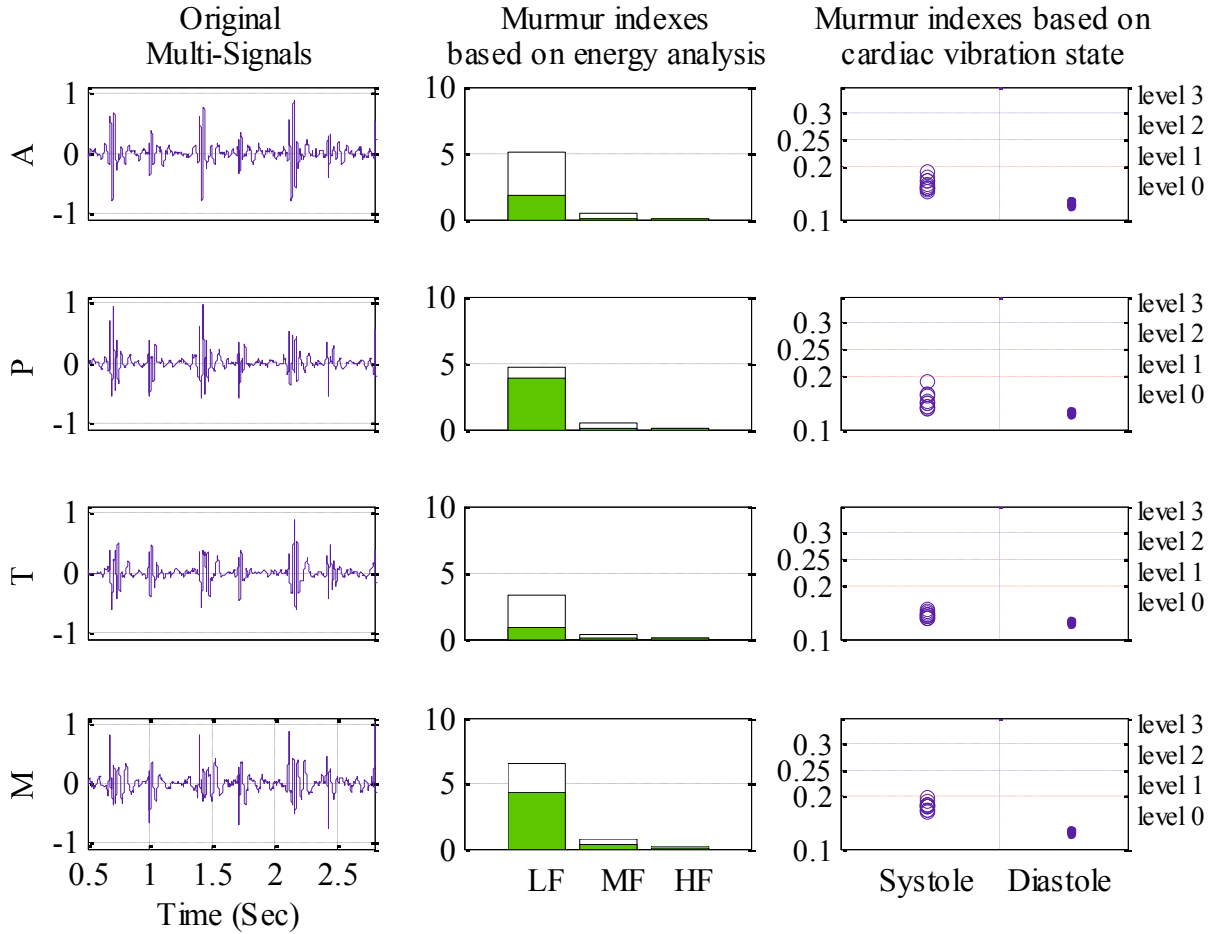


Fig.5. The multichannel cardiac murmur diagnosis parameters of NHS case (WBD).

Furthermore, there are another NHS case, which is showed in Fig.6~8, the HR is 72bpm, which is also within the normal range (60~100) bpm. The cardiac murmur evaluation parameters which showed in Fig.7 (middle column), the multichannel signals from A, P and T positions are displayed with green bar meaning there are no murmur at these three frequencies (LF, MF and HF), while at M position it shows there are murmurs at LF and MF frequencies, that because there are some body organ sounds which appeared near the end part (red box part) showed in Fig.8. And the murmur appearance period and intensity level parameters which showed in Fig.7 (right column), are revealed the MIL is 0 (level 0) that means there are no murmur at systolic and diastolic periods. The judgment values of the multichannel signals from the four positions are displayed in Fig.6.

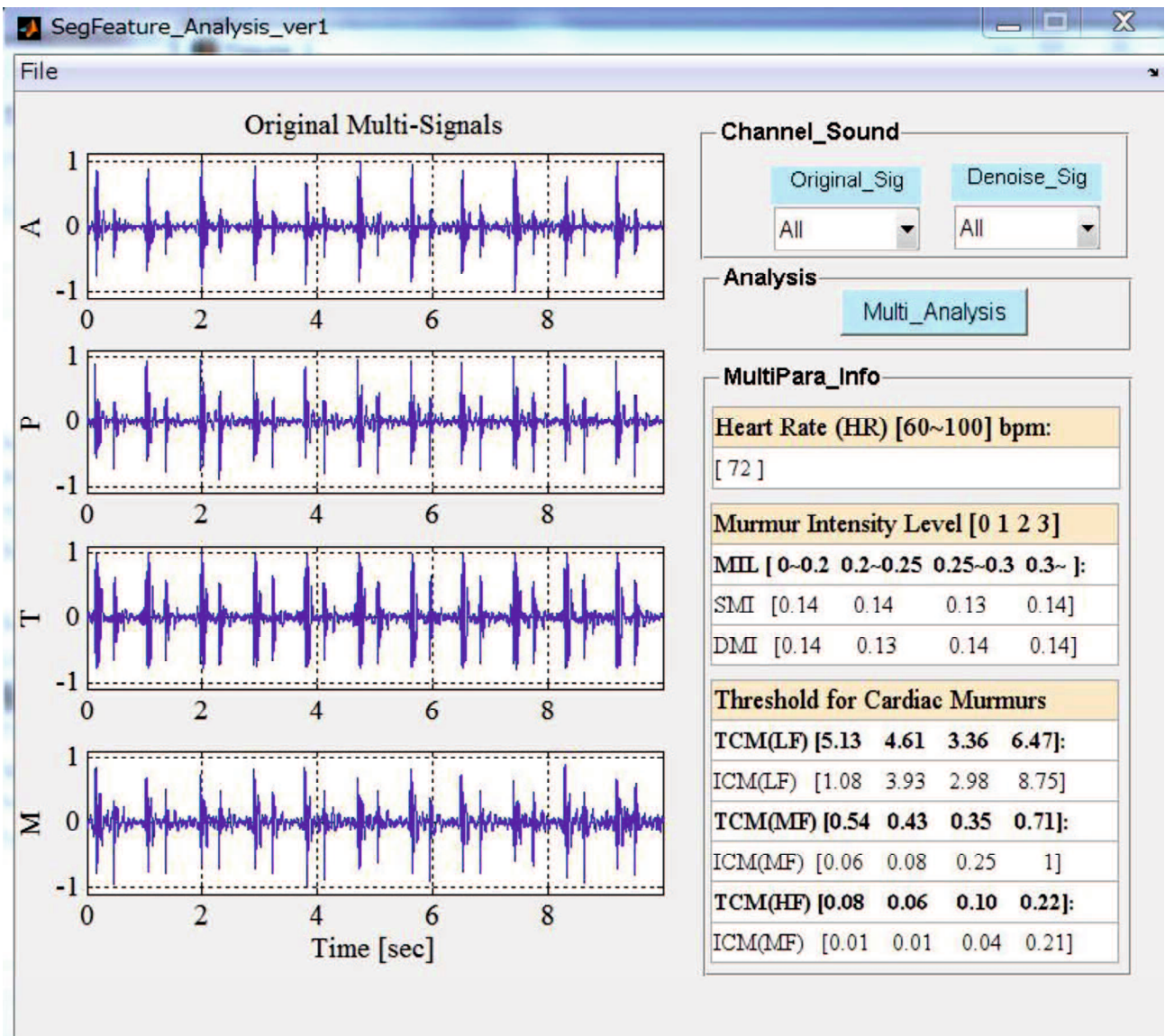


Fig.6. The GUI monitoring system of NHS case (CSY).

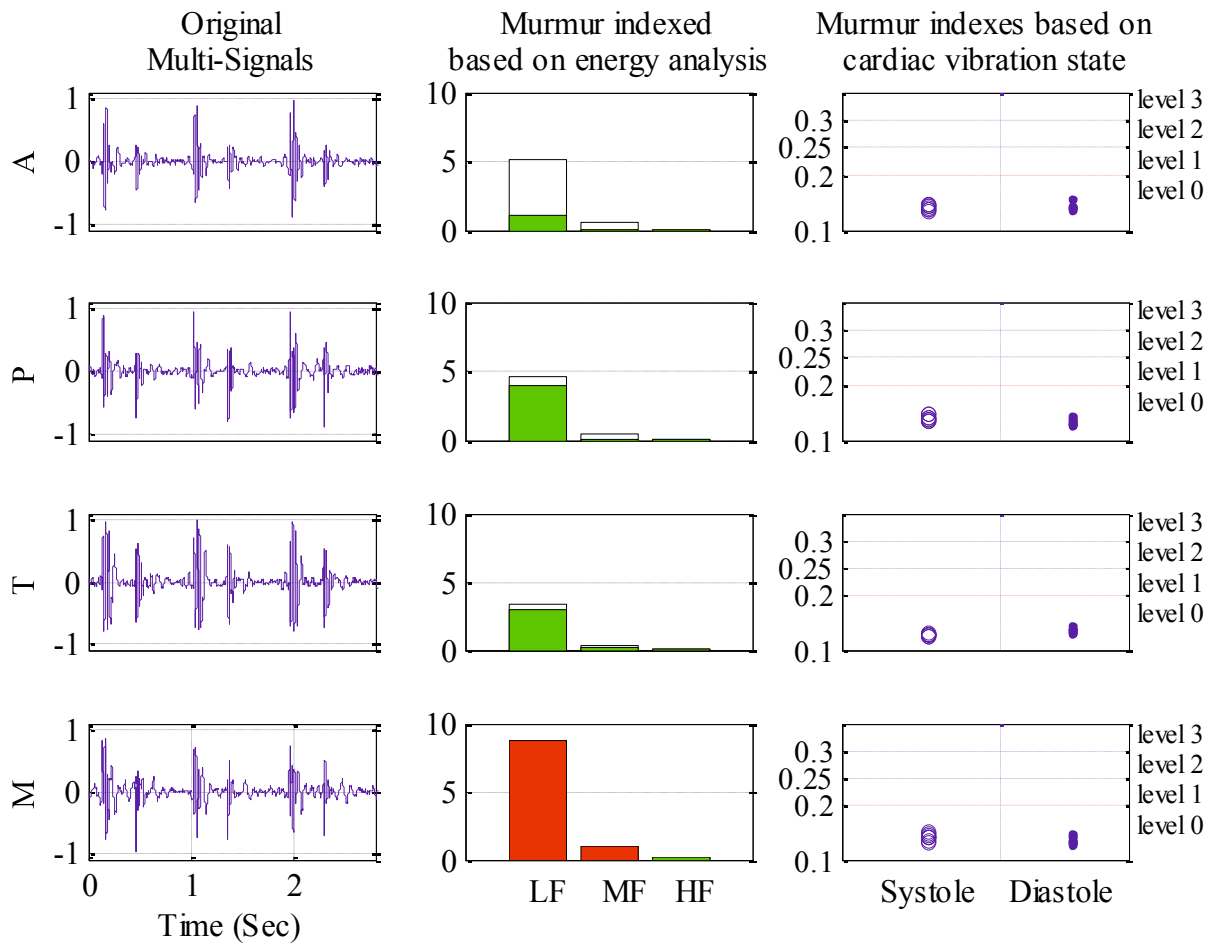


Fig.7. The multichannel cardiac murmur diagnosis parameters of NHS case (CSY).

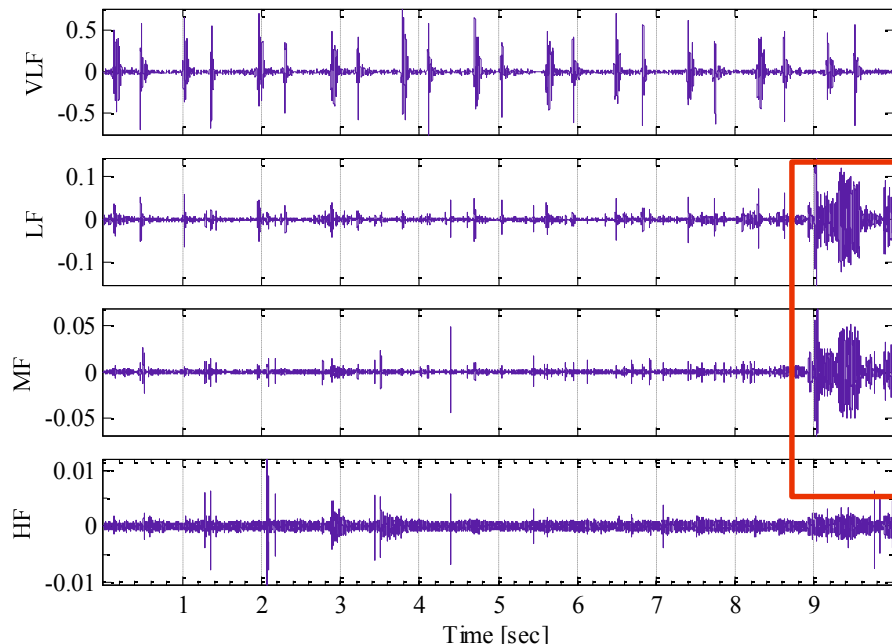


Fig.8. Waveforms of NHS case (CSY) at different frequencies in Mitral position (M), and the part in the red box showed the body organ sounds at LF and MF bands.

3.2 Discussion of atrioventricular septal defect (ASD) case

The common CHDs (ASD, VSD and TOF) cases will be discussed as following. As for ASD case, which is showed in Fig.9~12, the HR is 84 bpm. The murmur appearance period and intensity level parameters which showed in Fig.10 (right column), are revealed that there are level 1 systolic murmurs at A, P and M positions, and there are no diastolic murmurs, while there are no murmurs from T position, which showed in Fig.10~11 marked with red box. However, the cardiac murmur evaluation parameters from T position signal which showed in Fig.10 (middle column), there are murmurs at MF and HF bands, that because there are some strong external sounds which appeared from 3.5~4 seconds (red box part) showed in Fig.11~12. And the judgment values of the multichannel signals from the four positions are displayed in Fig.9.

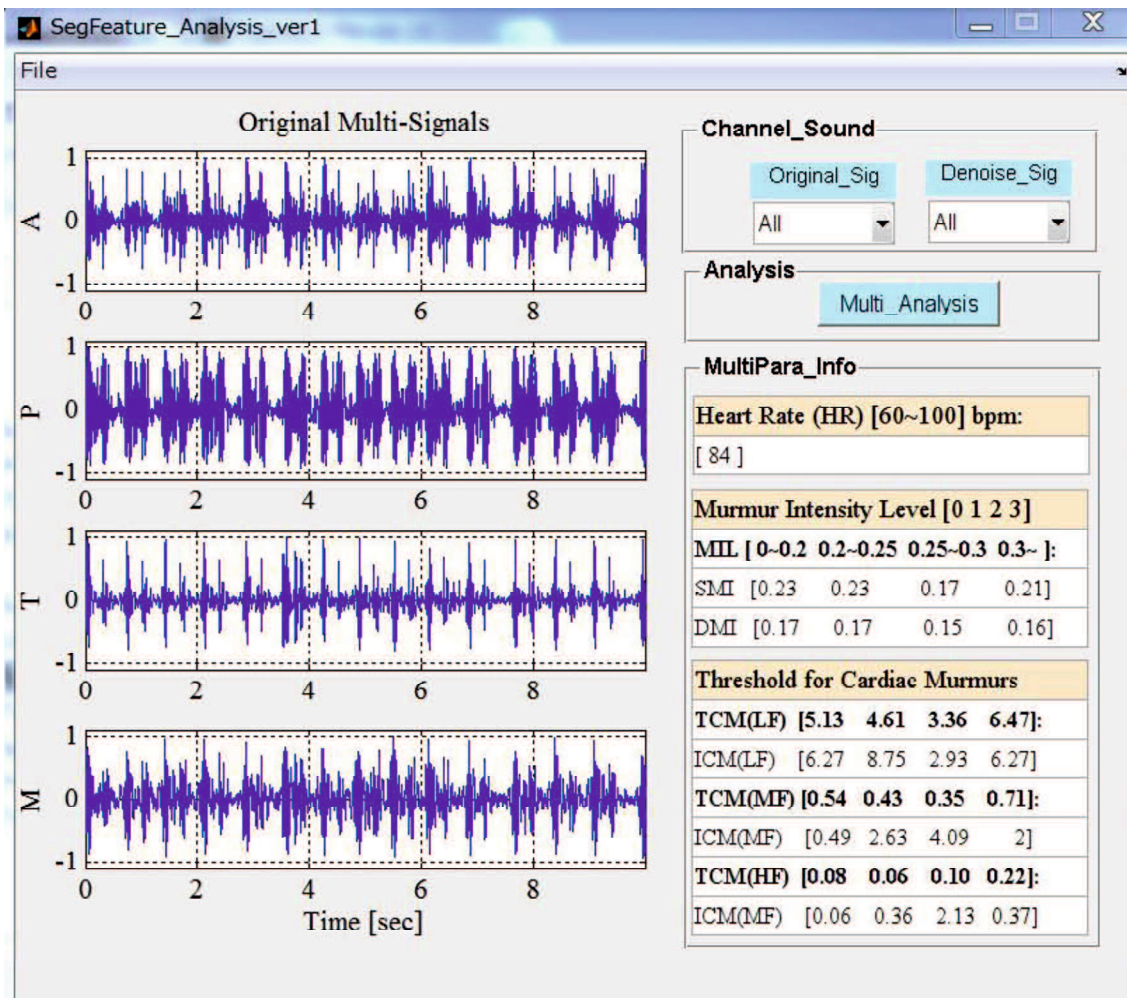


Fig.9. The GUI monitoring system of ASD case (MSJ).

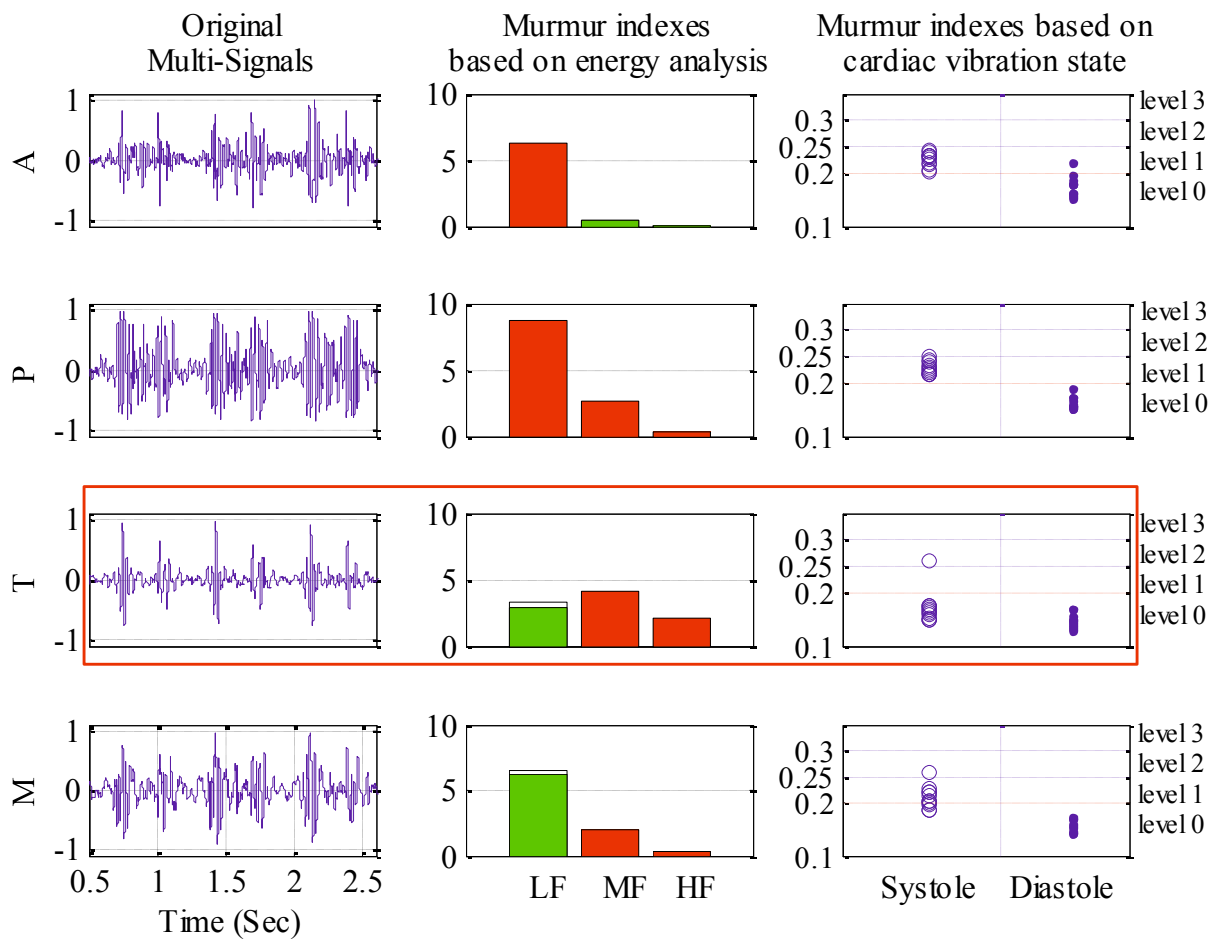


Fig.10. The multichannel cardiac murmur diagnosis parameters of ASD case (MSJ).

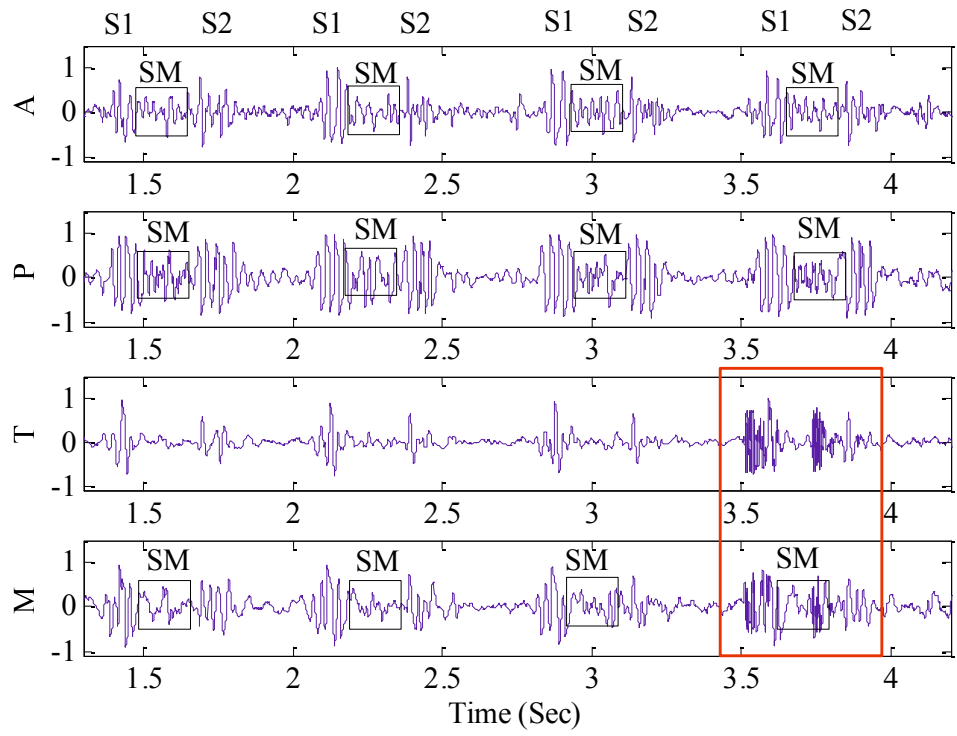


Fig.11. The multichannel signals of ASD case (MSJ), the basic HS (S1 and S2), systolic murmur (SM) are marked, and the strong external noise at T and M positions are marked with red box.

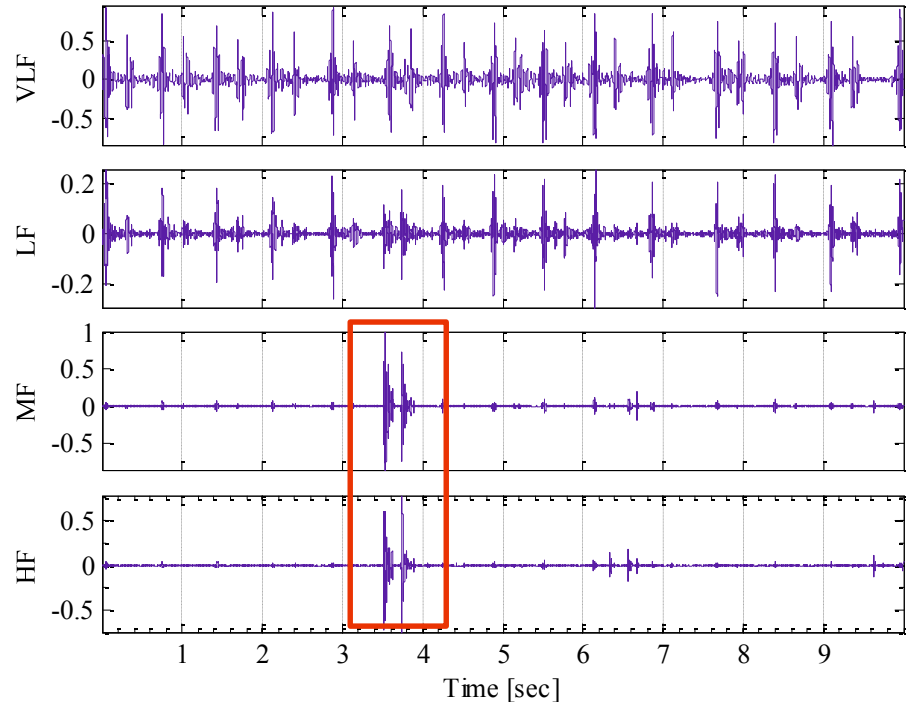


Fig.12. Waveforms of ASD case (MSJ) at different frequencies in Tricuspid position (T), and the part in the red box showed the strong external sound at MF and HF bands.

3.3 Discussion of ventricular septal defect (VSD) case

As for VSD case, which is showed in Fig.13~16, the HR is 84 bpm. The murmur appearance period and intensity level parameters which showed in Fig.14 (right column), are revealed that there are level 1 systolic murmurs from A position, and level 1~2 systolic murmur from P position, furthermore, there are some systolic murmurs from T and M positions. However, there are no diastolic murmurs from these four positions. The systolic murmurs from P position are strongest, which is also described with the cardiac murmur evaluation parameters showed in Fig.14 (middle column), there are murmurs at LF, MF and HF bands shown in Fig.16 (red box part). And the judgment values of the multichannel signals from the four positions are displayed in Fig.13.

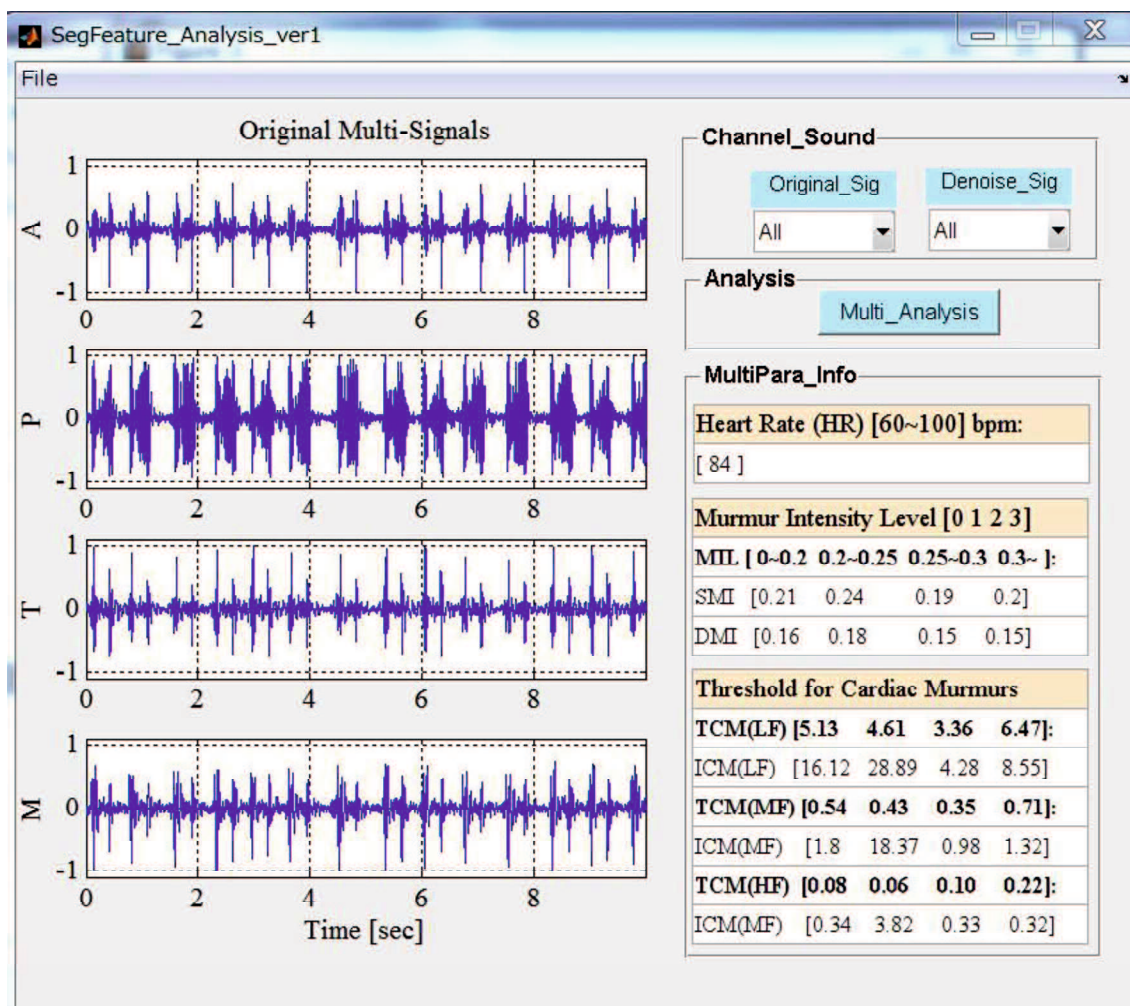


Fig.13. The GUI monitoring system of VSD case (XY).

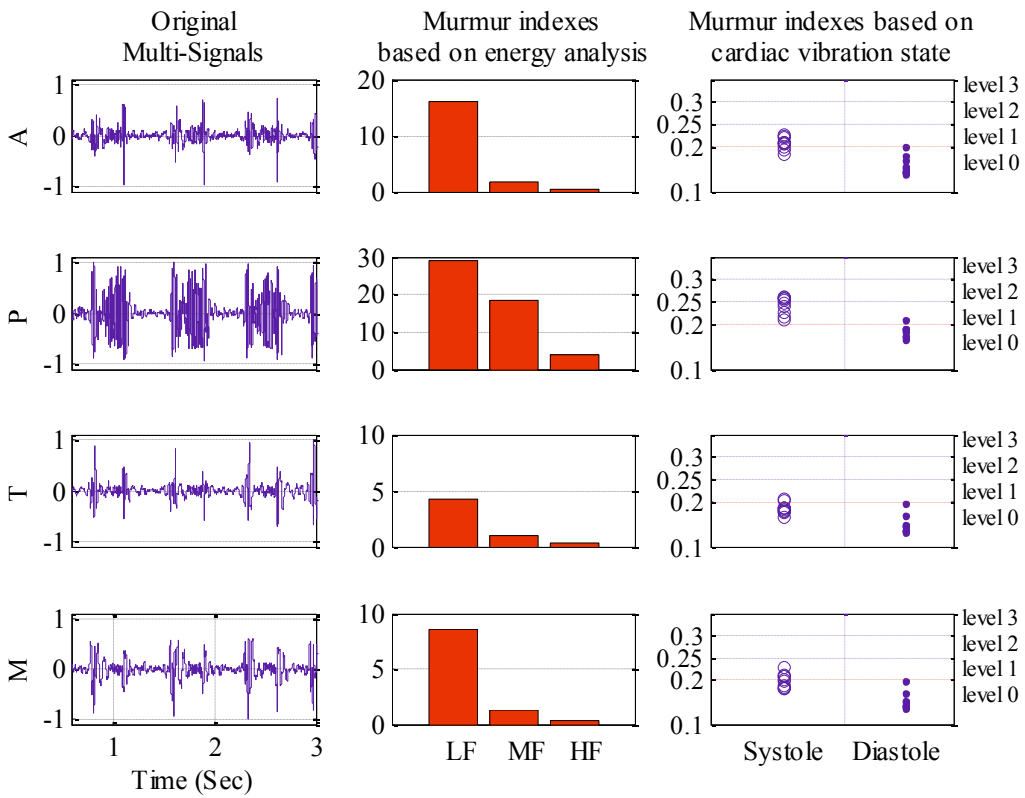


Fig.14. The multichannel cardiac murmur diagnosis parameters of VSD case (XY).

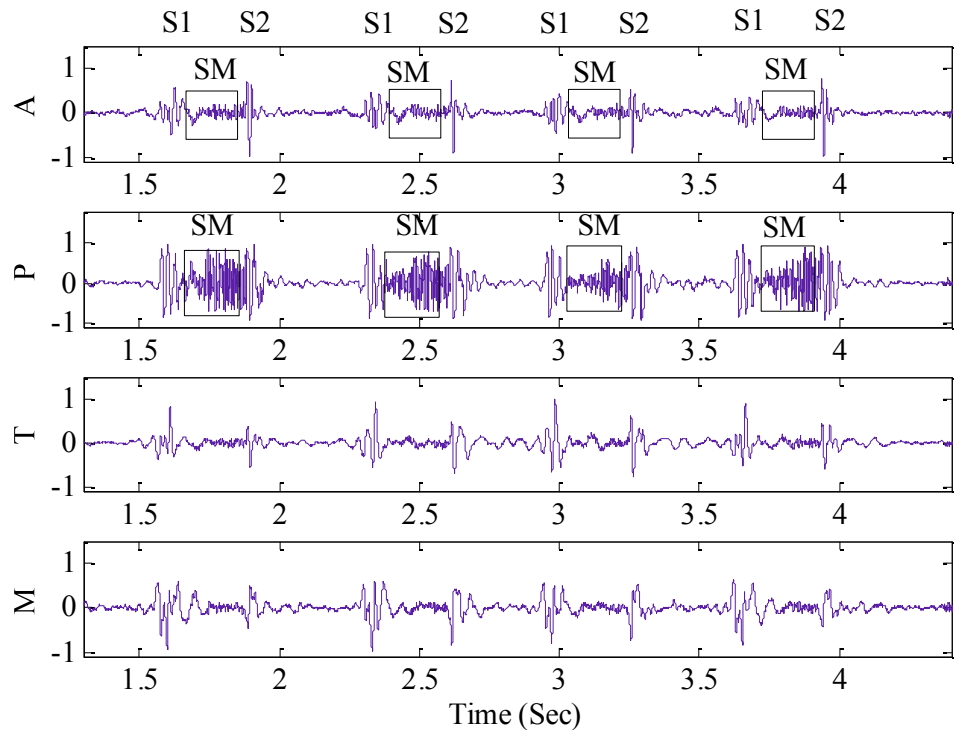


Fig.15. The multichannel signals of VSD case (XY), the basic HS (S1 and S2), systolic murmur (SM) are marked, and some systolic murmurs at T and M positions.

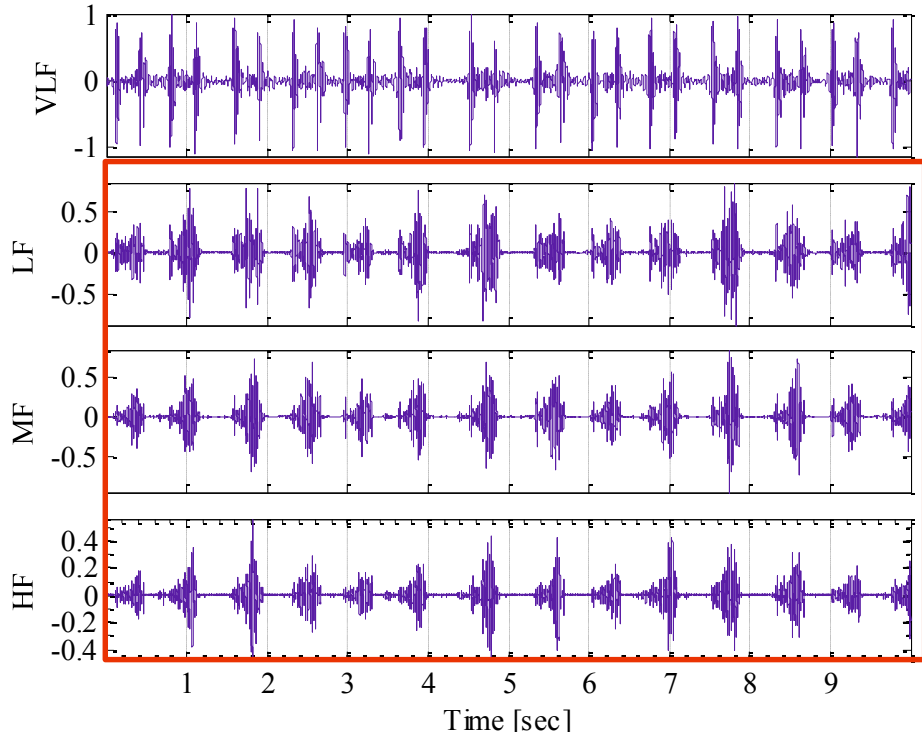


Fig.16. Waveforms of VSD case (XY) at different frequencies in Pulmonary (P) position, and the part in the red box showed the strongest at LF, MF and HF bands.

3.4 Discussion of Tetralogy of Fallot (TOF) case

As for TOF case, which is showed in Fig.17~19, the HR is 66 bpm. The murmur appearance period and intensity level parameters which showed in Fig.18 (right column), are revealed that there are level 2 systolic murmurs from A position, level 2~3 systolic murmur from P position, level 2 from T position, and level 1~2 from M position, furthermore, there are level 1 diastolic murmurs from P positions. However, there are no diastolic murmurs from A, T and M positions. The systolic murmurs from P position are strongest, which is also described with the cardiac murmur evaluation parameters at LF, MF and HF bands showed in Fig.18 (middle column). And the judgment values of the multichannel signals from the four positions are displayed in Fig.17.

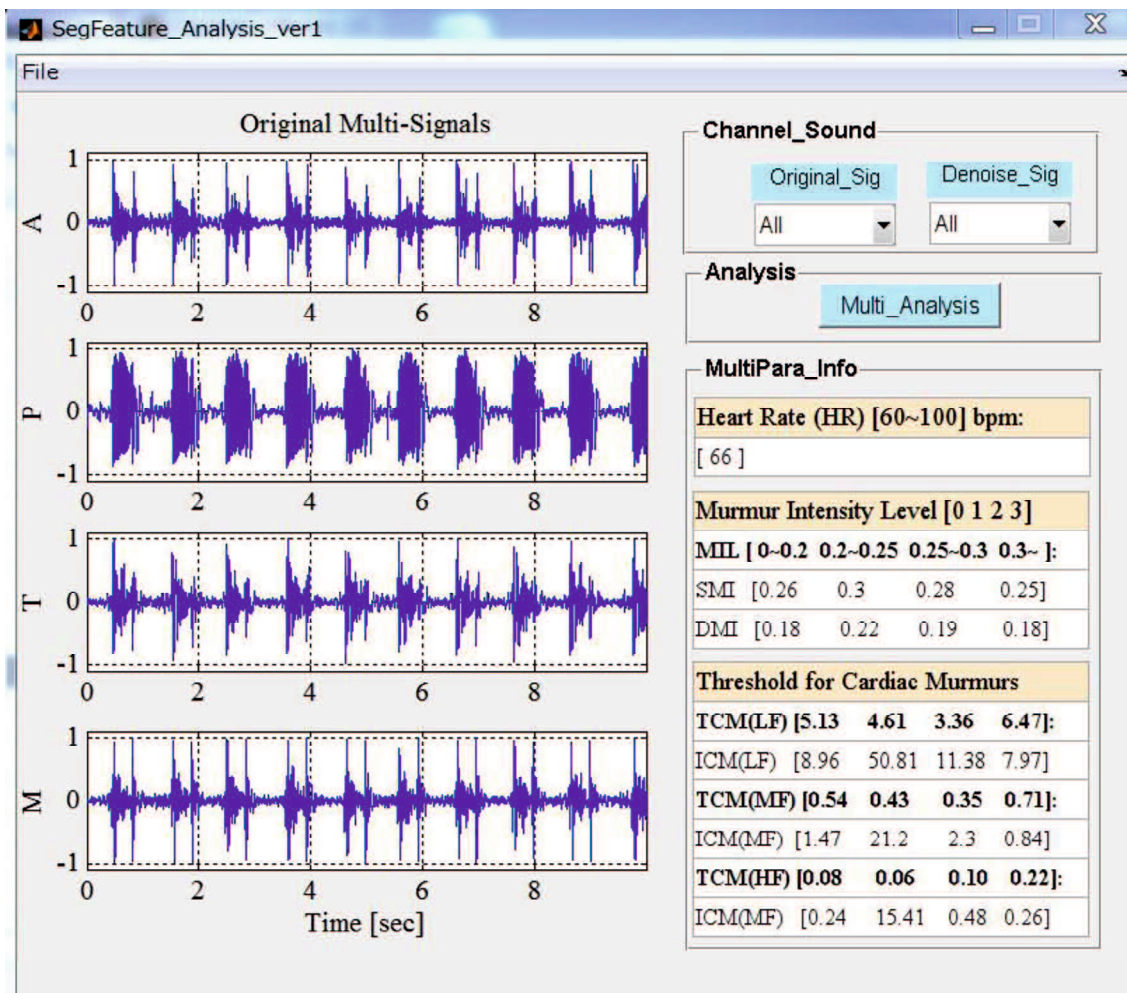


Fig.17. The GUI monitoring system of TOF case (ZZL).

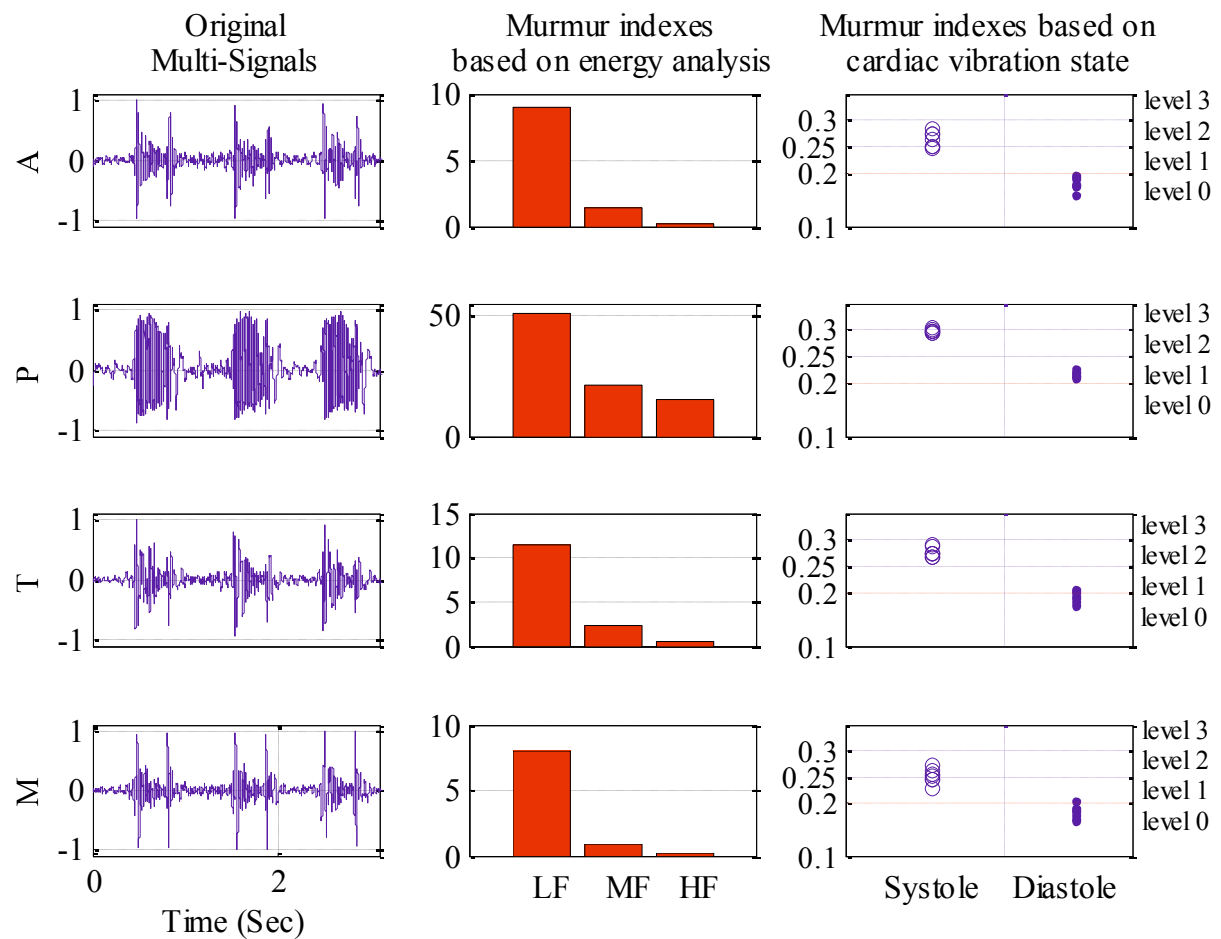


Fig.18. The multichannel cardiac murmur diagnosis parameters of TOF case (ZZL).

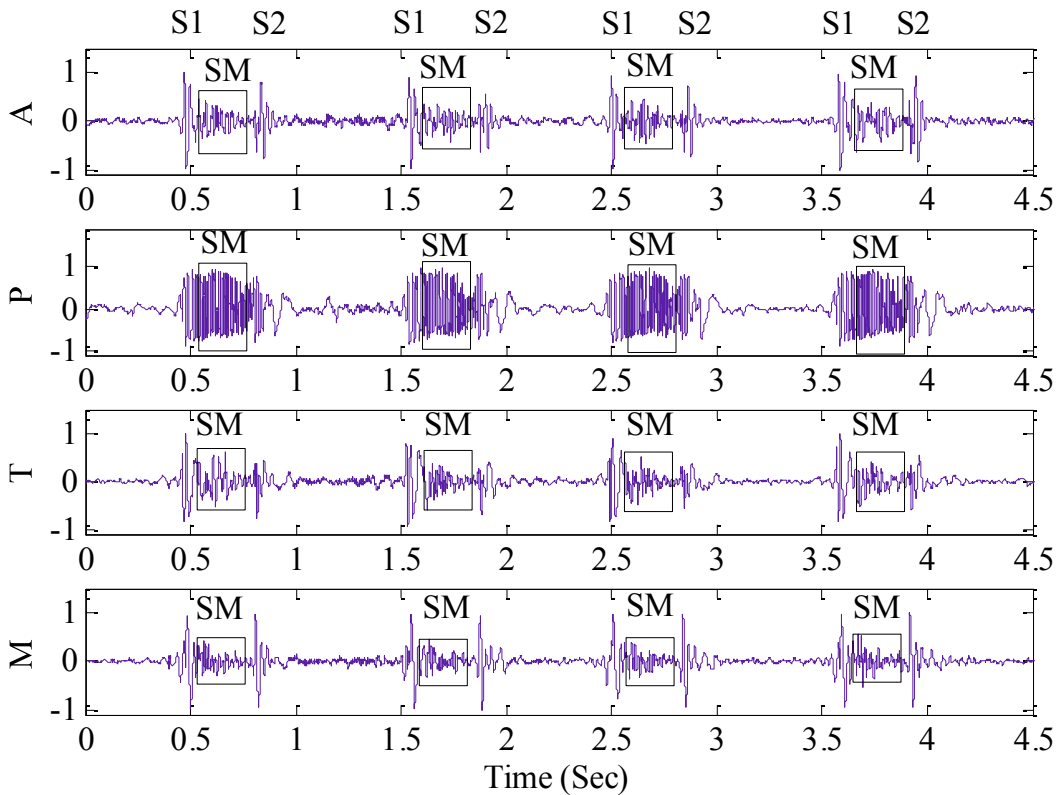


Fig.19. The multichannel signals of TOF case (ZZL, the basic HS (S1 and S2), systolic murmur (SM) are marked, and some diastolic murmurs at P position.

4. Summary

In this chapter, the multichannel murmurs monitoring system which is composed of multichannel HSs measuring system, analysis server and analysis result display was designed. The measuring system which consists of multichannel cardiac signals recorders acquires the signals and sends them to analysis server through internet network by computer. And the data transmission (upload and download) and analysis were implemented by the analysis server.

Furthermore, the analysis result display realized by the GUI monitoring system, the functions which consist of the file reading, original multichannel signals display, each channel listening selection, including the original signals and de-noised signals, multi-signals analysis and multichannel parameters information, are introduced. Meantime, the four-channel murmurs indexes information from four positions can be displayed timely, it is easy and convenient for researchers, medical staff and general users to understand and use.

Furthermore, the murmurs of four channels signals are analyzed based on analysis methodologies which were proposed in our study. The multichannel murmur parameters which were proposed can be used to diagnose the clinical murmurs. Firstly, the judgment of whether the cardiac murmurs existed or not. And then, the appearance periods of the cardiac murmurs, such as systole or diastole murmurs. Further, the murmur intensity level is also can be decided in this study. Meanwhile, the murmur evaluation at LF, MF and HF bands was also discussed. The NHS and common CHDs cases were discussed in this Chapter. Finally, these murmur indexes are contributed to multichannel cardiac signals' pathology analysis in our future study. We also found much more information about the multi-signals from their four positions.

This monitoring on CHDs by clinical HSs auscultation and analysis remain important for general daily health care. The pre-monitoring for CHD sounds will greatly improve the prevention of clinical CHD in advance, and helpful to the primary screening examination, and becomes stronger for the general users to perform the auscultation at home.

References

- [1] The Heart Foundation, HEART DISEASE FACTS, ABOUT HEART DISEASE, 2015. Available at, <http://www.theheartfoundation.org/heart-disease-facts/heart-disease-statistics>. Accessed in 2015.02.03.
- [2] Congenital Heart Defects UK, 2007-2015. Available at, <http://www.chd-uk.co.uk/what-is-chd-abbreviation-for-congenital-heart-defects>. Accessed in 2015.02.03.
- [3] Danford DA¹, Nasir A, Gumbiner C, Cost assessment of the evaluation of heart murmurs in children, Pediatrics. 1993, 91(2):365-8.

Chapter 6

Conclusions

Heart disease is the leading or the second cause of death for people in the world, the mortality occurs in low and middle-income countries. And a type of heart disease called congenital heart defects (CHD) is the most frequent form of major birth defects in newborns, CHDs are not always found during pregnancy or at birth, they also can not be cured, and they must be monitored throughout life. Thus, if life-style related diseases could not be monitored continuously during a long period in the early stage, they might be difficult to be diagnosed appropriately in an early step. Furthermore, the need for the primary health care physicians to improve the cardiac auscultation skill is still strong in the primary screening examination, and becomes stronger for the general users to perform the auscultation at home.

The aim of this study is to develop a multichannel cardiac murmurs analysis method and monitoring system on CHD. Firstly, the background of CHD, HS and common murmurs, reviews of cardiac murmurs analysis were introduced in Chapter one. Next, the HSs measuring system which consisted of four electronic stethoscopes, two IC recorders, auscultation cloth and a note computer was introduced in Chapter 2. The acquired data were transformed to analysis server by network for data transmission, save and analysis.

Heart murmurs are pathological sounds produced by turbulent blood flow due to cardiac defects. In order to quantitatively analyze cardiac murmurs, the murmur index extraction methods based on murmur energy analysis was proposed in Chapter 3. Firstly, In order to extract the murmur indexes

for analyzing the entire cardiac murmurs at different frequency bands, the approach on analysis of the pathologic cardiac murmurs based on the wavelet packet decomposition technique were described. The HS signals were divided into five bands and the energy ratios at each frequency band were calculated and compared. Based on the analysis of clinic HSs data, three evaluation indexes of cardiac murmurs (ICM) were proposed for the analysis of the pathologic murmurs. Finally, the threshold values between the innocent and pathologic murmurs were determined based on the statistical results of the normal HSs. The performance measures of ICM_{HF} yielded the highest sensitivity of 95.7%, specificity of 91.4% and accuracy of 93.9%, respectively. Furthermore, considering the analysis result of evaluation indexes ICM_{HF} at HF (312.5-1250Hz) and the two special cases at VLF band (4.88-19.53Hz), we can obtain the improved performance measures with a sensitivity of 100%, and accuracy of 96.3%, respectively. The statistic results showed that ICM of multichannel signals not only evaluated the murmur quantitatively, but also revealed the murmurs generating reason by analyzing signals from four positions simultaneously.

Furthermore, in order to further quantitatively analyze the cardiac murmurs at each cardiac cycle, the murmur index extraction based on cardiac vibration state by describing the shape of different-scale window moment waveform (MW) was proposed in Chapter 3. Firstly, the homomorphic segmentation of multichannel HS cycle (T) and fundamental HS (S1S2) is proposed based on homomorphic MW extraction with window length l ($T/2$), the HS cycle and S1S2 segmentation were implemented by locating the maximum and minimum of MW respectively. And the HR was also calculated, the cycle automatic segmentation accuracy yielded the highest of 100%, the lowest accuracy was even up to 98.1%. Meanwhile, the S1S2 segmentation accuracy yielded the highest of 100%, the lowest accuracy was even up to 97.5%. Secondly, considering the segmentation points of HS S1S2 and cycle as MW centers respectively, to extract the systolic MW and diastolic MW with different window lengths ($T/8$ and $3T/8$), furthermore, extracting DWF such as systolic murmur index (SMI) and diastolic murmur index (DMI) which were proposed based on systolic and diastolic MW with window length $T/4$. And many experiments showed that the original clinical HS signal included more murmur components when the DMF was high and its value over 0.20. The MIL was defined to evaluate murmur quantitatively, MIL which is less than 0.20, it is defined that there is no murmur, and MIL is belong to 0.20~0.25, it is murmur level 1, and belong to 0.25~0.30, it means

murmur level 2, and If MIL is more than 0.30, it is defined that the murmur level is 3. These simple evaluation limits are used to estimate the clinical CHD murmur quantitatively. Finally, many experiments show that the murmur indexes are efficient to judge the murmur occurring periods and degree. Importantly, DMF can be computed by moment analysis very fast and simple, and therefore it's very useful to auto-diagnosis or aided-diagnosis in an artificial intelligence cardiac murmur analysis system.

The noises coming from various sources contaminate HS signals and affect HS auscultation, in order to improve the auscultation, an unexpected noise reduction method based on frequency slice wavelet transform (FSWT) that can consummate the filtrating in time and frequency domain simultaneously was proposed. This method was assessed by signal noise ratio (SNR), correlation coefficient (CC) and mean square error (MSE) evaluation indicators and comparing with the total variation de-noise (TVD) and discrete wavelet transform (DWT) methods, experimental results showed HCA method was much more effective for external (ambient noise, speech noise, stethoscope device power interference) and internal (respiratory or lung sounds, and skin movements) disturbances noise reduction.

Finally, the multichannel murmurs monitoring system which is composed of multichannel HSs measuring system, analysis server and analysis result display was designed. The measuring system which consists of multichannel cardiac signals recorders acquires the signals and sends them to analysis server though internet network by computer. And the data transmission (upload and download) and analysis were implemented by the analysis server. The analysis results which show the multichannel heart murmur analysis indexes are useful and efficient to diagnose the CHDs, meanwhile, further reveal the heart murmurs physiological and pathological information. And the results data were not only saved in the server, but also displayed in the website for murmurs auscultation and diagnosis. Therefore, monitoring on CHDs by clinical HSs auscultation and analysis remain important for general daily health care. The pre-monitoring for CHD sounds will greatly improve the prevention of clinical CHD in advance, and helpful to the primary screening examination, and becomes stronger for the general users to perform the auscultation at home.

Acknowledgment

It has been sincerely good fortune to have Prof. Zhongwei JIANG as my research adviser. His profound knowledge and scrupulous attitude help my research, dissertation and life in Japan. Moreover, thanks to his sensible encouragement, I can enlarge my views of life. I sincerely appreciate his gratitude for support. Meanwhile, I would like to thank Prof. JIANG's wife Mrs. Yi LIU, who care for my life in Japan in every possible way.

I would like to thank all the members of the committees: Prof. Kanya TANAKA, Prof. Syouji KIDO, Prof. Masanao OBAYASHI and assistant Prof. Minoru MORITA, for their thoroughly reviewing my thesis, and the valuable comments and suggestions,

I gratefully acknowledge Prof. Haibin WANG and Prof. Zhonghong YAN for their advice, supervision, and crucial contribution, I am grateful in every possible way to keep up our collaboration in the future.

I also would like to express my appreciation to Doctor Jinbao ZHANG and Xiaochen WU who are from Chengdu Military General Hospital of People's Liberation Army, Cardiothoracic Surgery. Thanks them to provide the valuable clinical cardiac sound signal data.

I would like to thank all of my colleagues in the Micro-mechatronics laboratory, especially assistant Prof. MORITA, Yu FANG and Jingjing YANG, for their necessary help during my PhD study and life.

I also would like to thank the Rotary Yoneyama Memorial Foundation which support my research and life two years in Japan, especially the all members from Ube Higashi Rotary Club, they are very friendly and kind to me, and teach me the program's mission which is to foster a large cadre of young people who, imbued with the Rotary spirit, will play active roles in international society while building bridges of understanding and cooperation between China and Japan. And further I

would like to appreciate my counselor Mr. Takeo OURIN from Ube Higashi Rotary Club and his wife Mrs. Tamiko OURIN and family, thanks for their love to me, consider me as their own daughter and family member, support my research and life, and encourage me to go towards my dream bravely.

Finally, I would like to thank my parents, who raise me, support me and encourage me several decades. And thank everybody who support and help me during these abroad education lifetimes in Japan. As well as expressing my apology that I can not mention personally one by one.

Ting TAO